5-1-2014

Novel α-MSH Peptide Analogs for Melanoma Targeting

Adam Flook

Adam Michael Flook
Candidate

Biomedical Sciences
Department

This dissertation is approved, and it is acceptable in quality and form for publication:

Approved by the Dissertation Committee:

Dr. Yubin Miao, Chairperson

Dr. Eric Prossnitz

Dr. Helen Hathaway

Dr. Changjian Feng

NOVEL α-MSH PEPTIDE ANALOGS FOR MELANOMA TARGETING

BY

ADAM MICHAEL FLOOK

Bachelor of Science, Biology, University of Redlands, 2009

DISSERTATION

Submitted in Partial Fulfillment of the
Requirements for the Degree of

Doctor of Philosophy

Biomedical Sciences

The University of New Mexico
Albuquerque, New Mexico

March, 2014

ACKNOWLEDGMENTS

I would like to acknowledge Dr. Yubin Miao, my graduate student advisor, principal investigator, and dissertation committee chairperson, for granting me the opportunity to join the lab and work on this exciting and challenging project in fulfillment of my graduate studies. I will take the knowledge and experience gained while under his direction with me throughout my career. I appreciate all that Dr. Miao has taught me and enjoyed being his first graduate student.

I would also like to thank my committee members, Dr. Eric Prossnitz, Dr. Helen Hathaway, and Dr. Changjian Feng for all of their guidance and support throughout this whole process and my time here. Your insights into my project and discussions during committee meetings allowed me to critically analyze and interpret my project, allowing me to become a better scientist.

Finally, I would like to thank Dr. Fabio Gallazzi for his technical assistance and dedication to synthesis of all the α-MSH analogs used for this project, without which, I would have never completed. I would also like to thank the Keck-UNM Small-Animal Imaging Resource (KUSAIR) with funding from the W.M Keck Foundation and UNM Cancer Research and Treatment Center for allowing me access to the SPECT/CT to perform my imaging studies.

NOVEL α-MSH PEPTIDE ANALOGS FOR MELANOMA TARGETING

BY

ADAM MICHAEL FLOOK

Bachelor of Science, Biology, University of Redlands, 2009

ABSTRACT OF DISSERTATION

Submitted in Partial Fulfillment of the
Requirements for the Degree of

Doctor of Philosophy

Biomedical Sciences

The University of New Mexico
Albuquerque, New Mexico

March, 2014

NOVEL α-MSH PEPTIDE ANALOGS FOR MELANOMA TARGETING

By

Adam Michael Flook

Bachelor of Science, Biology, University of Redlands, 2009

Ph.D; Biomedical Sciences, University of New Mexico, 2014

ABSTRACT

Skin cancer is the one of the most diagnosed cancers in the United States with increasing incidence over the past two decades. There are three major forms of skin cancer but melanoma is the deadliest. It is estimated that 76,690 new diagnoses of melanoma and 9,480 deaths will occur in 2013. Melanoma accounts for approximately 1.6% of all cancer related deaths and is the 5th leading diagnosed cancer in the United States. The mean survival rate of patients diagnosed with metastatic melanoma is six months, with five year survival rates of less than 5%. In this project, we describe the design and characterization of novel melanoma-targeting peptide analogs for use in diagnostic imaging of both primary and metastatic melanoma lesions.

Novel α-MSH peptide conjugates were designed to target the melanocortin-1 receptor present and over-expressed on melanoma cells. These peptides were synthesized and their *in-vitro* melanocortin-1 receptor binding affinities were established in murine melanoma cells. Once binding affinities were determined, the peptides were radiolabeled with ^{99m}Tc utilizing a novel direct

radiolabeling technique developed in our laboratory. The peptides were purified via reverse-phase high performance liquid chromatography and *in-vivo* melanoma targeting and pharmacokinetic properties were determined in B16/F1 melanoma-bearing female C57BL/6 mice. Biodistribution and SPECT/CT imaging studies were performed with the promising ^{99m}Tc-labeled peptide conjugates.

All α-MSH peptide conjugates tested showed low nanomolar binding affinity for the melanocortin-1 receptor. All peptides were readily radiolabeld with ^{99m}Tc with greater than 95% radiochemical purity. All ^{99m}Tc-labeled peptides displayed high specific *in-vivo* melanoma tumor uptake while maintaining low normal organ accumulation, and were excreted through the urinary system in a timely fashion. In addition, all tested ^{99m}Tc-labeld α-MSH peptides demonstrated clear visualization of *in-vivo* tumor lesions with SPECT/CT. While all peptides exhibited high melanoma uptake, extremely high non-specific renal uptake was of concern. After synthesis of α-MSH peptide conjugates containing a different amino acid linker, renal uptake was drastically reduced and a lead compound had emerged, showing favorable *in-vivo* melanoma targeting and uptake properties with limited amounts of non-specific renal accumulation.

TABLE OF CONTENTS

LIST OF FIGURES

LIST OF TABLES

Chapter 1

Introduction

Carcinogenesis

Over the last half of a century, cancer research has spawned a vast and complex body of knowledge into the underlying mechanisms of cancerous cell development. The research to date reveals cancer to be a complex disease involving dynamic alterations at both a genomic and proteomic level [1, 2]. These alterations allow for the process of carcinogenesis to take place. Carcinogenesis is a highly complicated, multi-step mechanism of malignant transformation by genomic mutations producing both oncogenic and tumor suppressive genes capable of transforming normal cells into highly malignant cells [1, 2]. The combination of oncogenic gene activation and tumor suppressive capabilities allows for excessive, uncontrolled cellular proliferation and development of clinically diagnosed tumors. These processes have been reiteratively studied and classified utilizing transgenic mouse models and cancerous cell lines (both human and animal) to determine the multi-step modality of which carcinogenesis takes place [1, 2].

Deemed the “Hallmarks of Cancer” by Hanahan and Weinberg in 2000, the acquired capabilities of cancerous cells necessary for cancer development and progression can be categorized into six functional traits: self-sufficiency in growth signals, insensitivity to anti-growth signals, limitless replicative potential, sustained angiogenesis, evasion of apoptosis, and tissue invasion and metastasis. It is believed that all cancers acquire these traits during their

transformation from normal cells, albeit through a tremendous variety of molecular mechanisms and genetic mutations.

Melanoma epidemiology and carcinogenesis

Skin cancer is the one of the most diagnosed cancers in the United States with increasing incidence over the past two decades. Different types of skin cancer include basal cell carcinoma, squamous cell carcinoma, and melanoma. Of these three types of skin cancer, melanoma is by far the deadliest. It is estimated that 76,690 new diagnoses of melanoma and 9,480 deaths will occur in 2013. Melanoma accounts for approximately 1.6% of all cancer related deaths and is the 5th leading diagnosed cancer in the United States [3]. Metastatic melanoma is the leading cause of skin cancer related deaths with a poor prognosis. The mean survival rate of patients diagnosed with metastatic melanoma is six months, with five year survival rates of less than 5% [4, 5]. The rise in incidence and diagnoses is due to both increased awareness of cutaneous lesions and lifestyle changes that have led to increased ultraviolet light exposure over the past few decades [6, 7]. Melanomas are derived from the malignant transformation of cutaneous melanocytes, the cells residing in the basal layer of the epidermis that are solely responsible for human pigmentation [8]. The majority of melanomas arise de novo although some may originate in existing nevi [8, 9].

Exposure to ultraviolet light sources such as the sun and an ever increasing proclivity towards cosmetic enhancement of the skin through the use

of tanning beds have presented as important causative factors in melanoma carcinogenesis. Intermittent UV exposure and sunburn history in melanoma development have been identified as major contributors in epidemiological studies [5, 7] . The pathogenic effects of UV exposure could involve genotoxic, mitogenic, or immunosuppressive responses to damage induced by both Ultraviolet A (UVA) and Ultraviolet B (UVB) radiation. UVA, also known as long wave radiation, has a particle wavelength of 320-400 nM and can penetrate the skin past the epidermal layers and into the dermal tissue. UVA radiation indirectly damages DNA through reactive oxygen species (ROS) generation and formation of Guanine to Thymine transversion mutations. UVB, also known as short wave radiation, has a particle wavelength of 290-320 nM and is the chief cause of skin reddening and sun burning, damage occurring to the more superficial epidermal tissues of the skin. UVB radiation can directly damage DNA through mutagenesis at dipyrimidine sites, inducing apoptosis in normal keratinocytes [7, 10].

While the strong correlation between UV exposure and melanoma development exists, it is extremely difficult to accurately delineate the precise exposure patterns of individuals and entire populations to both UVA and UVB exposure. Clinically cutaneous melanomas have been categorized into four distinct subtypes: superficial spreading melanoma on intermittently exposed skin such as the upper back, lentigo maligma melanoma in chronically exposed skin, acral lentiginous melanoma on the hairless skin of the palms and soles, and nodular melanoma with vertical growth, not associated with a macular component [7, 11]. The potential targets of UV-induced damage from a molecular

point of view include the signaling cascades of the melanocortin-1 receptor (MC1R) and BRAF genes. The BRAF gene is an important molecule in the mitogen-activated protein kinase (MAPK) pathway, which regulates cell growth, survival, and invasion. MAPK signaling initiates at the cell membrane through receptor tyrosine kinases binding their respective ligand or via RAS-GTPase activation upon adhesion of integrin molecules to extracellular matrices [7, 12]. BRAF, a serine-threonine kinase, can become constitutively activated upon mutation of a single amino acid substitution of valine with glutamic acid at position 600 (known as the V600E mutation). This BRAF mutation, which activates a 500-fold induction of BRAF, constitutively activates downstream MAPK/ERK signaling in cells without upstream activation of RAS, in a growth factor-independent manner [13]. Constitutive MAPK/ERK activity stimulates proliferation, survival, and can induce the expression of the microphthalmia-associated transcription factor (MITF) gene in cutaneous melanocytes. The MITF gene has been shown to be the master regulator of melanocytes with induced activation resulting in increased pigmentation, survival, and proliferation through a mechanism that triggers cell cycle exit [6, 7, 14-17]. While the discovery of the BRAF mutations elicit the potential for therapeutic intervention, due to the extensive heterogeneity of this disease, BRAF mutations have only been identified in approximately 50-60% of all cutaneous melanomas [6, 13, 18].

Current diagnostic procedures for detecting both melanoma and non-melanoma related skin cancers remain fickle to this day, even with clinical knowledge that detection of any form of skin cancer in the early treatable phases

is critical for favorable prognosis. The American Cancer Society recommends "careful skin check by a clinician as part of a routine cancer-related checkup", however, many clinicians do not perform any routine skin screenings during regular checkups [19]. In order to diagnosis a melanocytic lesion on a patient, clinicians utilize the ABCDE rule to guide naked eye examinations: A= lesion asymmetry, B= border irregularity, C= color variability, D= diameter usually larger than 6mm, E= evolution or change in shape, color, size, elevation, or any emerging symptoms such as bleeding, itching or crusting [19, 20]. Once a melanoma diagnosis has been given, some clinicians will opt for the utilization of imaging modalities to rule out any clinically resectable distant disease. This is done to avoid potential surgery when curative resection is not a viable option, as well as ease patient anxiety by confirming the absence of distant disease [21]. Currently, the most commonly used imaging modalities for melanoma patients include chest x-ray, computed tomographic (CT) imaging, magnetic resonance imaging (MRI), ultrasonography, positron-emission tomographic (PET) imaging, and PET-CT [21]. While these imaging modalities are powerful tools to help aide clinicians in patient diagnosis, several studies have demonstrated that the detection rate of metastatic disease is lower than the rate of false positivity [21, 22]. False positivity rates with staging x-ray studies range from 7-15% as compared to a 0.0-0.2% detection rate for metastatic disease. Similar results have been obtained with current CT imaging, ultrasonography, and FDG-PET scans [21-24]. It is imperative that new diagnostic imaging procedures be

implemented in order to aide clinicians in successful diagnosis of both primary melanoma lesions and metastatic disease.

Clinical treatment of metastatic melanoma

Melanoma is notoriously difficult to treat and has been considered as one of the most therapeutically challenging malignancies due to its genetic heterogeneity, dysregulation of cell cycle events allowing for evasion of apoptosis and constitutive proliferative potential, and increased drug resistance to current chemotherapeutic and immunotherapeutic agents [18, 25-28]. Through the years many novel systemic therapeutic approaches have been developed to treat metastatic melanoma but have proven largely ineffective. Cytotoxic chemotherapeutic agents deployed as the "standard of care" for treatment of metastatic melanoma include Dacarbazine (DTIC), Temozolomide (TMZ), and taxanes such as paclitaxel or docetaxel [25, 29, 30]. Dacarbazine is the only FDA approved chemotherapy agent for metastatic melanoma and is closely related to its more bioavailable and orally tolerable derivative, TMZ [30-33]. Both chemotherapeutic agents are prodrugs that are transformed into 5-(3-methyltriazen-1-yl)imidazole-4-carboximide (MITC), which can then methylate guanine residues in the DNA, forming O^6-methylguanine adducts, repair of which is vital and necessary for cell integrity and survival. These adducts work to generate single and double-strand DNA breaks when repair of adducts is attempted by cellular mismatch repair enzymes, causing activation of apoptotic pathways [31, 34]. Response from treatment with these chemotherapeutic

agents on malignant metastatic melanoma have been less than promising since their development, with overall response rates ranging between 15-20%, and a median survival of approximately 7 months [31, 32, 35, 36]. Paclitaxel and docetaxel are both mitotic inhibitors that can stabilize microtubules, interfering with the normal breakdown of microtubules during cellular division. Both drugs have not shown significant activity in melanoma with response rates in metastatic melanoma not exceeding 15%, and a median survival of 5 months [32, 33, 37, 38]. Multidrug combination therapy of these agents combined with tamoxifen and cisplatin showed no significant benefit to overall survival and increased toxicity when compared to DTIC alone [32, 33, 39, 40].

Treatments of metastatic melanoma with systemic immunotherapeutic or biochemotherapeutic treatment regimens have not encountered much more success than chemotherapeutic agents alone [32, 33]. Interferon as a single agent, has shown modest activity against metastatic melanoma with an average response rate ranging from 10-15%, while high dose interleukin-2 (IL-2), which has recently garnished FDA approval for late stage metastatic melanoma, showed an overall response rate of 16%, but can achieve durable complete remissions in a small percentage of patients [32, 33, 41-43]. Biochemotherapeutic regimens, utilizing both chemotherapeutic and immunotherapeutic agents, with combined DTIC, cisplatin,IL-2, and IFN have shown promise in Phase III clinical trials with response rates ranging from 30-60% with some durable complete remissions in patients [32, 33, 44]. Targeted therapies such as Sorafenib or Vemurafenib, FDA approved oral multikinase

inhibitors targeting the MAPK pathway and oncogenic *B-raf* V600E mutation, when added to conventional treatments with paclitaxel and/or carboplatin have shown a high partial response rate of 40% and median survival of 13.6 months, but antitumor activity was independent of BRAF mutational status [43, 45-51].

Metastatic melanoma chemo and immunoresistance

Melanoma resistance to exogenous drug and immunotherapies is a multifaceted and complex problem involving a multitude of molecular mechanisms. Chemotherapeutic efficacy is often impaired by intrinsic or acquired tumor resistance, known as multi-drug resistance (MDR). MDR can be the result of varying mechanistic alterations to cancer cells including changes in tumor cell cycle checkpoints, impairment of apoptotic pathways, increased repair of damaged cellular targets, and a vast reduction in drug accumulation within the tumor cells [25, 30]. The mechanism encountered in the vast majority of laboratory research has been that of the enhanced efflux of hydrophobic cytotoxic drugs mediated by one of a family of transporters, known as the ATP-binding cassette (ABC) transporters [25]. The ABC transporters are an energy-dependent family of proteins that typically efflux exogenous hydrophobic solutes and structurally diverse molecules out of the cytoplasm of the cell and back into the extracellular environment [25, 26, 30, 52-55]. In human melanoma, the transport proteins with elevated mRNA expression in both primary and metastatic melanoma cells contributing to increased MDR are ABCA5, ABCB2, ABCB6, ABCD3, ABCD4, ABCF1, ABCF2 and ABCF3 [52, 55]. Expression of the most

common and extensively studied ABC transport proteins, ABCB1 and ABCC1, remain controversial and may be induced by chemotherapy treatment itself, but their role in the high chemoresistance of human melanoma may be limited [52, 56, 57]. The ABCB5 transport protein, which shares high homology with its structural analog ABCB1, has demonstrated high expression in both clinical melanomas and specifically within cells of melanocytic origin, and may represent an novel chemoresistance mediator in human melanoma [52, 58, 59].

Resistance of human melanoma to chemo and immunotherapeutic regimens may also be conferred by an increased expression and activation of DNA repair enzymes. Increasing evidence indicates that damage to highly proliferating cells, such as melanoma, induced by the use of cytostatic drugs can be counteracted and compensated for by modulation of DNA-repair mechanisms [30, 60]. Decreased efficacy of cytostatic drugs such as TMZ and other therapeutic agents can be conferred by the inhibition of the DNA-mismatch repair pathway (MMR) and over expression of O^6-methylguanine-DNA methyltransferase (MGMT) [30, 54]. DNA-mismatch repair deficiency imparts drug resistance by enervating the ability of cells to repair DNA damage generated from alkylating agents and activate cellular apoptosis [30, 60]. In particular, O^6-methylguanine adducts invoked by the use of TMZ or DTIC, are not properly reconstituted due to the up-regulation of MGMT in melanoma cells. MGMT encodes the DNA-repair protein O^6-alkylguanine DNA alkyltransferase (AGT) and is a singular protein pathway that recognizes and repairs DNA through its specificity for O^6-substituted purines without the use of any other

multi-enzyme complexes such as the nucleotide excision repair (NER) pathway [61, 62]. Specifically, AGT recognizes the O^6-guanine base lesion induced by alkylating agents and transfers the aberrant methyl group to a cysteine residue in its active site, thus repairing the guanine base. Removal of the methylation on the guanine residue prevents cytotoxicity by regenerating intact DNA. Regular cellular replication and transcription is allowed to proceed, while the AGT molecule is ubiquitinated and eventually degraded [54, 61, 63, 64]. Loss of MMR protein expression in melanoma cell lines confers resistance to apoptotic stimuli and causes destabilization of the melanotic genome, resulting in high mutation rates, increased proliferation, invasion, and survival [30, 60, 65].

Melanoma targeting via alpha-melanocyte stimulating hormone (α-MSH) ligand biding to the melanocortin-1 receptor

Melanocortin-1 receptor

The melanocortin-1 receptor (MC1R) is part of a superfamily of G-protein coupled receptors (GPCR's) expressed in melanocytes and melanoma cells, initially authenticated by ligand-binding studies [66-68]. At the present time, five melanocortin receptors have been identified, namely the MC1R-MC5R. The MC1R is expressed largely in melanocytes and leukocytes and involved in skin pigmentation and animal coat coloration [69]. Expression levels of functional MC1R are 100-fold higher in melanocytes than immune derived lymphoblastoid cells with an estimated number of MC1R transcripts of 20-200 receptors per cell for normal melanocytes and 1-10 receptors per cell for normal keratinocytes [70]. The MC2R is expressed in the adrenal glands and regulates glucocorticoneogenesis [71]. The MC3R and MC4R are expressed in brain tissues and are found to regulate feeding behavior and energy homeostasis [72]. The MC5R is widely expressed throughout peripheral tissues and may participate in the mediation of exocrine gland function [73].

The MC1R is an integral membrane protein consisting of 317 amino acids and harboring all the structural hallmarks of classical GPCR's; an extra cellular N-terminus, seven transmembrane (TM) fragments, and an intracellular C-terminus [68, 74]. According to several 3-D ligand-receptor models and site directed mutagenesis, the ligand binding site of the MC1R forms a pocket located

below the plasma membrane-extracellular matrix interface [74, 75]. The 3-D models developed suggest a highly charged region containing a Glu residue from TM2 and two Asp residues from TM3 interact with an Arg residue on the pharmacophore binding sequence of the native MCR agonists, the family of peptide hormone derivatives known as the melanocortins. In addition, a network of aromatic residues on the extracellular side of TM4, TM5, and TM6 may also play an important role in agonist binding by interacting with other aromatic residues of the pharmacophore sequence of the melanocortins (**Fig. 1.1**) [68, 76].

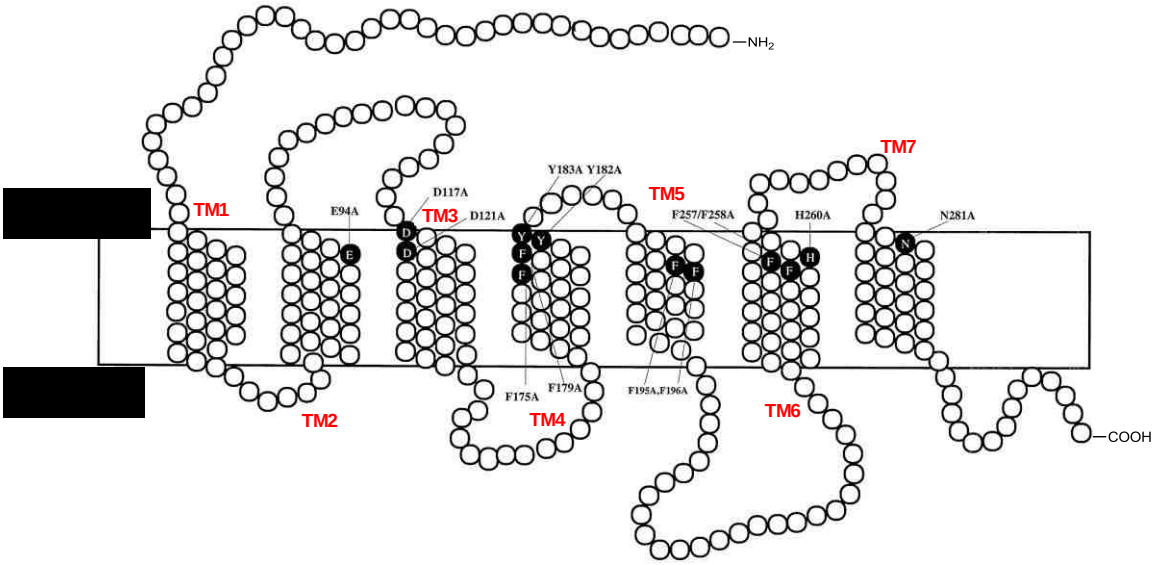

Fig. 1.1- Schematic structure of the human melanocortin-1 receptor. (Adapted from Yang, 1997).

The MC1R is a significant contributor to skin phenotype and sensitivity to UV light induced DNA damage and photocarcinogenesis through regulation and production of the amount and type of pigments produced in the skin [68, 77-80]. The total amount of melanin content present and relative contributions of

pheomelanin (a red/ yellow pigment) and eumelanin (a brown/ black pigment) synthesized by human epidermal melanocytes are a key contributor of epidermal pigmentation and UV protection [68, 81]. Epidermal pigmentation is directly correlated with eumelanin content, which is more abundant in dark pigmented skin than lighter pigmented skin. Eumelanin is considered to be the primary photo-protective mechanism as it reduces the penetration of UV radiation (UVR) through the epidermal layers and into the underlying dermis; known as the tanning response. Eumelanin is superior to pheomelanin in its photoprotection properties as it is less resistant to degradation from UVR exposure and boasts the ability to quench reactive oxygen species generated during UVR that can cause cellular lipid peroxidation and protein/ DNA damage [77, 78, 81, 82].

Activation of eumelanin production within wild type melanocytes upon UVR exposure occurs through a cascade of autocrine and paracrine signaling within the skin. Upon exposure of the human epidermis to UVR, a variety of factors will be released by keratinocytes, including the native MC1R ligand, α-MSH. Binding of α-MSH to the MC1R on melanocytes activates the cAMP/PKA signaling cascade and production of cAMP through adenylyl cyclase. cAMP accumulation in the cytoplasm activates the MAPK and ERK1/2 kinases leading to phosphorylation of cAMP responsive-element-binding protein (CREB) transcription factor family members. CREB phosphorylation transcriptionally activates the microphthalmia transcription factor (MITF), which is used to activate production of tyrosinase and tyrosinase related protein-1 (TRP-1) and TRP-2 as well as promote survival and proliferation of melanocytes. Cooperatively in a

storage organelle called the melanosome, tyrosinase, TRP-1, and TRP-2 enzymatically convert the precursor molecule, tyrosine, into eumelanin. Eumelanin will stay deposited in the melanosome to exert its biological effects of UV protection and skin pigmentation [68, 77-79, 81-84].

In addition to the important biological role of the MC1R in reducing UV induced damage in the epidermis, the process of ligand binding induces several other important molecular mechanisms including cell survival through evasion of apoptosis and cellular internalization of the ligand-receptor complex. Upon binding of α-MSH, the MC1R also activates the inositol triphosphate (IP3) kinase survival pathway, an important survival pathway in many different cell types [77, 85]. Induction of this pathway ultimately leads to the activation of protein kinase B (Akt/PKB). Activated Akt inhibits apoptosis by phosphorylating and inactivating pro-apoptotic proteins Bad and caspase 9. This evasion of apoptosis was seen independent of α-MSH melanogenic or mitogenic effects [77, 85, 86].

Agonist binding to the MC1R triggers an important cellular process of internalization of the ligand-receptor complex. The process of agonist dependent internalization is initiated upon MC1R binding of its native agonist, α-MSH. Binding of the receptor initiates a phosphorylation of the MC1R by the GRK family of kinases. This phosphorylation targets the receptor, with bound ligand, for internalization into an endocytic vesicle. This process has been determined for the MCR4 and can be speculated with the MC1R due to the presence of melanocortins in melanoma cells following their addition to external medium and time-dependent appearance of acid-resistant binding [87]. The fate of the

MC1R-ligand complex remains unclear upon endocytosis into the cell but evidence has been presented that radiolabeled α-MSH agonists are rapidly internalized into the cell and translocated to the lysosome, where they remain within cellular cytoplasm for a prolonged period of time [68, 88, 89].

MC1R expression on both human and murine melanoma cells makes this receptor system an attractive molecular target for melanoma specific targeting. Radioligand binding studies have demonstrated functional MC1 receptor populations ranging from 1,000-6,000 receptor sites per cell on human melanotic and amelonotic melanoma cells and between 5,000-8,000 receptors sites per cell for murine melanoma cells [90, 91]. The relatively low number of receptor sites per cell necessitates the need for high affinity ligand molecules for successful molecular targeting of the MC1R.

Wild type α-MSH ligand for MC1R

α-melanocyte stimulating hormone (α-MSH) is a tridecapeptide derived from the posttranslational processing of proopiomelanocortin (POMC) produced in the pituitary gland [92, 93]. Wild type α-MSH (Ac-Ser^{1}-Tyr^{2}-Ser^{3}-Met^{4}-Glu^{5}-His^{6}-Phe^{7}-Arg^{8}-Trp^{9}-Gly^{10}-Lys^{11}-Pro^{12}-Val^{13}-NH_2) is a potent MC1R agonist that exerts its biological effects in the regulation of eumelanin production, as previously stated. Structure bio-activity analyses have demonstrated that the four peptide pharmacophore binding sequence of His^{6}-Phe^{7}-Arg^{8}-Trp^{9}, is solely responsible for binding the MC1R and exerting melanotropic activity [93, 94]. With over 80% of all human melanoma tumor samples obtained from patients

with metastatic disease harboring receptors for α-MSH and the intrinsic nanomolar binding affinity of wild-type α-MSH for the MC1R, underscores the potential use of this ligand-receptor complex for selective delivery of either diagnostic or therapeutic radiopharmaceuticals for melanoma imaging or therapy [95].

Radiolabeled α-MSH peptide analogs used in targeting of the MC1R

Linear α-MSH tritium-labeled radiopharmaceuticals were first developed during the 1970's and 1980's for tissue distribution and melanoma detection but suffered with low specific activity, making tumor targeting inefficient. In addition, the linear structure of these peptide analogs allowed for increased conformational freedom attributing to less potent MC1 receptor binding and decreased *in-vivo* stability. Currently the "gold standard" in linear α-MSH peptide analogs is ^{125}I-[Nle^{4},$_{D}$-Phe^{7}]-α-MSH (NDP-MSH), due to its sub-nanomolar binding affinity to the MC1 receptor [93, 96]. Utilization of this peptide analog was limited to *in-vitro* studies as dehalogenation of ^{125}I-NDP-MSH occurs *in-vivo*. Radiolabeling linear α-MSH peptide analogs through conjugation of radionuclide chelators was another method employed to develop potent melanoma imaging probes. 1,4,7,10-tetraazacyclododecane-1,4,7,10-tetraacetic acid (DOTA) and diethylene triamine pentaacetic acid (DTPA) metal chelators conjugated to the N-terminus of the peptides are able to form stable complexes with a variety of radiometals and were demonstrated to increase melanoma imaging sensitivity,

tumor uptake, and decrease normal organ uptake compared to their linear peptide analog counterparts [93, 97, 98].

In more recent years, new targeting peptide design methods have been employed with increasing promise. Peptide cyclization strategies were employed to enhance *in-vivo* stability, receptor selectivity, and receptor binding affinity of the α-MSH peptides [99-102]. Cyclization of the α-MSH peptide allowed for decreased conformational freedom due to stabilization of peptide secondary structures, including beta turns, as compared to the linear peptide. This decrease in conformational freedom allows for increased receptor binding affinity [100-102]. Cyclization strategies can be classified into four types: (1) backbone to backbone; (2) N-terminus to C-terminus; (3) side chain to C-terminus; (4) two side chains via disulfide, metal, or lactam bridges [4]. Unique lactam bridge cyclization occurs by an amide bridge formed between two amino acid side chains within the peptide such as a positively-charged Lysine and a negatively-charged Aspartic acid [101-103]. Lactam bridge, disulfide bond, and metal cyclization strategies were employed to improve the stability of the α-MSH peptides against *in-vivo* proteolytic degradation as well as further enhance the binding affinity of the α-MSH peptides to the MC1 receptor [104, 105].

Research into the potential use of these cyclized α-MSH radiopeptides was thoroughly conducted over the last decade. Through this research it was determined that the different cyclization strategies may have a profound effect on pharmacokinetic and biodistribution properties of radiopeptides with comparable *in-vitro* binding affinities. A comparison of DOTA-conjugated Re-metal-cyclized

peptides with disulfide bridge-cyclized α-MSH analogs showed that metal cyclization results in increased receptor-mediated tumor uptake and decreased renal uptake values compared to disulfide bridge-cyclization, correlating to more favorable pharmacokinetic and biodistribution properties [106].

Lactam cyclization and substitution of Phe^7 with $_D$-Phe^7 in α-MSH peptides along with radiolabeling of ^{67}Ga and ^{111}In to form ^{67}Ga-DOTA-GlyGlu-CycMSH and ^{111}In-DOTA-GlyGlu-CycMSH, showed improved cellular internalization and retention in B16/F1 mouse melanoma cells as well as fast whole body clearance [100, 104]. In addition, visualization of *in-vivo* tumor formation in B16/F1 melanoma-bearing C57 mice utilizing whole body SPECT/CT imaging of ^{111}In-DOTA-GlyGlu-CycMSH, demonstrated clear potential for diagnostic applications [104]. The data showed the significant improvement and utilization of the lactam bridge-cyclized α-MSH radiolabeled peptides as a melanoma specific imaging and therapeutic agent.

Recent research has been focused on fine tuning the use of the lactam bridge-cyclized peptides by both adjusting the position of the DOTA metal chelator and reducing the ring size of the cyclized peptide. DOTA position had previously been shown to have a profound effect on radiolabeled linear α-MSH peptide tumor and renal uptake whereas conjugation of the DOTA chelator to the C-terminus in the ^{111}In-DOTA-NAPamide complex exhibited 75% greater melanoma uptake and 63% less renal uptake than the N-terminus conjugated ^{111}In-MSH_{oct} [102]. Thus, alternate conjugation of the DOTA chelator to ^{111}In-labeled lactam bridge-cyclized α-MSH was a logical next step. Indeed

conjugation of the DOTA chelator to the α-amino group of Lys in the cyclic ring of Ac-GluGlu-CycMSH[DOTA]-^{111}In exhibited increased MC1 receptor binding affinity of 0.6 nM, high tumor uptake (11.42 ± 2.20 % injected dose/gram (%ID/g) 2 h post injection), increased cellular retention (9.42 ± 2.41 %ID/g 4 h post injection), and low non-target organ uptake values (<1.3 %ID/g) [102].

Reduction in the ring size of the cyclized α-MSH peptide from 12 amino acids to 6 amino acids in the ^{111}In-DOTA-Nle-CycMSH$_{hex}$ complex exhibited increased tumor uptake values (24.94 ± 4.58 %ID/g 0.5 h post injection), rapid clearance of 82% of injected radioactivity through the urinary system by 2 h post Injection, and clear, defined whole body melanoma visualization through SPECT/CT imaging. In addition, linker modifications have demonstrated profound effects on the melanoma-targeting and pharmacokinetic properties of the ^{111}In-labeled lactam-bridge cyclized α-MSH peptides. Hydrocarbon, amino acid, and polyethylene glycol linkers were previously shown to have favorable pharmacokinetic and melanoma-targeting profiles on radiolabeled bombesin[107], RGD[108], and α-MSH peptides[100]. Introduction of the GluGlu linker in the ^{111}In-DOTA-Nle-CycMSH$_{hex}$ peptides produced ^{111}In-DOTA-GGNle-CycMSH$_{hex}$, which demonstrated high melanoma uptake while reducing both kidney and liver uptake values by 28-42% and 61-68% respectively.

In nuclear medicine, both ^{111}In and ^{99m}Tc radionuclides are widely used as diagnostic imaging agents due to their unique imaging properties. ^{99m}Tc is an ideal imaging radionuclide due to its favorable nuclear decay properties and ease

of coordination with imaging probes, such as small peptides like the α-MSH peptides previously discussed.

^{99m}Tc-radiolabeling of α-MSH peptides

Background of technetium

Technetium, a second-row transition metal and element 43 on the Periodic Table, was discovered in 1937 by a pair of Italian scientists in a sample of molybdenum that had been irradiated by deuterons for some years in the U.C. Berkeley cyclotron [109-111]. Stemming from the Greek word technetos, meaning artificial, technetium was the first previously unknown element on earth to be artificially made by man. Since its discovery, 21 isotopes of technetium have been produced ranging from Tc-90 to Tc-110. All technetium isotopes produced are radioactive with nuclear half-lives ranging from 0.86 sec (short-lived ^{110}Tc , $T_{1/2}$= 0.86 sec) to 2.6 x10^6 years (long-lived ^{97}Tc, $T_{1/2}$= 2.6 x10^6 y) [110, 112].

Currently, ^{99m}Tc is the most commonly used radioisotope in diagnostic nuclear medicine. ^{99m}Tc can be produced through the use of the ^{99}Mo/^{99m}Tc commercial generator first developed in 1957 at the Brookhaven National Laboratory (BNL) in Upton, New York [110, 112, 113]. Purification work on the ^{132}Te/ ^{132}I generator at BNL in the late 1950's turned up a contaminant which was discovered to be ^{99}Tc after the presence of ^{99}Mo was found in the chemical separation process [109, 114]. The ^{99}Mo/^{99m}Tc generator uses the parent isotope (^{99}Mo), obtained as a fission by-product of ^{235}U or by bombardment of ^{98}Mo with neutrons, loaded onto an alumina column as molybdate, $^{99}MoO_4^{2-}$. The positively-charged alumina absorbs the negatively-charged molybdate ions.

Through a β-decay process, ^{99m}Tc is produced as $^{99m}TcO_4^-$ pertechnetate (**Fig. 1.2**) [112]. The $^{99m}TcO_4^-$ is then eluted off the column with sterile normal saline to generate the final product of $Na^{99m}TcO_4^-$, sodium pertechnetate, at high specific activity with only diminutive quantities of chemical contaminants such as carrier molybdate and ^{99}Tc.

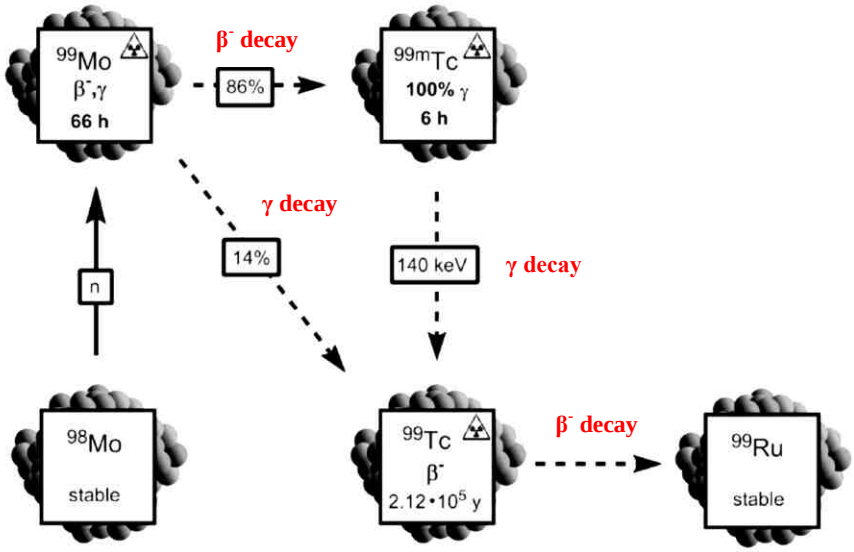

Fig. 1.2- Generation and decay of ^{99m}Tc through the use of the $^{99}Mo/^{99m}Tc$ generator. (Adapted from Bartholomä, 2010).

The $^{99}Mo/^{99m}Tc$ generator can be eluted multiple times per day as ^{99}Mo radioactivity remaining on the column continues to decay, yielding fresh ^{99m}Tc activity. The worldwide use of this generator system in nuclear medicine is due to the ease of operation, high elution efficiency, extraordinary radionuclide purity, and remarkable specific activity [110-112] . Other methods used for separating ^{99m}Tc from ^{99}Mo include: solvent extraction of “instant technetium” with methylethyl ketone, sublimation of technetium oxides from Mo complexes at

temperatures exceeding 850°C, and elution of ^{99m}Tc from zirconium molybdate gel columns [111].

Technetium-99m is an ideal SPECT (single photon emission computed tomography) imaging radionuclide due to its nuclear decay properties. Decay of the metastable ^{99m}Tc to the ground state, and virtually stable, ^{99}Tc element, releases three gamma photons of 2.2, 140, and 143 KeV, with the monochromatic 140 KeV photon in highest abundance with 89.1% of all nuclear transitions [110, 113]. The 140 KeV photon emission is strong enough to penetrate tissues *in-vivo* but can be readily collimated and absorbed by commercial gamma camera detectors to give images with superior spatial resolution. In addition to the 140 KeV photon emission, the convenient physical half-life of ^{99m}Tc ($T_{1/2}$= 6.03 hours) also renders the radionuclide an ideal SPECT imaging agent [109, 110, 112, 115]. The physical half-life of this isotope is long enough to synthesize ^{99m}Tc-labeled radiopharmaceuticals, perform quality controls, administer ^{99m}Tc-labeled compounds to a patient as well as allow compound accumulation in a target tissue and collection of imaging data, while minimizing the total radiation dose the patient. The wide use of ^{99m}Tc for diagnostic radioimaging studies is demonstrated by the fact that 19 million injections of ^{99m}Tc radiopharmaceuticals were performed in the United States in 2007 for cardiac, lung, kidney, bone, liver, and gall bladder studies, representing nearly 85% of radiopharmaceuticals used as nuclear medicine [112].

Coordination geometries of technetium

As a transitional metal element, technetium displays some unique chemistry characteristics, including its rich and diverse redox chemistry, with compounds of technetium exhibiting all formal oxidation states between +7 and -1 [115, 116]. **Table 1.1** summarizes the oxidation states and coordination geometries of technetium. The existence of technetium in these many oxidation states suggests an advantage in structural diversity for ^{99m}Tc-labeled radiopharmaceuticals. However, the existence of the technetium in these diverse redox states also demonstrates the potential reactions for undesirable side products.

Oxidation State	Example	Coordination Chemistry	Coordination number
+7 (d^0)	$[TcH_9]^{2-}$ TcO_4^-	trigonal prism tetrahedron	9 4
+6 (d^1)	TcO_4^{2-}	tetrahedron	4
+5 (d^2)	$TcOCl^{4-}$ $[Tc(NCS)_6]^-$ $[Tc(Diars)_2Cl_4]^+$	square pyramid octahedron dodecahedron	5 6 8
+4 (d^3)	$[TcCl_6]^{2-}$	octahedron	6
+3 (d^4)	$[Tc(diars)_2Cl_2]^+$	octahedron	6
+2 (d^5)	$[TcCl_2(PhP(Oet)_2)_4]$	octahedron	6
+1 (d^6)	$[Tc(CNC(CH_3)_3)_6]^+$	octahedron	6
0 (d^7)	$[Tc_2(C0)_{10}]$	octahedron	6
-1 (d^8)	$[Tc(CO)_5]^-$	trigonal bipyramid	5

Table 1.1- Oxidation states and coordination geometries of technetium. (Adapted from Liu, 1999).

Technetium must be reduced to a lower oxidation state in order to produce stable and effective ^{99m}Tc-labled biomolecules. The choice of reducing agents and reaction conditions play a pivotal role on determining the final redox state of the technetium complex. These reducing agents will be discussed later in ^{99m}Tc

radiolabeling approaches. The most stable oxidation states of technetium for use in radiopharmaceuticals can be characterized by chemically robust core structures depicted in **Fig. 1.3** [115]. The most studied and utilized core moiety is that of $[^{99m}TcO]^{3+}$ (B), characteristic of the Tc(V) oxidation state. Complexes of this core generally yield a square pyramidal geometry and are stabilized via N_xS_{4-x} tetradentate ligands. The use of this technetium core produces ^{99m}Tc-complexes containing both syn- and anti- isomers [116]. These isomeric compounds generally contain different lipophilicity and biodistribution properties in biological systems, so it is critical to determine the species desired, and perform optimized radiosynthesis under specific conditions to obtain that single species.

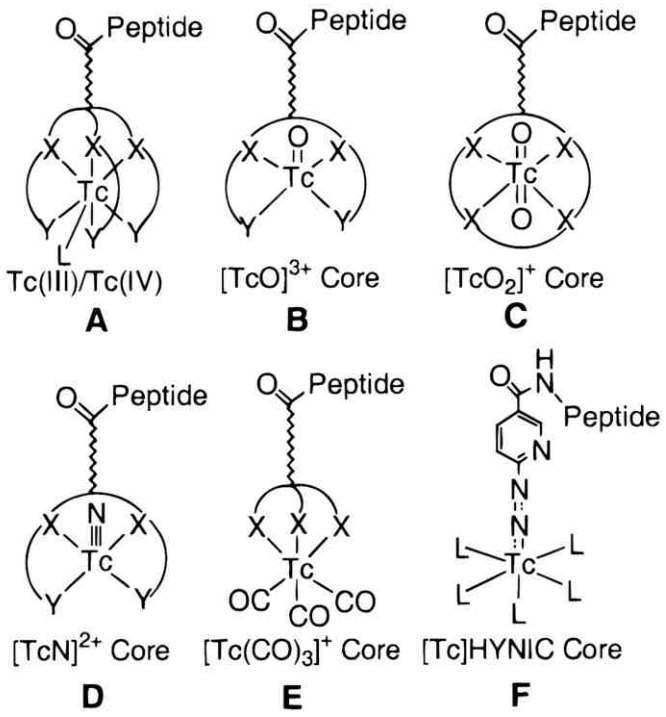

Fig. 1.3- Technetium cores used in ^{99m}Tc labeling of biomolecules. X= N or S, Y= N or S, L= neutral donor ligand. (Cited from Liu, 1999).

Design of ^{99m}Tc radiopharmaceuticals

The early design of ^{99m}Tc radiopharmaceuticals in the 1970's and 1980's was directed toward investigating ligands that were able to stabilize technetium in lower oxidation states for localized direction of the radionuclide *in-vivo*, known as technetium-essential radiopharmaceuticals. These compounds use technetium as the essential core atom around which other conjugating ligands are arranged. The first stable core structures were demonstrated by a group at MIT in which the Tc(V)O core could be stabilized utilizing bisdithiolate (S_4) or diamidedithiolate (N_2S_2) ligands to form square pyramidal complexes [109, 117]. This initial finding permitted the development of newer generations of technetium-labeled, technetium-essential radiopharmaceuticals with differing core structures [115, 117]. Many of these core structures are still in use today as the basis for diagnostic ^{99m}Tc radiopharmaceuticals [109, 115, 118].

Throughout the years various strategies have been employed for receptor-based ^{99m}Tc radiopharmaceuticals targeting both intra- and extra-cellular receptors, also known as technetium-tagged receptor targeting radiopharmaceuticals. As the basis of these compounds, technetium is conjugated to a receptor-targeting moiety for site specific localized targeting. Design strategies for these compounds fall into three categories: the integrated approach, the bifunctional approach, and the peptide-hybrid approach [109, 115, 118]. The integrated approach for receptor-based ^{99m}Tc radiopharmaceuticals integrates or replaces part of a known receptor-binding ligand with the ^{99m}Tc chelate (**Fig. 1.4**) [115, 118]. In this approach the ^{99m}Tc metal chelate becomes

a pivotal component of the receptor-binding ligand and all parts are arranged in such a way that the whole metal complex becomes a high affinity receptor ligand. This approach often results in challenging synthetic synthesis of target molecules with low receptor binding affinity. Therefore, it is crucial to comprehensively consider the effects of the ^{99m}Tc chelator on a ligand's size, charge, conformation, and lipophilicity during the structural design [118].

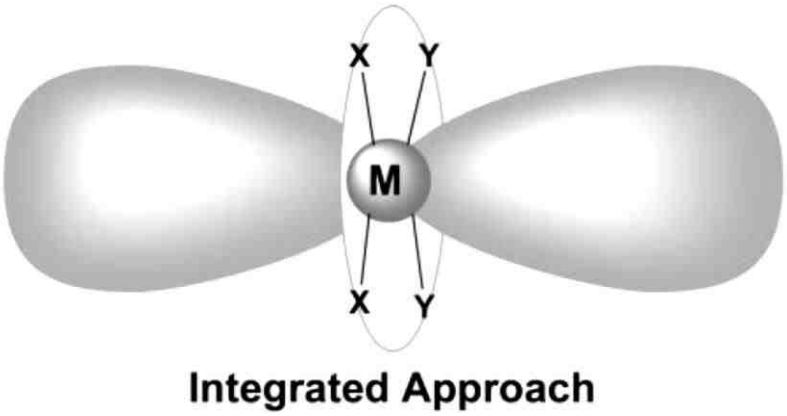

Fig. 1.4- Schematic representation of the integrated design strategy of receptor targeted radiopharmaceuticals. M=^{99m}Tc, X &Y= donor atoms. (Cited from Liu, 2004).

The second design strategy is the bifunctional approach. In this approach, a receptor-binding ligand is used as the targeting biomolecule, a bifunctional coupling agent (BFCA) is used for ^{99m}Tc chelation, and a chemical linker is used to covalently attach the two components (**Fig. 1.5**) [118]. This design is a more popular approach for target-specific radiopharmaceutical development due to the likelihood of retaining high receptor binding affinity with the targeted tissue. The receptor-targeting biomolecule in this design serves as a vehicle to carry the radionuclide to the targeted disease tissue, which should be

known to harbor a substantial concentration of the target receptor. In this design, the biomolecule can be monoclonal antibodies, small peptides, or other non-peptide small molecule receptor ligands. The high specificity of receptor binding to the biomolecule is essential and will result in selective uptake and distribution of the radiolabeled receptor ligand in the disease tissue. Many biomolecules including antibody fragments and small peptides have been studied as “carriers” for radionuclides and have been FDA approved for both diagnostic and therapeutic treatment of disease. Examples of FDA approved target-specific radiopharmaceuticals include Octreoscan® (^{111}In-pentetreotide) for imaging of neuroendocrine tumors and Zevalin® (^{90}Y-Ibitumomab tiuxetan) for treatment of non-Hodgkin’s lymphoma [118].

Different chemical linkers can be used to modify the binding affinity and pharmacokinetic properties of the radiolabeled biomolecule as well as structurally keep the radiometal chelate far enough away from the biomolecule to limit any possible interference it may have with the receptor binding motif of the biomolecule. The choice of linker depends on the pharmacokinetic requirements for the radiopharmaceutical. The linker can range from a simple hydrocarbon chain to increase lipophilicity, to a poly amino acid sequence to increase hydrophilicity to facilitate renal clearance, to a long polyethylene glycol (PEG) molecule to slow extraction by hepatocytes.[115, 118, 119].

The requirements for an ideal BFCA are the selective stability of an intermediate or lower oxidation state of technetium to minimize the redox reactions pertaining to the ^{99m}Tc complex, formation of a complex with the

minimum number of isomers possible, ease of attachment to the biomolecule, and high radiolabeling efficiency [115, 118, 119]. Attachment of the BFCA to the biomolecule in these complexes is performed by a reactive conjugation group. These reactive groups can be either intrinsic to the peptide (e.g. an amino group from lysine, phenol moiety from tyrosine, thiol group from cysteine, or carboxylate group from aspartic or glutamic acid) or can be chemically introduced into a peptide. The attachment of the BFCA/ radiometal complex occurs through the following reactive groups: N-Hydroxysuccinimide (NHS) esters, isothiocyanates, or maleimide moieties (**Fig 1.6**) [113]. The NHS-esters can attach to a lysine amine or linker amino group through an amide bond and is very stable under physiological conditions. Hence, the NHS-esters are the most widely used and powerful conjugation groups. The isothiocyanates are amine reactive groups as well and can form thiourea bonds with primary amino acid amines. The maleimide moiety is a thiol-reactive group that can selectively react with a thiol from a peptide to form a thioether bond [115].

Fig. 1.5- Schematic representation of the bifunctional design strategy of receptor targeted radiopharmaceuticals. (Cited from Liu, 2004).

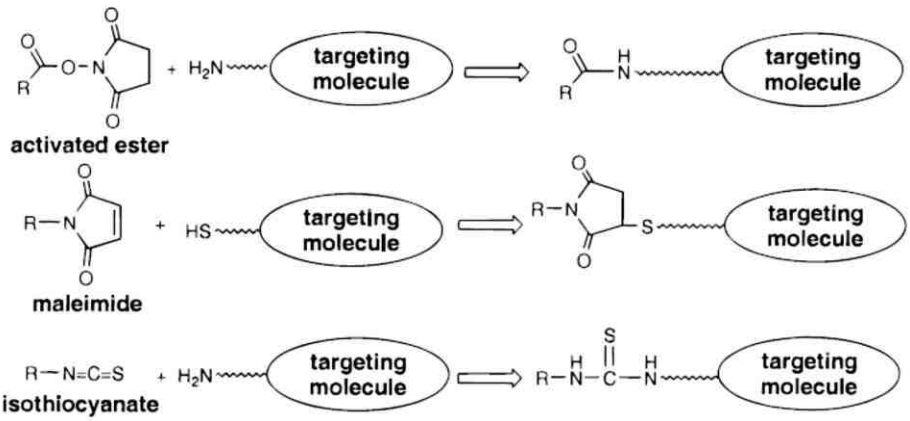

Fig. 1.6- Representative conjugation groups capable of attaching the BFCA to the targeting biomolecule. (Cited from Liu, 1999).

The third radiopharmaceutical design strategy is the peptide-hybrid approach. In this approach, the ^{99m}Tc is chelated and conjugated by a tripeptide sequence (such as Gly-Gly-Gly, Cys-Gly-Gly, Cys-Gly-Cys, or Cys-Cys-Cys) within the targeting peptide which contain a N_4, N_3S, N_2S_2, or NS_3 donor set respectively. The radiometal can be conjugated to either a linear polypeptide or cyclic peptide backbone, incorporating it as a component of the macrocyclic peptide framework (**Fig. 1.7**) [117]. Coordination of the radiometal to a linear peptide increases receptor binding affinity by creating a constrained macrocyclic metallopeptide with less conformational freedom to its intended receptor [118, 120]. The site-specific metal cyclization can also improve the stability of the radiolabeled peptide *in-vivo* [99, 101].

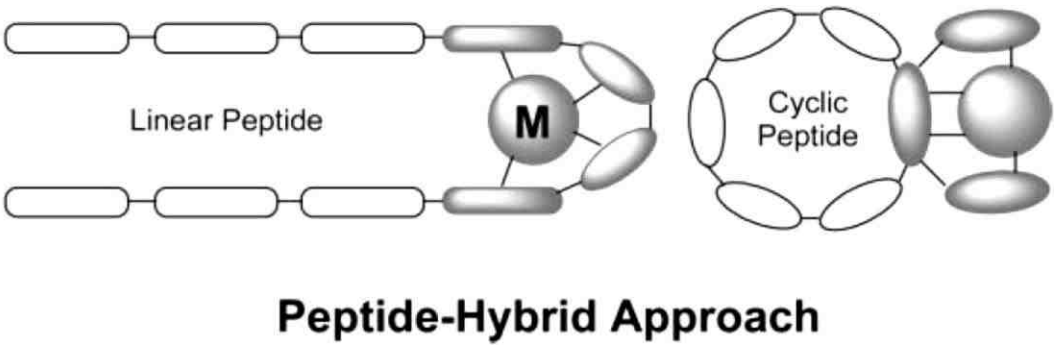

Fig. 1.7- Schematic representation of the peptide-hybrid design strategy of receptor targeted radiopharmaceuticals. M= ^{99m}Tc. (Cited from Liu, 2004).

In addition to ^{99m}Tc-radiolabeling design on these pharmaceuticals, it is also important to consider the pharmacokinetics of each compound. The pharmacokinetic considerations to include are absorption, distribution, metabolism, and excretion. The main goal of any diagnostic radiopharmaceutical is to acquire the highest target-to-background ratio possible in the shortest amount of time. In optimizing this ratio, the patient will receive the least amount of non-target radiation, as the radioactivity will be quickly excreted from the body through the urinary system. When applied systematically and in most cases intravenously, radiopharmaceutical blood residence time should be short enough to quickly release the diagnostic agent into the target tissue, but long enough to adequately accumulate in target tissue as well. For receptor-targeting radiopharmaceuticals, the receptor binding affinity should be extremely high, binding rate should be fast, and the radiopharmaceutical should have adequate cellular retention to eliminate the potential of non-targeted radiation doses to healthy tissue, as well as achieving optimal imaging characteristics in the targeted tissue [118, 119].

Radiolabeling approaches of technetium

^{99m}Tc-radiolabeling techniques have advanced throughout the years, and labeling approaches depend on the type of biomolecules being used (e.g. antibodies or small peptides) and the purpose of the study being conducted (e.g. product development or proof of concept). Many techniques have been established for ^{99m}Tc-radiolabeling of biomolecules such as antibodies, small peptides, and other non-peptide small molecules. These radiolabeling approaches usually fall into three main categories: the pre-labeling approach, the post-labeling (or indirect labeling) approach, and the direct labeling approach.

The pre-labeling approach (also referred to as the pre-formed chelate approach) involves the chelation of ^{99m}Tc with the BFCA, activation of the BFCA, and conjugation of the ^{99m}Tc-BFCA complex to the biomolecule in a separate step (**Fig. 1.8**) [109, 119]. This approach has been more extensively researched and the chemistry involved is better defined than that of the direct labeling approach. One advantage of this approach is that the peptide or protein being labeled is not exposed to the harsh environment that is sometimes necessary for the chelation step (e.g. pH extremes or high temperatures). For research purposes this labeling approach is very useful for developing proof of concept studies, but the complex and time consuming radiosynthesis process is not suitable for routine clinical use or kit formulation. This approach has been successfully used to ^{99m}Tc-radiolabel antibodies and small peptides in a variety of studies including the use in cyclic platelet glycoprotein GPIIb/IIIa receptor antagonists coordinated with HYNIC [109, 115, 119, 121].

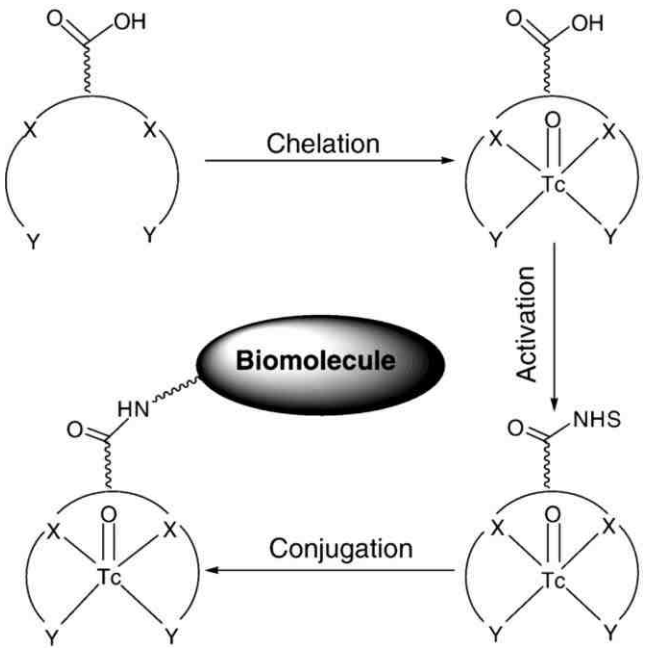

Fig. 1.8- Schematic of the ^{99m}Tc pre-labeling approach. X & Y= donor atoms. (Cited from Liu, 2008).

The post-labeling approach (also known as the indirect labeling approach) involves attachment of the BFCA to the biomolecule, forming a BFCA-biomolecule conjugate. In this instance the BFCA can be attached to either the C- or N-terminus of the peptide or protein, as well as to an amino acid side chain, or directly incorporated into the peptide backbone utilizing multi-step organic synthesis. Once the BFCA-biomolecule conjugate is prepared, radiolabeling with ^{99m}Tc can be accomplished through multiple mechanisms including direct reduction of $^{99m}TcO_4^-$ in the presence of the BFCA-biomolecule conjugate, ligand exchange with an intermediate ^{99m}Tc complex, or a reduction-substitution reaction (**Fig. 1.9**) [119]. This labeling approach utilizes the ease of direct radiolabeling and well-defined chemistry of the pre-labeling approach, making it

the most practical approach for development of target-specific radiopharmaceuticals [109, 115, 119].

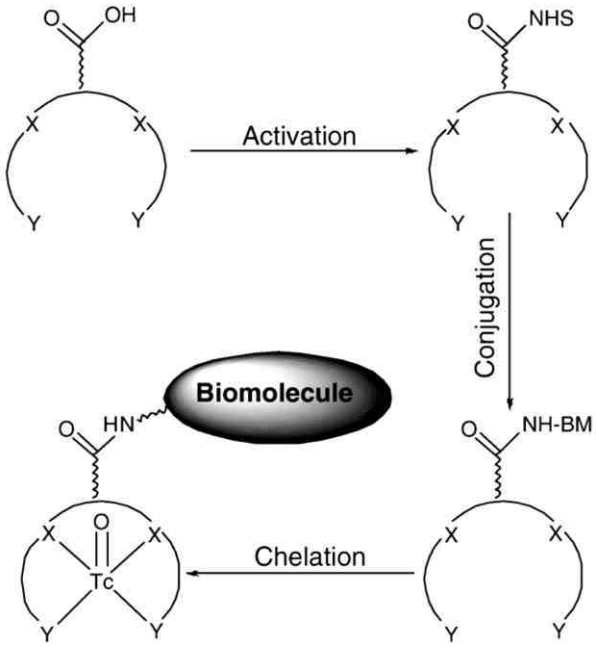

Fig. 1.9- Schematic of the ^{99m}Tc post-labeling (indirect labeling) approach. X & Y= donor atoms. (Cited from Liu, 2008).

^{99m}Tc radiolabeling of the BFCA-biomolecule complex through the direct reduction approach involves directly reducing $^{99m}TcO_4^-$ pertechnetate in one step by a variety of reducing agents ($SnCl_2$, $NaBH_4$, $Na_2S_2O_4$, H_3PO_4, NH_2NH_2, ascorbic acid, and HCl, among many others), in the presence of adequate BFCA-peptide conjugate. This reaction generally produces mixed ^{99m}Tc reduction species, but can be controlled and prepared into a single ^{99m}Tc-BFCA-biomolecule species through the use of a particular reducing agent and BFCA under well-controlled labeling conditions. The most commonly used reducing agent is $SnCl_2$ for its rapid reduction kinetics. The use of Sn(II) however can lead to production of the Tc (VI) intermediate ($^{99m}TcO_4^{2-}$) and Tc [122] intermediate (

$^{99m}TcO_2$); both of which form unstable complexes capable of undergoing hydrolysis and compromising the radiolabeling yield of the ^{99m}Tc-BFCA-biomolecule complex [109, 115, 119].

Another way of ^{99m}Tc radiolabeling the BFCA-biomolecule complex is through a two-step ligand exchange. In this process, the pertechnetate ion is reduced by a reducing agent in the presence of a weak chelating agent to form a ^{99m}Tc-chelate intermediate. This intermediate is then allowed to react with the BFCA-biomolecule complex under milder conditions to form the final desired ^{99m}Tc-BFCA-biomolecule complex. This route is often used to limit the exposure of the BFCA-biomolecule conjugate to the sometimes harsh radiolabeling conditions. One example of a ligand exchange process is the use of glucoheptonate (GH) as a weak chelating agent to aid in radiolabeling the α-MSH peptide with ^{99m}Tc. In this process, a reducing agent such as $SnCl_2$ is used to reduce the pertechnetate ion to the Tc(V) state containing the $[^{99m}TcO]^{3+}$ core in the presence of the glucoheptonate. Once reduced, the glucoheptonate chelates and stabilizes the $[^{99m}TcO]^{3+}$ core and protects from redox reactions with the aqueous environment. Once stabilized, the BFCA-biomolecule conjugate (α-MSH in this case) is allowed to react and conjugate with $[^{99m}TcO]^{3+}$ to form the final radiolabeled product of ^{99m}Tc-(Arg^{11})CCMSH (**Fig. 1.10**) [115, 119, 123-125].

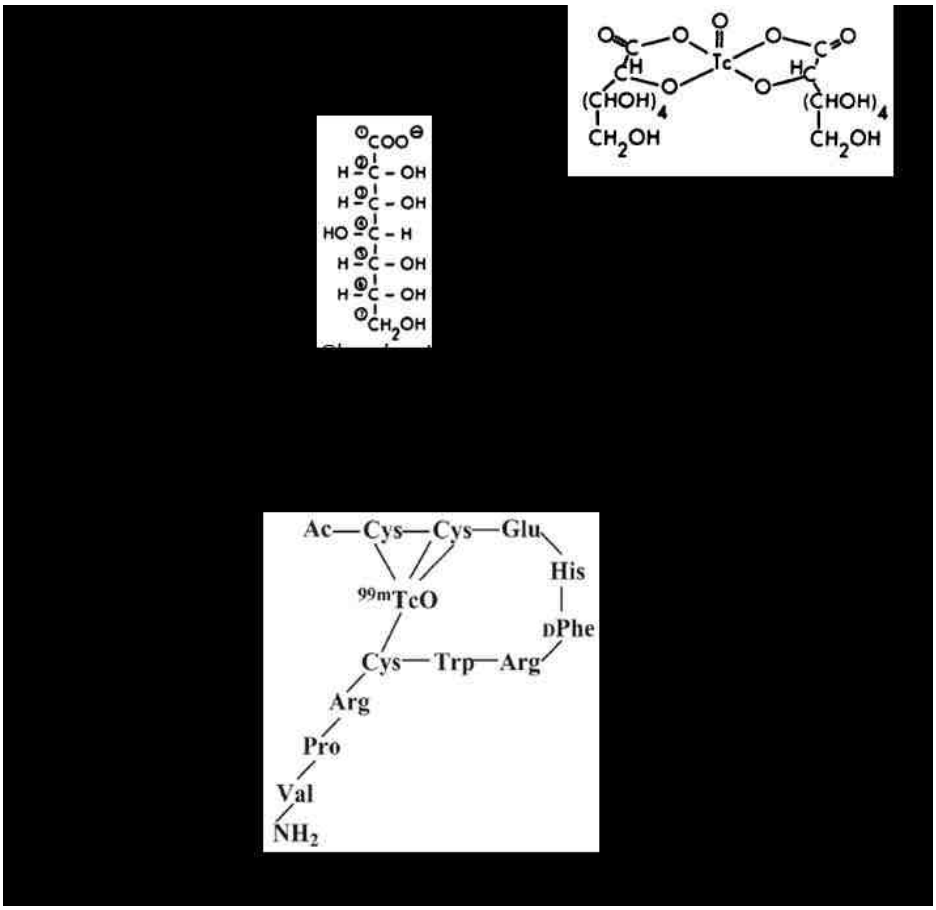

Fig. 1.10- Schematic representation of ligand-exchange radiolabeling with glucoheptonate of ^{99m}Tc-(Arg^{11})CCMSH. (Adapted from Miao, 2007 and de Kieviet, 1981).

The direct labeling approach uses a reducing agent to convert disulfide linkages into free thiols, which are then able to strongly bind technetium (**Fig. 1.11**). Many reducing agents can be used (e.g. $NaBH_4$, $Na_2S_2O_4$, H_3PO_4, NH_2NH_2, ascorbic acid, and HCl, among many others) but stannous chloride ($SnCl_2$) is the most commonly used. $SnCl_2$ is used to break the disulfide linkage as well as reduce the $^{99m}TcO_4^-$, Tc(VII), to a lower oxidation state such as Tc(V) [110]. This approach applies mainly to antibodies and antibody fragments as many small peptides do not have disulfide linkages, or if one exists, the linkage

may be critical for maintaining biological properties and therefore should not be reduced. For this approach however there are some critical questions that must be addressed: the desired oxidation state of ^{99m}Tc, the number of ^{99m}Tc conjugations to the biomolecule, purity of the desired ^{99m}Tc-labeled species, and impact on the targeting molecules biological activity after ^{99m}Tc-radiolabeling. Examples of direct ^{99m}Tc-radiolabeling can be seen with many ^{99m}Tc-labeled monoclonal antibodies including those to aid in detection of colorectal and ovarian cancer.

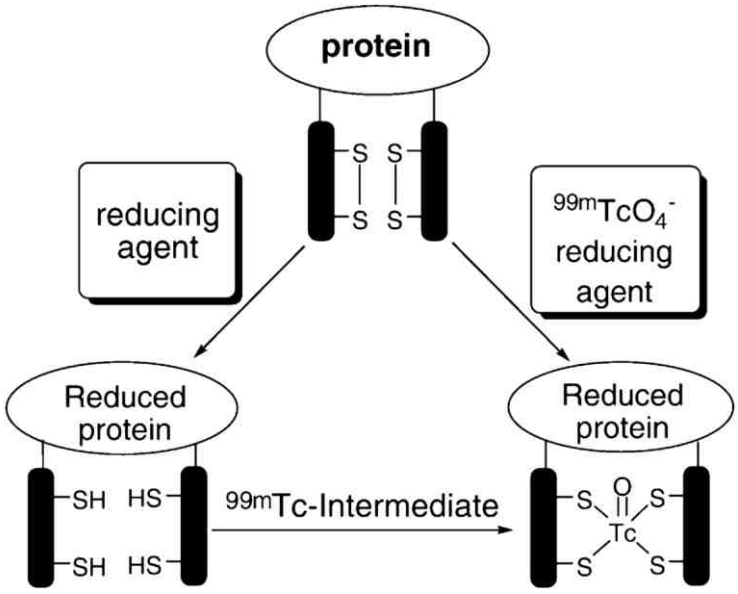

Fig. 1.11- Schematic of the ^{99m}Tc direct labeling approach. (Cited from Liu, 2008).

Recently, our lab has developed a unique one-step radiolabeling procedure utilized for ^{99m}Tc-radiolabeling of hybrid peptides. These hybrid peptides coordinate the technetium into the cyclic backbone of the peptide via three cysteine amino acid additions. The sulfhydryl side chains of the cysteine residues strongly conjugate to the ^{99m}Tc(V)O core, stabilizing the technetium

within the cyclic peptide backbone via an NS_3 coordination system. Radiolabeling of the peptide is performed through direct reduction of $^{99m}TcO_4^-$ with $SnCl_2$. Since the sulfhydryl side chains on the cysteine residues are already fully reduced, the $^{99m}Tc(V)$ core, $[TcO]^{3+}$, is allowed to covalently conjugate directly to those residues without the need for attachment to a BFCA. Meanwhile, the hybrid peptide can be simultaneously cyclized during the radiolabeling of ^{99m}Tc, allowing for diminished conformational freedom of the peptide secondary structure and reduced *in-vivo* proteolytic degradation. The cyclization process increases *in-vivo* stability as well as binding affinity of the peptide for its targeted receptor. Radiolabeling synthesis is performed by incubation of the peptide, sodium pertechnetate, $SnCl_2$, and buffer solutions (NH_4OAc/ Na_2 tartate•$2H_2O$) for twenty minutes at room temperature. Upon radiolabeling synthesis, collection of a single species of ^{99m}Tc-labeled peptide can be performed through RP-HPLC (**Fig 1.12**). This labeling approach is well suited for use in clinical applications as it can be performed in a single step at room temperature.

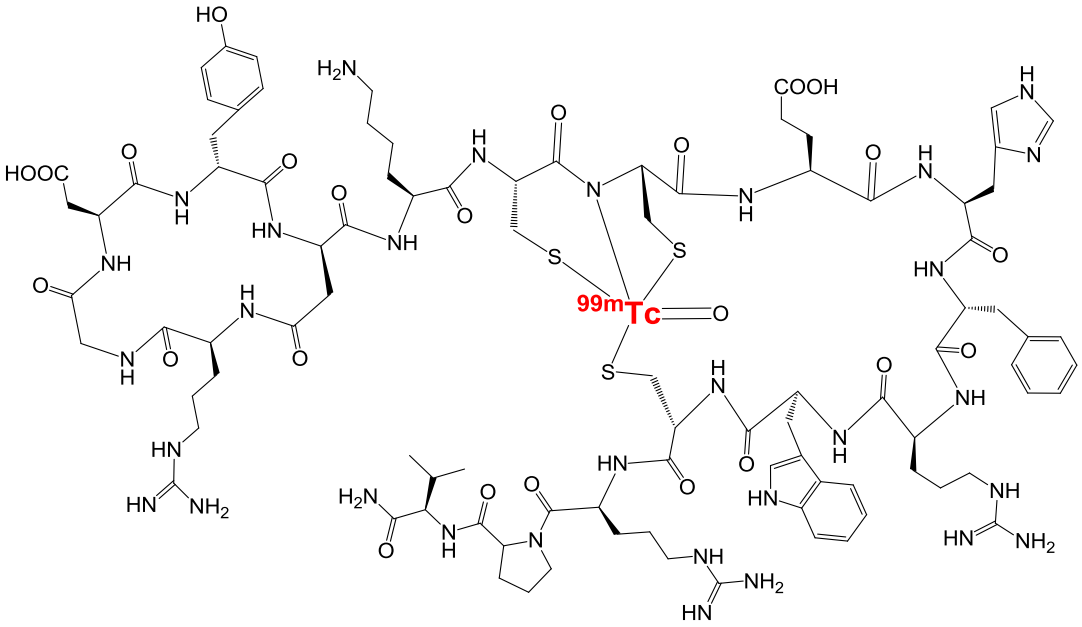

Fig. 1.12- Structure of ^{99m}Tc-RGD-Lys-(Arg^{11})CCMSH peptide after direct reduction radiolabeling synthesis. (Adapted from Yang, 2010).

^{99m}Tc-Labeled α-MSH analogs

Throughout the past two decades, novel ^{99m}Tc-labeled α-MSH peptide analogs have been employed for development of diagnostic or therapeutic targeting molecules for metastatic melanoma with varying success. One of the first attempts at utilizing ^{99m}Tc-labeled α-MSH peptide analogs was the development of ^{99m}Tc-CGCG-NDP, which employed a tetrapeptide chelator of Cys-Gly-Cys-Gly on the amino terminus of the synthetic α-MSH analog NDP-MSH. ^{99m}Tc-CGCG-NDP showed moderate melanoma uptake in B16/F1 melanoma bearing C57 mice with a peak tumor uptake at 30 minutes post-injection of 6.52 ± 1.11 %ID/g [97, 120]. A novel α-MSH peptide analog, [Cys^{3,4,10},$_{D}$-Phe^{7}]α-MSH$_{3-13}$ (CCMSH), was created utilizing the peptide-hybrid

approach of chelation within the backbone of the α-MSH peptide via addition of three cysteine residues at amino acid positions 3, 4, and 10 [97, 98]. The metal cyclized portion of the peptide contained the potent α-MSH pharmacophore consensus sequence. ^{99m}Tc-CCMSH exhibited rapid and high tumor uptake as well as fast whole-body clearance in B16/F1 melanoma bearing mice. The peak tumor uptake was seen at 30 min post-inject with an uptake value of 12.97 ± 2.38 %ID/g [126]. In an effort to decrease non-specific renal uptake of the ^{99m}Tc-CCMSH peptide, a substitution to the Lys^{11} for Arg^{11} was made to establish the novel peptide analog (Arg^{11})CCMSH. ^{99m}Tc-(Arg^{11})CCMSH exhibited a peak tumor uptake value of 14.03 ± 2.58 %ID/g at 1 h post-injection while demonstrating a 62% reduction in non-specific renal uptake at 4 h post-injection [97, 125, 126].

Newer generations of ^{99m}Tc-labeled α-MSH peptides generated in our lab emerged as dual receptor targeting molecules. Arg-Gly-Asp-conjugated α-MSH hybrid peptides were developed to target both the MC1R and the $\alpha_V\beta_3$ integrin present on melanoma cells. The cyclized Arg-Gly-Asp (RGD) $\alpha_V\beta_3$ integrin binding motif was attached to the hybrid α-MSH peptide containing the MC1R pharmacophore binding sequence via a Lys amino acid linker, forming a novel RGD-Lys-(Arg^{11})CCMSH hybrid peptide [127]. It was hypothesized that targeting of both the MC1R and $\alpha_V\beta_3$ integrin would provide for superior melanoma targeting as compared to MC1R targeting alone. As a control, the cyclic RGD motif was also substituted into a cyclic RAD motif in order to ablate $\alpha_V\beta_3$ binding, producing the RAD-Lys-(Arg^{11})CCMSH peptide. Receptor binding studies with

both peptides in human M21 melanoma cells demonstrated that indeed substitution of the Gly residue in the RGD motif for an Ala residue ablated $\alpha_V\beta_3$ integrin binding, with IC_{50} values of 403 nM for RGD-Lys-(Arg^{11})CCMSH compared with greater than 100,000 nM for RAD-Lys-(Arg^{11})CCMSH.

Surprisingly, MC1R binding affinity of the RAD-Lys-(Arg^{11})CCMSH peptide was nearly 10-fold higher than the original RGD-Lys-(Arg^{11})CCMSH M21 human melanoma cells, with IC_{50} values of 0.3 nM and 2.0 nM, respectively [127]. This elevated MC1 receptor binding affinity resulted in enhanced melanoma tumor uptake of ^{99m}Tc-RAD-Lys-(Arg^{11})CCMSH as compared with ^{99m}Tc-RGD-Lys-(Arg^{11})CCMSH (19.91± 4.02 vs 14.83 ± 2.93% ID/g at 2 h post-injection) in B16/F1 melanoma-bearing C57 mice as well [128]. The minor structural difference of the addition of one extra methyl group on the Ala residue as compared to the Gly residue, indicated that the existence of the methyl group enhanced the *in-vivo* melanoma tumor uptake of ^{99m}Tc-RAD-Lys-(Arg^{11})CCMSH. Therefore, it was of interest to determine how other minor structural differences to the ^{99m}Tc-RAD-Lys-(Arg^{11})CCMSH peptide could further enhance the MC1R binding affinity and *in-vivo* tumor targeting and pharmacokinetics, as well as determine the optimal structure for use as a melanoma SPECT imaging probe.

Purpose, hypothesis, and specific aims

Currently, no curative treatment options exist for metastatic melanoma. A patient's best opportunity for a cure is early detection of melanocytic lesions and prompt surgical removal of cancerous tissues [3, 6, 27]. The development of novel targeting radiopharmaceuticals capable of both early detection and imaging of primary melanoma lesions and metastases represents a potential innovative tool suited for a patient's best chance at survival. At present, the work being conducted in the development of novel radiolabeled α-MSH peptide analogs is still in the pre-clinical stage. Proper optimization and characterization of the newest generations of these peptides is of importance to ascertain the most promising compounds capable of utilization in a clinical setting.

The research emphasis for this project entails combining the knowledge from different biomedical sciences in the fields of oncology, cellular and molecular biology, chemistry, and radiopharmacology to develop, optimize, and characterize novel radiolabeled α-MSH peptide analogs for targeting and radioimaging of melanoma lesions. The development of which can potentially aide clinicians in determining the location and size of both primary melanoma lesions and their metastatic counterparts for prompt surgical removal and monitoring the growth and spread of disease over the periods of progression, remission, and recurrence.

With the promising results seen by the modification of α-MSH analogs in respect to increased MC1 receptor binding affinity and increased *in-vivo*

melanoma targeting and uptake in B16/F1 melanoma-bearing C57 mice, it was the purpose of this study to determine the optimal α-MSH peptide structure necessary for development of an ideal melanoma targeting probe suitable for diagnostic imaging.

Central Hypothesis

Our central hypothesis states that structural modifications of novel α-MSH peptides targeting the melanocortin-1 receptor will enhance melanoma targeting and pharmacokinetic properties of ^{99m}Tc-labeled α-MSH peptide analogs for SPECT radioimaging and may provide a distinct non-invasive tool for early detection and diagnosis of melanocytic disease, both primary and disseminated.

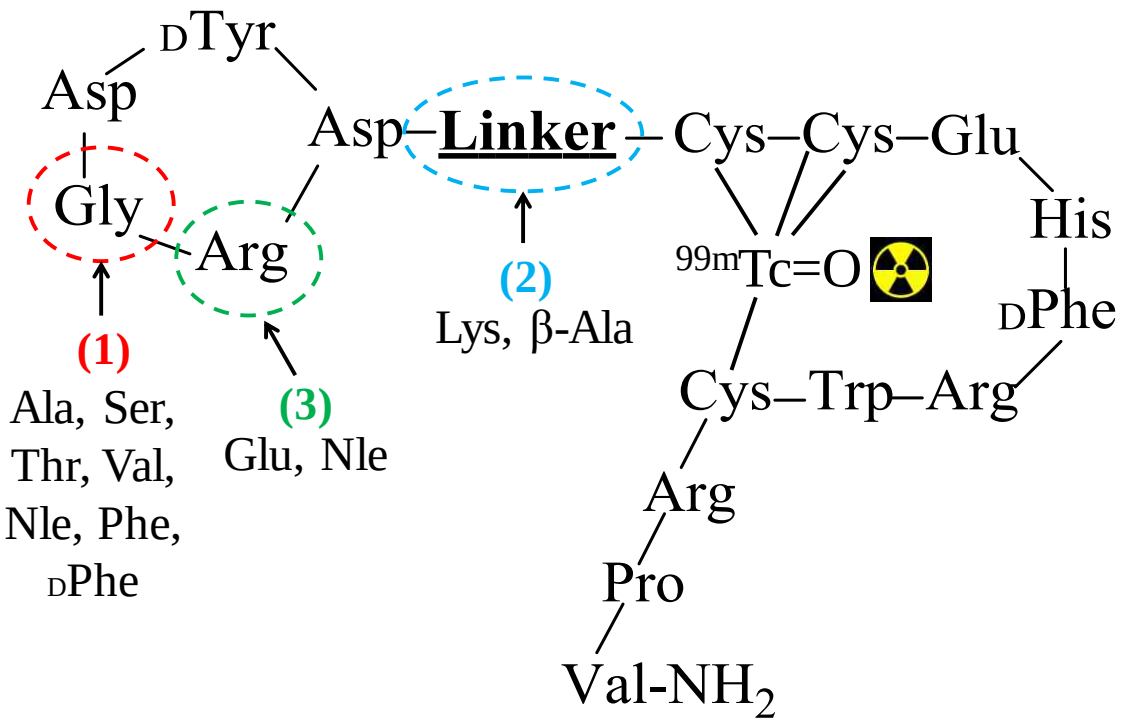

Figure 1.13- Schematic representation of the modifications made to the novel α-MSH peptides in the RXD motif (1), linker (2), and XAD motif (3).

Specific aims

I will attempt to examine our central hypothesis through the following specific aims:

1. To determine the effect of single amino acid substitutions to the RXD motif on the targeting and biodistribution properties of RXD-Lys-(Arg^{11})CCMSH peptides.

In order to evaluate specific aim #1, α-MSH peptides will be designed and synthesized containing amino acid substitutions to the Ala residue on the RXD motif. The *in-vitro* MC1 receptor targeting properties of the RXD-Lys-(Arg^{11})CCMSH peptides will be determined in the B16/F1 murine melanoma cell line. The *in-vivo* melanoma targeting and pharmacokinetic properties of the ^{99m}Tc-RXD-Lys-(Arg^{11})CCMSH peptides will be evaluated in B16/F1 melanoma-bearing C57 mice.

2. To reduce *in-vivo* non-specific renal uptake of α-MSH peptide analogs via L-Lys co-injection and linker modification through substitution of the positively charged Lys linker with a neutral β-Ala linker, without disrupting melanoma tumor uptake.

In order to evaluate specific aim #2, as a proof of concept study, reduction of *in-vivo* non-specific renal uptake of the ^{99m}Tc-RXD-Lys-(Arg^{11})CCMSH peptides will be determined with the use of a purified L-Lys co-injection. Based

on the results of the L-Lys co-injection study, α-MSH peptides will then be designed and synthesized containing an amino acid substitution of the positively charged Lys linker with a neutral β-Ala linker. The *in-vitro* MC1 receptor targeting properties of the RXD-β-Ala-(Arg^{11})CCMSH peptides will be determined in the B16/F1 murine melanoma cell line. The *in-vivo* reduction of renal radiopharmaceutical uptake and pharmacokinetic properties of the ^{99m}Tc-RXD-β-Ala-(Arg^{11})CCMSH peptides will be evaluated in B16/F1 melanoma-bearing C57 mice.

3. To further reduce *in-vivo* non-specific renal uptake of α-MSH peptides by amino acid substitutions to XAD motif on XAD-β-Ala-(Arg^{11})CCMSH peptides, without disrupting melanoma tumor uptake.

In order to evaluate specific aim #3, α-MSH peptides will be designed and synthesized containing amino acid substitutions to reduce the overall net charge of the peptides by replacing the Arg residue in the RXD motif, creating the XAD-β-Ala-(Arg^{11})CCMSH peptides. The *in-vitro* MC1 receptor targeting properties of the XAD-β-Ala-(Arg^{11})CCMSH peptides will be determined in the B16/F1 murine melanoma cell line. The further *in-vivo* reduction of renal radiopharmaceutical uptake and pharmacokinetic properties of the ^{99m}Tc-XAD-β-Ala-(Arg^{11})CCMSH peptides will be evaluated in B16/F1 melanoma-bearing C57 mice.

Chapter 2

Evaluation of new Tc-99m-labeled Arg-X-Asp-conjugated α-melanocyte stimulating hormone peptides for melanoma imaging

Introduction

Malignant melanoma is the most lethal form of skin cancer with an increasing incidence [3]. Melanoma leads to greater than 75% of deaths from skin cancer although it only accounts for less than 5% of skin cancer cases. There is no curative treatment available for metastatic melanoma. Both melanocortin-1 (MC1) and $\alpha_v\beta_3$ integrin receptors have been utilized as targets for developing melanoma imaging probes [91, 100, 103, 105, 129-145]. The radiolabeled α-melanocyte stimulating hormone (α-MSH) peptides were used to target the MC1 receptors [91, 100, 103, 105, 129-137], whereas the radiolabeled Arg-Gly-Asp (RGD) peptides were reported to target the $\alpha_v\beta_3$ integrin receptors [138-145]. In our previous report, we developed a novel Arg-Gly-Asp (RGD)-conjugated α-MSH hybrid peptide {RGD-Lys-(Arg^{11})CCMSH} to target both MC1 and $\alpha_v\beta_3$ integrin receptors for M21 human melanoma imaging [127]. The dual receptor-targeting ^{99m}Tc-RGD-Lys-(Arg^{11})CCMSH exhibited significantly higher melanoma uptake than single receptor-targeting ^{99m}Tc-RAD-Lys-(Arg^{11})CCMSH or ^{99m}Tc-RGD-Lys-(Arg^{11})CCMSH$_{scramble}$ in M21 human melanoma-xenografted nude mice. Interestingly, the switch from RGD to Arg-Ala-Asp (RAD) in the hybrid peptide dramatically improved the MC1 receptor binding affinity of RAD-Lys-(Arg^{11})CCMSH as compared to RGD-Lys-(Arg^{11})CCMSH (0.3 vs. 2.0 nM) in M21

melanoma cells [127]. The stronger MC1 receptor binding resulted in enhanced melanoma uptake of ^{99m}Tc-RAD-Lys-(Arg^{11})CCMSH as compared with ^{99m}Tc-RGD-Lys-(Arg^{11})CCMSH (19.91 ± 4.02 vs. 14.83 ± 2.93% ID/g at 2 h post-injection) in B16/F1 melanoma-bearing C57 mice [128].

The minor structural difference between ^{99m}Tc-RAD-Lys-(Arg^{11})CCMSH and ^{99m}Tc-RGD-Lys-(Arg^{11})CCMSH is Ala and Gly. The Ala has one more methyl group as compared with the Gly. The biodistribution results indicated that the existence of methyl group in Ala enhanced the melanoma uptake of ^{99m}Tc-RAD-Lys-(Arg^{11})CCMSH [128]. Therefore, we were interested in whether the substitution of Gly with other amino acids could affect the melanoma targeting and pharmacokinetic properties of ^{99m}Tc-labeled peptides. In this study, we replaced the Gly with Thr and Val to generate RTD-Lys-(Arg^{11})CCMSH and RVD-Lys-(Arg^{11})CCMSH peptides. The MC1 receptor binding affinities of RTD-Lys-(Arg^{11})CCMSH and RVD-Lys-(Arg^{11})CCMSH were examined in B16/F1 melanoma cells. Thereafter, we determined the biodistribution and imaging properties of ^{99m}Tc-RTD-Lys-(Arg^{11})CCMSH and ^{99m}Tc-RVD-Lys-(Arg^{11})CCMSH in B16/F1 melanoma-bearing C57 mice.

Experimental design and methods

Chemicals and Reagents

Amino acids and resin were purchased from Advanced ChemTech Inc. (Louisville, KY) and Novabiochem (San Diego, CA). ^{125}I-Tyr^{2}-[Nle^{4}, DPhe^{7}]-α-MSH {^{125}I-(Tyr^{2})-NDP-MSH} was obtained from PerkinElmer, Inc. (Waltham, MA) for receptor binding assay. $^{99m}TcO_4^-$ was purchased from Cardinal Health (Albuquerque, NM). *L*-lysine was purchased from Sigma-Aldrich (St. Louis, MO). All other chemicals used in this study were purchased from Thermo Fischer Scientific (Waltham, MA) and used without further purification. B16/F1 murine melanoma cells were obtained from American Type Culture Collection (Manassas, VA).

Peptide Synthesis and In Vitro Competitive Binding Assay

The RTD-Lys-(Arg^{11})CCMSH and RVD-Lys-(Arg^{11})CCMSH peptides were synthesized according to our previously published procedure [146] with slight modification on Sieber amide resin by an Advanced ChemTech multiple-peptide synthesizer (Louisville, KY). Briefly, 70 µmol of Sieber amide resin and 210 µmol of Fmoc-protected amino acids were used for the synthesis. Fmoc-Lys(Boc) was used to generate a Lys linker in the hybrid peptide. The RTD-Lys-(Arg^{11})CCMSH and RVD-Lys-(Arg^{11})CCMSH were purified by reverse phase-high performance

liquid chromatography (RP-HPLC) and characterized by liquid chromatography-mass spectroscopy (LC-MS).

The IC_{50} values RTD-Lys-(Arg^{11})CCMSH and RVD-Lys-(Arg^{11})CCMSH for the MC1 receptor were determined in B16/F1 melanoma cells. The receptor binding assay was replicated in triplicate for each peptide. The B16/F1 cells were seeded into a 24-well cell culture plate at a density of 2.5×10^5 cells/well and incubated at 37° C overnight. After being washed with binding medium {modified Eagle's medium with 25 mM N-(2-hydroxyethyl)-piperazine-N′-(2-ethanesulfonic acid) (HEPES), pH 7.4, 0.2% bovine serum albumin (BSA), 0.3 mM 1,10-phenathroline}, the cells were incubated at 25 °C for 2 h with approximately 30,000 counts per minute (cpm) of ^{125}I-(Tyr^2)-NDP-MSH in the presence of increasing concentrations (10^{-13} M to 10^{-6} M) of RTD-Lys-(Arg^{11})CCMSH or RVD-Lys-(Arg^{11})CCMSH in 0.3 mL of binding medium. The reaction medium was aspirated after the incubation. The cells were rinsed twice with 0.5 mL of ice-cold pH 7.4, 0.2% BSA/0.01 M phosphate buffered saline (PBS) to remove any unbound radioactivity and lysed in 0.5 mL of 1 M NaOH for 5 min. The activities associated with the cells were measured in a Wallac 1480 automated gamma counter (PerkinElmer, NJ). The IC_{50} value for each peptide was calculated using Prism software (GraphPad Software, La Jolla, CA).

Peptide Radiolabeling

RTD-Lys-(Arg^{11})CCMSH and RVD-Lys-(Arg^{11})CCMSH peptides were labeled with ^{99m}Tc via a direct reduction reaction with $SnCl_2$. Briefly, 10 µL of 1 mg/mL $SnCl_2$ in 0.1 M HCl, 40 µL of 0.5 M NH_4OAc (pH 5.2), 100 µL of 0.2 M Na_2tartate (pH 9.2), 100 µL of fresh $^{99m}TcO_4^-$ solution (37-74 MBq), and 10 µL of 1 mg/mL RTD-Lys-(Arg^{11})CCMSH or RVD-Lys-(Arg^{11})CCMSH peptide in aqueous solution were added into a reaction vial and incubated at 25 °C for 20 min to form ^{99m}Tc-labeled peptide. Each ^{99m}Tc-peptide was purified to a single species by Waters RP-HPLC (Milford, MA) on a Grace Vydac C-18 reverse phase analytic column (Deerfield, IL) using a 20-min gradient of 16-26% acetonitrile in 20 mM HCl aqueous solution at a flow rate of 1 mL/min. Each purified peptide was purged with N_2 gas for 20 mins to remove the acetonitrile. The pH of final peptide solution was adjusted to 7.4 with 0.1 N NaOH and sterile normal saline for stability, biodistribution and imaging studies. The serum stability of ^{99m}Tc-RTD-Lys-(Arg^{11})CCMSH and ^{99m}Tc-RVD-Lys-(Arg^{11})CCMSH was determined by incubation in mouse serum at 37 °C for 24 h and monitored for degradation by RP-HPLC. Briefly, 100 µL of HPLC-purified peptide solution (~7.4 MBq) was added into 100 µL of mouse serum (Sigma-Aldrich Corp, St. Louis, MO) and incubated at 37 ^oC for 24 h. After the incubation, 200 µL of a mixture of ethanol and acetonitrile (V:V = 1:1) was added to precipitate the serum proteins. The resulting mixture was centrifuged at 16,000 g for 5 min to collect the supernatant. The supernatant was purged with N_2 gas for 30 min to remove the

ethanol and acetonitrile. The resulting sample was mixed with 500 µL of water and injected into RP-HPLC for analysis using the gradient described above.

Cellular Internalization and Efflux

Cellular internalization and efflux of ^{99m}Tc-RTD-Lys-(Arg^{11})CCMSH and ^{99m}Tc-RVD-Lys-(Arg^{11})CCMSH were evaluated in B16/F1 melanoma cells. The B16/F1 cells were seeded into a 24-well cell culture plate at a density of 2.5×10^5 cells/well and incubated at 37° C overnight. After being washed twice with binding medium [modified Eagle's medium with 25 mM *N*-(2-hydroxyethyl)-piperazine-*N'*-(2-ethanesulfonic acid), pH 7.4, 0.2% bovine serum albumin (BSA), 0.3 mM 1,10-phenathroline], the B16/F1 cells were incubated at 25°C for 20, 40, 60, 90 and 120 min (n=3) in the presence of approximate 200,000 counts per minute (cpm) of HPLC-purified of ^{99m}Tc-RTD-Lys-(Arg^{11})CCMSH or ^{99m}Tc-RVD-Lys-(Arg^{11})CCMSH. After incubation, the reaction medium was aspirated and the cells were rinsed with 2 × 0.5 mL of ice-cold pH 7.4, 0.2% BSA / 0.01 M PBS. Cellular internalization was assessed by washing the cells with acidic buffer [40 mM sodium acetate (pH 4.5) containing 0.9% NaCl and 0.2% BSA] to remove the membrane-bound radioactivity. The remaining internalized radioactivity was obtained by lysing the cells with 0.5 mL of 1 N NaOH for 5 min. Membrane-bound and internalized activities were counted in a gamma counter. Cellular efflux was determined by incubating the B16/F1 cells with ^{99m}Tc-RTD-Lys-(Arg^{11})CCMSH or ^{99m}Tc-RVD-Lys-(Arg^{11})CCMSH for 2 h at 25°C, removing non-specific-bound

activity with 2 × 0.5 mL of ice-cold PBS rinse, and monitoring radioactivity released into cell culture medium. At time points of 20, 40, 60, 90 and 120 min, the radioactivities on the cell surface and inside the cells were separately collected and counted in a gamma counter.

Biodistribution Studies

All the animal studies were conducted in compliance with Institutional Animal Care and Use Committee approval. The biodistribution properties of ^{99m}Tc-RTD-Lys-(Arg^{11})CCMSH and ^{99m}Tc-RVD-Lys-(Arg^{11})CCMSH were determined in B16/F1 melanoma-bearing C57 female mice (Harlan, Indianapolis, IN). Each C57 mouse was subcutaneously inoculated on the right flank with 1×10^6 B16/F1 cells. The weight of tumors reached approximately 0.2 g 10 days post cell inoculation. Each melanoma-bearing mouse was injected with 0.037 MBq of ^{99m}Tc-RTD-Lys-(Arg^{11})CCMSH and ^{99m}Tc-RVD-Lys-(Arg^{11})CCMSH via the tail vein. Groups of 4 mice were sacrificed at 0.5, 2, 4 and 24 h post-injection, and tumors and organs of interest were harvested, weighed and counted. Blood values were taken as 6.5% of the body weight. The specificity of tumor uptake was determined by co-injecting ^{99m}Tc-RTD-Lys-(Arg^{11})CCMSH or ^{99m}Tc-RVD-Lys-(Arg^{11})CCMSH with 10 μg (6.1 nmol) of unlabeled NDP-MSH at 2 h post-injection.

L-lysine co-injection is effective in decreasing the renal uptake of radiolabeled α-MSH peptides. To determine the effect of *L*-lysine co-injection on

the renal uptake of ^{99m}Tc-RTD-Lys-(Arg^{11})CCMSH and ^{99m}Tc-RVD-Lys-(Arg^{11})CCMSH, a group of 4 mice were injected with a mixture of 0.037 MBq of ^{99m}Tc-RTD-Lys-(Arg^{11})CCMSH or ^{99m}Tc-RVD-Lys-(Arg^{11})CCMSH and 15 mg of *L*-lysine. The mice were sacrificed at 2 h post-injection, and tumors and organs of interest were harvested, weighed and counted in a gamma counter.

Melanoma Imaging with ^{99m}Tc-RTD-Lys-(Arg^{11})CCMSH and ^{99m}Tc-RVD-Lys-(Arg^{11})CCMSH

To determine the melanoma imaging properties, approximately 7.4 MBq of ^{99m}Tc-RTD-Lys-(Arg^{11})CCMSH or ^{99m}Tc-RVD-Lys-(Arg^{11})CCMSH was injected into two B16/F1 melanoma-bearing C57 mice via the tail vein, respectively. The mice were euthanized for small animal SPECT/CT (Nano-SPECT/CT®, Bioscan, Washington DC) imaging 2 h post-injection. The 9-min CT imaging was immediately followed by the SPECT imaging of whole-body. The SPECT scans of 24 projections were acquired. Reconstructed data from SPECT and CT were visualized and co-registered using InVivoScope (Bioscan, Washington DC).

Urinary Metabolites of ^{99m}Tc-RTD-Lys-(Arg^{11})CCMSH and ^{99m}Tc-RVD-Lys-(Arg^{11})CCMSH

Approximately 3.7 MBq of ^{99m}Tc-RTD-Lys-(Arg^{11})CCMSH or ^{99m}Tc-RVD-Lys-(Arg^{11})CCMSH was injected into two B16/F1 melanoma-bearing C57 mice

via the tail vein to determine the urinary metabolites. The mice were euthanized to collect urine at 2 h post-injection. The collected urine samples were centrifuged at 16,000 g for 5 min before the HPLC analysis. Thereafter, aliquots of the urine were injected into the HPLC. A 20-minute gradient of 16-26% acetonitrile / 20 mM HCl with a flow rate of 1 mL/min was used for urine analysis.

Statistical Analysis

Statistical analysis was performed using the Student's t-test for unpaired data to determine the significance of differences in tumor and kidney uptake with/without peptide blockade or with/without *L*-lysine co-injection in biodistribution studies described above. Differences at the 95% confidence level ($p<0.05$) were considered significant.

Results

The schematic structures of RTD-Lys-(Arg^{11})CCMSH and RVD-Lys-(Arg^{11})CCMSH are presented in **Figure 2.1**. RTD-Lys-(Arg^{11})CCMSH and RVD-Lys-(Arg^{11})CCMSH were synthesized and purified by RP-HPLC. The overall synthetic yields were 30% for RTD-Lys-(Arg^{11})CCMSH and RVD-Lys-(Arg^{11})CCMSH. The chemical purities of RTD-Lys-(Arg^{11})CCMSH and RVD-Lys-(Arg^{11})CCMSH were greater than 95% after the HPLC purification. The peptide identities were confirmed by electrospray mass spectrometry. The measured molecular weights for RTD-Lys-(Arg^{11})CCMSH and RVD-Lys-(Arg^{11})CCMSH were 2194 and 2192. The competitive binding curves of the peptides are shown in **Figure 2.2**. The IC_{50} values of RTD-Lys-(Arg^{11})CCMSH and RVD-Lys-(Arg^{11})CCMSH were 0.7 ± 0.07 and 1.0 ± 0.3 nM in B16/F1 melanoma cells.

RTD-Lys-(Arg^{11})CCMSH and RVD-Lys-(Arg^{11})CCMSH were readily radiolabeled with ^{99m}Tc with greater than 95% radiolabeling yields. The ^{99m}Tc-RTD-Lys-(Arg^{11})CCMSH and ^{99m}Tc-RVD-Lys-(Arg^{11})CCMSH peptides were purified and separated from their excess non-labeled peptides by RP-HPLC. The retention times of ^{99m}Tc-RTD-Lys-(Arg^{11})CCMSH and ^{99m}Tc-RVD-Lys-(Arg^{11})CCMSH were 12.7 and 14.6 min. ^{99m}Tc-RTD-Lys-(Arg^{11})CCMSH and ^{99m}Tc-RVD-Lys-(Arg^{11})CCMSH were stable in mouse serum at 37°C for 24 h (**Figure 2.3**). Cellular internalization and efflux properties of ^{99m}Tc-RTD-Lys-(Arg^{11})CCMSH and ^{99m}Tc-RVD-Lys-(Arg^{11})CCMSH were examined in B16/F1 cells. **Figure 2.4** illustrates the internalization and efflux properties of ^{99m}Tc-RTD-Lys-(Arg^{11})CCMSH and ^{99m}Tc-RVD-Lys-(Arg^{11})CCMSH. ^{99m}Tc-RTD-Lys-

(Arg^{11})CCMSH and ^{99m}Tc-RVD-Lys-(Arg^{11})CCMSH exhibited rapid cellular internalization and prolonged cellular retention. Approximately 71% of ^{99m}Tc-RTD-Lys-(Arg^{11})CCMSH and 72% of ^{99m}Tc-RVD-Lys-(Arg^{11})CCMSH activities were internalized in the cells after 20 min of incubation. Cellular efflux results indicated that 75% of ^{99m}Tc-RTD-Lys-(Arg^{11})CCMSH and 70% of ^{99m}Tc-RVD-Lys-(Arg^{11})CCMSH activities remained inside the cells at 2 h of incubation in the culture medium.

The melanoma targeting and pharmacokinetic properties of ^{99m}Tc-RTD-Lys-(Arg^{11})CCMSH and ^{99m}Tc-RVD-Lys-(Arg^{11})CCMSH are shown in **Tables 2.1 and 2.2**. Both ^{99m}Tc-RTD-Lys-(Arg^{11})CCMSH and ^{99m}Tc-RVD-Lys-(Arg^{11})CCMSH exhibited rapid and high tumor uptake in B16/F1 melanoma-bearing C57 mice. ^{99m}Tc-RTD-Lys-(Arg^{11})CCMSH exhibited the peak tumor uptake of 18.77 ± 5.13% ID/g at 2 h post-injection, whereas ^{99m}Tc-RVD-Lys-(Arg^{11})CCMSH reached the peak tumor uptake of 19.63 ± 4.68% ID/g at 4 h post-injection. The tumor uptake values gradually decreased to 5.84 ± 0.50 and 8.81 ± 2.13% ID/g by 24 h post-injection. The tumor blocking studies (**Tables 2.1-2.2**) demonstrated that co-injection of 10 μg (6.1 nM) of non-radiolabeled NDP-MSH with ^{99m}Tc-RTD-Lys-(Arg^{11})CCMSH or ^{99m}Tc-RVD-Lys-(Arg^{11})CCMSH decreased their tumor uptake values to 2.85 ± 1.43 and 1.51 ± 0.6% ID/g at 2 h post-injection, demonstrating that the tumor uptake was MC1 receptor-mediated.

Renal uptake values of ^{99m}Tc-RTD-Lys-(Arg^{11})CCMSH and ^{99m}Tc-RVD-Lys-(Arg^{11})CCMSH were 135.14 ± 23.62 and 94.01 ± 18.31% ID/g at 2 h post injection, respectively. The renal uptake values of ^{99m}Tc-RTD-Lys-

(Arg^{11})CCMSH and ^{99m}Tc-RVD-Lys-(Arg^{11})CCMSH decreased to 46.84 ± 14.83 and 44.34 ± 12.11% ID/g at 24 h post-injection. The effect of *L*-lysine co-injection on renal uptake is presented in **Figure 2.5**. Co-injection of 15 mg *L*-lysine significantly ($p<0.05$) decreased the renal uptake values of ^{99m}Tc-RTD-Lys-(Arg^{11})CCMSH and ^{99m}Tc-RVD-Lys-(Arg^{11})CCMSH to 60.66 ± 12.09 and 55.74 ± 9.14% ID/g at 2 h post-injection, respectively. The *L*-lysine co-injection didn't affect the tumor uptake of ^{99m}Tc-RTD-Lys-(Arg^{11})CCMSH and ^{99m}Tc-RVD-Lys-(Arg^{11})CCMSH ($p>0.05$) at 2 h post-injection. Whole-body clearance of ^{99m}Tc-RTD-Lys-(Arg^{11})CCMSH and ^{99m}Tc-RVD-Lys-(Arg^{11})CCMSH was rapid, with approximately 55% and 59% of the injected radioactivity clearance through the urinary system by 2 h post-injection (**Tables 2.1-2.2**). At 24 h post-injection, 82% of ^{99m}Tc-RTD-Lys-(Arg^{11})CCMSH and 77% of ^{99m}Tc-RVD-Lys-(Arg^{11})CCMSH activity cleared out the body. Normal organ uptakes of ^{99m}Tc-RTD-Lys-(Arg^{11})CCMSH and ^{99m}Tc-RVD-Lys-(Arg^{11})CCMSH was minimal (<2.1% ID/g) except for the kidneys after 2 h post-injection (**Tables 2.1-2.2**).

Whole-body SPECT/CT images are presented in **Figure 2.6**. Flank B16/F1 melanoma lesions were clearly visualized by SPECT using ^{99m}Tc-RTD-Lys-(Arg^{11})CCMSH and ^{99m}Tc-RVD-Lys-(Arg^{11})CCMSH) peptides as imaging probes. The SPECT image of tumor accurately matched its anatomical location obtained in the CT image. The SPECT image showed high contrast of tumor to normal organ except for kidneys, which was consistent with the biodistribution results. The urinary metabolites of ^{99m}Tc-RTD-Lys-(Arg^{11})CCMSH and ^{99m}Tc-RVD-Lys-(Arg^{11})CCMSH at 2 h post-injection are shown in **Figure 2.7**.

Approximately 70% of ^{99m}Tc-RTD-Lys-(Arg^{11})CCMSH or ^{99m}Tc-RVD-Lys-(Arg^{11})CCMSH remained intact in the urine at 2 h post-injection, while 30% of the ^{99m}Tc-RTD-Lys-(Arg^{11})CCMSH or ^{99m}Tc-RVD-Lys-(Arg^{11})CCMSH was transformed to a more hydrophobic compound.

Discussion

We have been interested in developing MC1 receptor-targeting α-MSH peptides for melanoma imaging [11-14, 23-25]. Recently, we have found that the substitution of RGD with RAD resulted in nearly a 10-fold increase in MC1 receptor binding affinity for RAD-Lys-(Arg^{11})CCMSH as compared to RGD-Lys-(Arg^{11})CCMSH in B16/F1 melanoma cells [128]. Furthermore, ^{99m}Tc-RAD-Lys-(Arg^{11})CCMSH displayed higher melanoma uptake than ^{99m}Tc-RGD-Lys-(Arg^{11})CCMSH (19.91 ± 4.02 vs. 14.83 ± 2.93% ID/g at 2 h post-injection) in B16/F1 melanoma-bearing C57 mice [128]. Because the only structural difference between ^{99m}Tc-RAD-Lys-(Arg^{11})CCMSH and ^{99m}Tc-RGD-Lys-(Arg^{11})CCMSH was the extra methyl group in Ala as compared to Gly, the enhanced melanoma uptake of ^{99m}Tc-RAD-Lys-(Arg^{11})CCMSH suggested that the methyl group in Ala dramatically affected the MC1 receptor binding motif (His-$_D$Phe-Trp-Arg) in the (Arg^{11})CCMSH moiety. Thus, we were interested in whether and how the replacement of Gly with other amino acids could affect the melanoma targeting and pharmacokinetic properties of ^{99m}Tc-labeled RXD-Lys-(Arg^{11})CCMSH peptides. Specifically, we substituted the Gly with Thr and Val to examine the effects of -$CH(CH_3)OH$ and -$CH(CH_3)_2$ groups on the biodistribution properties of ^{99m}Tc-labeled RTD-Lys-(Arg^{11})CCMSH and RVD-Lys-(Arg^{11})CCMSH peptides in this study.

The substitution of Gly with Thr and Val retained low nanomolar MC1 receptor binding affinities of the peptides in B16/F1 melanoma cells. RTD-Lys-(Arg^{11})CCMSH and RVD-Lys-(Arg^{11})CCMSH exhibited stronger MC1 receptor

binding affinities than RGD-Lys-(Arg^{11})CCMSH and weaker MC1 receptor binding affinities than RAD-Lys-(Arg^{11})CCMSH. The differences in MC1 receptor binding affinities among these peptides were attributed to the subtle structural differences among the amino acids (Gly, Ala, Thr and Val). We further radiolabeled RTD-Lys-(Arg^{11})CCMSH and RVD-Lys-(Arg^{11})CCMSH with ^{99m}Tc and determined their biodistribution and tumor imaging properties in B16/F1 melanoma-bearing C57 mice. Both ^{99m}Tc-RTD-Lys-(Arg^{11})CCMSH and ^{99m}Tc-RVD-Lys-(Arg^{11})CCMSH were stable in mouse serum for 24 h at 37 °C. ^{99m}Tc-RTD-Lys-(Arg^{11})CCMSH and ^{99m}Tc-RVD-Lys-(Arg^{11})CCMSH showed similar patterns in cellular internalization and efflux in B16/F1 melanoma cells. ^{99m}Tc-RTD-Lys-(Arg^{11})CCMSH and ^{99m}Tc-RVD-Lys-(Arg^{11})CCMSH exhibited comparable high receptor-mediated melanoma uptake as ^{99m}Tc-RAD-Lys-(Arg^{11})CCMSH. However, the tumor uptake pattern was different between ^{99m}Tc-RTD-Lys-(Arg^{11})CCMSH and ^{99m}Tc-RVD-Lys-(Arg^{11})CCMSH. ^{99m}Tc-RTD-Lys-(Arg^{11})CCMSH showed the highest tumor uptake of 18.77 ± 5.13% ID/g at 2 h post-injection, whereas ^{99m}Tc-RVD-Lys-(Arg^{11})CCMSH reached the highest tumor uptake of 19.63 ± 4.68% ID/g at 4 h post-injection. Meanwhile, ^{99m}Tc-RVD-Lys-(Arg^{11})CCMSH exhibited lower renal uptake than ^{99m}Tc-RTD-Lys-(Arg^{11})CCMSH at 0.5, 2, and 4 h post-injection. The renal uptake of ^{99m}Tc-RVD-Lys-(Arg^{11})CCMSH was 62, 70, and 70% of the renal uptake of ^{99m}Tc-RTD-Lys-(Arg^{11})CCMSH at 0.5, 2, and 4 h post-injection, respectively.

The B16/F1 melanoma lesions could be clearly visualized by SPECT using ^{99m}Tc-RTD-Lys-(Arg^{11})CCMSH and ^{99m}Tc-RVD-Lys-(Arg^{11})CCMSH as

imaging probes. Moreover, switching from the diagnostic ^{99m}Tc to therapeutic ^{188}Re/^{186}Re could further expand their therapeutic applications. Since ^{188}Re/^{186}Re share similar coordination chemistry with ^{99m}Tc, both RTD-Lys-(Arg^{11})CCMSH and RVD-Lys-(Arg^{11})CCMSH should be readily labeled with ^{188}Re/^{186}Re without structural modification of the peptides. Because the renal uptake of ^{99m}Tc-RVD-Lys-(Arg^{11})CCMSH was about 30% less than that of ^{99m}Tc-RTD-Lys-(Arg^{11})CCMSH, RVD-Lys-(Arg^{11})CCMSH could be a better candidate for melanoma therapy when labeled with ^{188}Re/^{186}Re. However, ^{99m}Tc-RVD-Lys-(Arg^{11})CCMSH displayed high non-specific renal uptake in this study. Thus, it is desirable to reduce the renal uptake to facilitate its therapeutic application. *L*-lysine co-injection dramatically decreased the renal uptake of ^{99m}Tc-RTD-Lys-(Arg^{11})CCMSH and ^{99m}Tc-RVD-Lys-(Arg^{11})CCMSH by 40-50% (Figure 2.5), suggesting that the overall positive charges of the ^{99m}Tc-RXD-Lys-(Arg^{11})CCMSH peptides played key roles in their non-specific renal uptake. The reduction of the overall positive charge of ^{111}In-DOTA-GlyGlu-CycMSH via a negatively-charged glutamic acid linker resulted in a decrease in renal uptake by 44% as compared to ^{111}In-DOTA-GlyGlu-CycMSH [100]. Accordingly, it is likely that the reduction of the overall positive charges of the ^{99m}Tc-RXD-Lys-(Arg^{11})CCMSH peptides through the structural modification would decrease their non-specific renal uptake. It is worthwhile to note that four positively-charged amino acids, namely three arginines and one lysine linker, contributed to the overall positive charges of the ^{99m}Tc-RXD-Lys-(Arg^{11})CCMSH peptides. Because two arginines in the (Arg^{11})CCMSH motif are critical for MC1 receptor binding, the structural

modification on the arginines in the (Arg^{11})CCMSH motif would likely decrease the receptor binding affinity of the peptide. Alternatively, the replacement of lysine linker or arginine in the RXD motif by neutral or negatively-charged amino acids would likely reduce the overall positive charges of ^{99m}Tc-RXD-Lys-(Arg^{11})CCMSH peptides without sacrificing their receptor binding affinities. It will be interesting to examine how the structural modification on the lysine linker or arginine in the RXD motif affects the tumor and renal uptake in future studies.

In conclusion, the substitution of Gly with Thr and Val retained low nanomolar MC1 receptor binding affinities of the peptides in B16/F1 melanoma cells. ^{99m}Tc-RVD-Lys-(Arg^{11})CCMSH exhibited comparable high melanoma uptake as ^{99m}Tc-RTD-Lys-(Arg^{11})CCMSH, but 30% less renal uptake than ^{99m}Tc-RTD-Lys-(Arg^{11})CCMSH. In spite of high receptor-mediated melanoma uptake, high non-specific renal uptake of ^{99m}Tc-RVD-Lys-(Arg^{11})CCMSH needs to be reduced to facilitate its future application.

Tables

Table 2.1. Biodistribution of ^{99m}Tc-RTD-Lys-(Arg^{11})CCMSH

Biodistribution of ^{99m}Tc-RTD-Lys-(Arg^{11})CCMSH in B16/F1 melanoma-bearing C57 mice. The data was presented as percent injected dose/gram or as percent injected dose (mean ± SD, n=4).

Tissue	0.5 h	2 h	4 h	24 h	2 h NDP Blockade
			Percent injected dose/gram (%ID/g)		
Tumor	14.56 ± 5.31	18.77 ± 5.13	13.84 ± 3.10	5.84 ± 0.50	2.85 ± 1.43*
Brain	0.14 ± 0.04	0.03 ± 0.01	0.02 ± 0.01	0.03 ± 0.01	0.08 ± 0.06
Blood	15.95 ± 3.97	0.44 ± 0.13	0.55 ± 0.41	0.40 ± 0.21	0.50 ± 0.20
Heart	1.86 ± 0.21	0.29 ± 0.08	0.19 ± 0.05	0.12 ± 0.02	0.42 ± 0.26
Lung	4.27 ± 0.27	0.51 ± 0.37	0.39 ± 0.24	0.23 ± 0.04	1.18 ± 0.40
Liver	2.09 ± 0.04	1.62 ± 0.14	2.01 ± 0.39	1.03 ± 0.10	2.09 ± 0.64
Skin	3.99 ± 0.42	0.50 ± 0.19	0.27 ± 0.13	1.01 ± 0.31	1.21 ± 0.64
Spleen	1.04 ± 0.33	0.48 ± 0.20	0.47 ± 0.18	0.19 ± 0.13	0.64 ± 0.37
Stomach	1.87 ± 0.21	0.67 ± 0.16	0.70 ± 0.23	0.21 ± 0.04	1.11 ± 0.82
Kidneys	144.56 ± 24.64	135.14 ± 23.62	105.54 ± 27.67	46.84 ± 14.83	96.23 ± 28.13
Muscle	0.80 ± 0.38	0.15 ± 0.05	0.07 ± 0.02	0.52 ± 0.10	0.33 ± 0.03
Pancreas	0.83 ± 0.40	0.11 ± 0.04	0.09 ± 0.05	0.13 ± 0.07	0.44 ± 0.34
Bone	1.66 ± 0.10	0.46 ± 0.11	0.39 ± 0.12	0.23 ± 0.09	0.91 ± 0.59
			Percent injected dose (%ID)		
Intestines	1.73 ± 0.17	0.84 ± 0.20	0.72 ± 0.18	0.48 ± 0.13	1.16 ± 0.61
Urine	28.64 ± 8.85	54.76 ± 5.65	61.21 ± 5.56	82.19 ± 4.69	48.53 ± 21.62
			Uptake ratio of tumor/normal tissue		
Tumor/Blood	0.91	42.66	25.16	14.60	5.70
Tumor/Kidneys	0.10	0.14	0.13	0.12	0.03
Tumor/Lung	3.41	36.80	35.49	25.39	2.42
Tumor/Liver	6.97	11.59	6.89	5.67	1.36
Tumor/Muscle	18.20	125.13	197.71	11.23	8.64

*$p<0.05$ ($p=0.01$) for determining the significance of differences in tumor and kidney uptake between ^{99m}Tc-RTD-Lys-(Arg^{11})CCMSH with or without NDP-MSH peptide blockade at 2 h post-injection.

Table 2.2. Biodistribution of ^{99m}Tc-RVD-Lys-(Arg^{11})CCMSH

Biodistribution of ^{99m}Tc-RVD-Lys-(Arg^{11})CCMSH in B16/F1 melanoma-bearing C57 mice. The data was presented as percent injected dose/gram or as percent injected dose (mean ± SD, n=4).

Tissue	0.5 h	2 h	4 h	24 h	2 h NDP Blockade
			Percent injected dose/gram (%ID/g)		
Tumor	16.70 ± 5.31	17.10 ± 3.82	19.63 ± 4.68	8.81 ± 2.13	1.51 ± 0.6*
Brain	0.15 ± 0.05	0.04 ± 0.01	0.02 ± 0.01	0.03 ± 0.01	0.03 ± 0.01
Blood	1.50 ± 0.52	0.49 ± 0.05	0.54 ± 0.45	0.07 ± 0.02	0.55 ± 0.35
Heart	0.74 ± 0.43	0.26 ± 0.15	0.16 ± 0.03	0.10 ± 0.07	0.26 ± 0.11
Lung	2.01 ± 0.97	0.87 ± 0.40	0.49 ± 0.43	0.19 ± 0.10	0.83 ± 0.24
Liver	1.86 ± 0.17	1.40 ± 0.34	1.59 ± 0.13	1.21 ± 0.26	1.32 ± 0.14
Skin	9.59 ± 0.62	0.69 ± 0.18	0.35 ± 0.08	0.42 ± 0.27	0.65 ± 0.10
Spleen	0.82 ± 0.43	0.40 ± 0.10	0.50 ± 0.15	0.34 ± 0.06	0.18 ± 0.14
Stomach	1.92 ± 0.53	1.21 ± 0.61	0.96 ± 0.27	0.40 ± 0.13	1.39 ± 0.79
Kidneys	90.19 ± 15.41	94.01 ± 18.31	73.92 ± 3.73	44.34 ± 12.11	67.24 ± 9.72
Muscle	11.25 ± 6.02	0.17 ± 0.10	0.10 ± 0.07	0.26 ± 0.02	0.03 ± 0.02
Pancreas	0.62 ± 0.25	0.10 ± 0.02	0.08 ± 0.08	0.18 ± 0.07	0.06 ± 0.03
Bone	1.6 ± 0.73	0.57 ± 0.08	0.54 ± 0.28	0.47 ± 0.05	0.46 ± 0.10
			Percent injected dose (%ID)		
Intestines	1.36 ± 0.27	1.59 ± 1.08	0.95 ± 0.30	0.44 ± 0.22	1.36 ± 0.48
Urine	44.47 ± 3.12	59.2 ± 9.65	67.47 ± 10.00	76.85 ± 8.21	76.07 ± 3.55
			Uptake ratio of tumor/normal tissue		
Tumor/Blood	11.13	34.89	36.35	125.86	2.75
Tumor/Kidneys	0.19	0.18	0.27	0.20	0.02
Tumor/Lung	8.31	19.66	40.06	46.37	1.82
Tumor/Liver	8.98	12.21	12.35	7.28	1.14
Tumor/Muscle	1.48	100.59	196.30	33.88	50.33

*$p<0.05$ ($p=0.002$) for determining the significance of differences in tumor and kidney uptake between ^{99m}Tc-RVD-Lys-(Arg^{11})CCMSH with or without NDP-MSH peptide blockade at 2 h post-injection.

Figure Legends

Figure 2.1. Schematic structures of RTD-Lys-(Arg^{11})CCMSH and RVD-Lys-(Arg^{11})CCMSH.

Figure 2.2. The competitive binding curves of RTD-Lys-(Arg^{11})CCMSH (■) and RVD-Lys-(Arg^{11})CCMSH (▲) in B16/F1 melanoma cells. The IC_{50} value of RTD-Lys-(Arg^{11})CCMSH and RVD-Lys-(Arg^{11})CCMSH was 0.7 ± 0.07 and 1.0 ± 0.3 nM, respectively.

Figure 2.3. Radioactive HPLC profiles of ^{99m}Tc-RTD-Lys-(Arg^{11})CCMSH **(A)** and ^{99m}Tc-RVD-Lys-(Arg^{11})CCMSH **(B)** in mouse serum after incubation at 37 °C for 24 h. The arrows denote the original retention times of ^{99m}Tc-RTD-Lys-(Arg^{11})CCMSH (12.7 min) and ^{99m}Tc-RVD-Lys-(Arg^{11})CCMSH (14.6 min) prior to the incubation in mouse serum.

Figure 2.4. Cellular internalization and efflux of ^{99m}Tc-RTD-Lys-(Arg^{11})CCMSH **(A and B)** and ^{99m}Tc-RVD-Lys-(Arg^{11})CCMSH **(C and D)** in B16/F1 melanoma cells. Total bound radioactivity (♦), internalized radioactivity (▲) and cell membrane radioactivity (■) were presented as counts per minute (cpm).

Figure 2.5. Effect of *L*-lysine co-injection on the tumor and kidney uptakes of ^{99m}Tc-RTD-Lys-(Arg^{11})CCMSH and ^{99m}Tc-RVD-Lys-(Arg^{11})CCMSH at 2 h post-injection in B16/F1 melanoma-bearing C57 mice. The white (□) and light grey (▫) columns represented the tumor and renal uptake of ^{99m}Tc-RTD-Lys-(Arg^{11})CCMSH with or without *L*-lysine co-injection. The heavy grey (▪) and black (■) columns represented the tumor and renal uptake of ^{99m}Tc-RVD-Lys-(Arg^{11})CCMSH with or without *L*-lysine co-injection. *L*-lysine co-injection significantly (*$p<0.05$) reduced the renal uptake of ^{99m}Tc-RTD-Lys-(Arg^{11})CCMSH by 55% and the renal uptake of ^{99m}Tc-RVD-Lys-(Arg^{11})CCMSH by 41% at 2 h post-injection without affecting their tumor uptake.

Figure 2.6. Representative whole-body SPECT/CT images of B16/F1 melanoma- bearing C57 mice 2 h post injection of 7.4 MBq of ^{99m}Tc-RTD-Lys-(Arg^{11})CCMSH **(A)** and ^{99m}Tc-RVD-Lys-(Arg^{11})CCMSH **(B)**. Flank melanoma lesions (T) and kidneys (K) were highlighted with arrows on the images.

Figure 2.7. Radioactive HPLC profiles of urinary metabolites at 2 h post-injection of ^{99m}Tc-RTD-Lys-(Arg^{11})CCMSH (A) and ^{99m}Tc-RVD-Lys-(Arg^{11})CCMSH (B). The arrows denote the original retention times of ^{99m}Tc-RTD-Lys-(Arg^{11})CCMSH (12.7 min) and ^{99m}Tc-RVD-Lys-(Arg^{11})CCMSH (14.6 min) prior to tail vein injection.

Figure 2.1

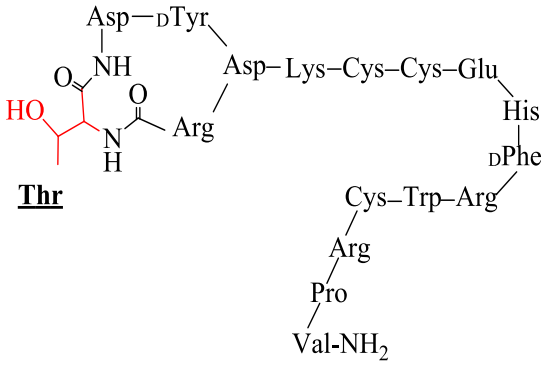

RTD-Lys-(Arg^{11})CCMSH

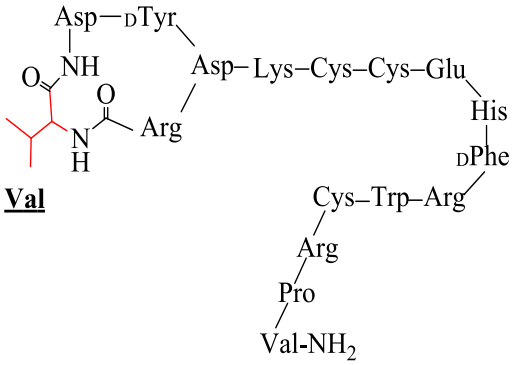

RVD-Lys-(Arg^{11})CCMSH

Figure 2.2

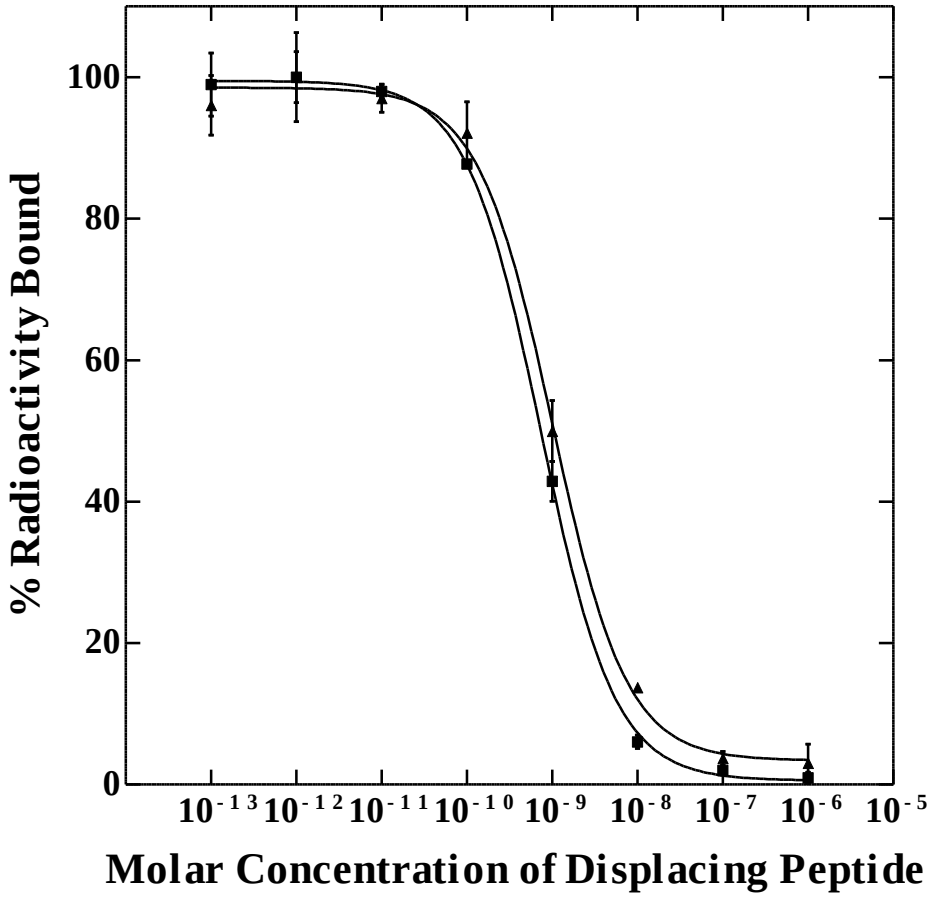
% Radioactivity Bound
100
80
60
40
20
0
10-13 10-12 10-11 10-10 10-9 10-8 10-7 10-6 10-5
Molar Concentration of Displacing Peptide

Figure 2.3

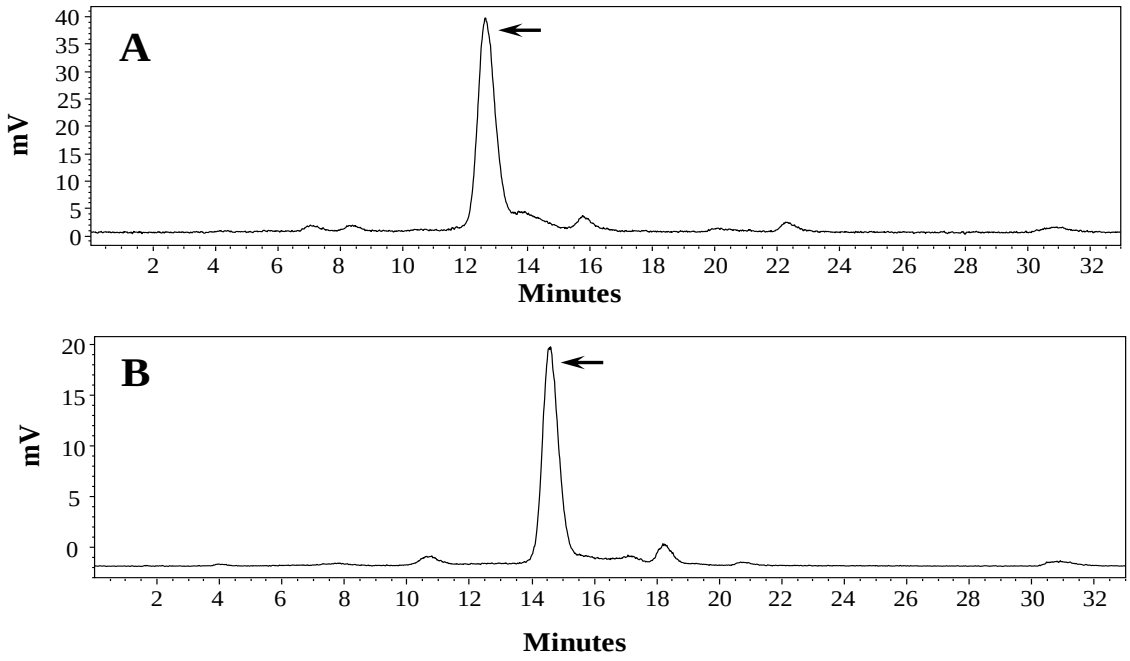
A
mV
40
35
30
25
20
15
10
5
0
2 4 6 8 10 12 14 16 18 20 22 24 26 28 30 32
Minutes
B
mV
20
15
10
5
0
2 4 6 8 10 12 14 16 18 20 22 24 26 28 30 32
Minutes

Figure 2.4

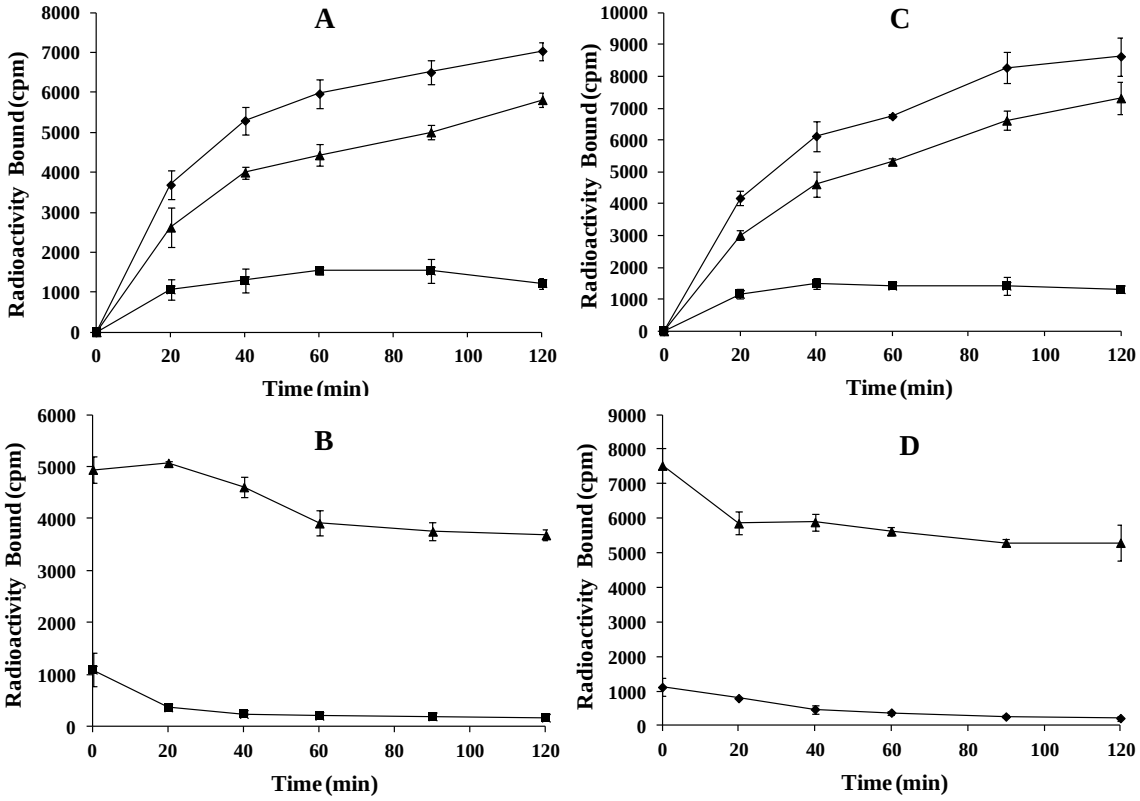
A
B
C
D
Radioactivity Bound (cpm)
Time (min)
0
20
40
60
80
100
120
1000
2000
3000
4000
5000
6000
7000
8000
9000
10000

Figure 2.5

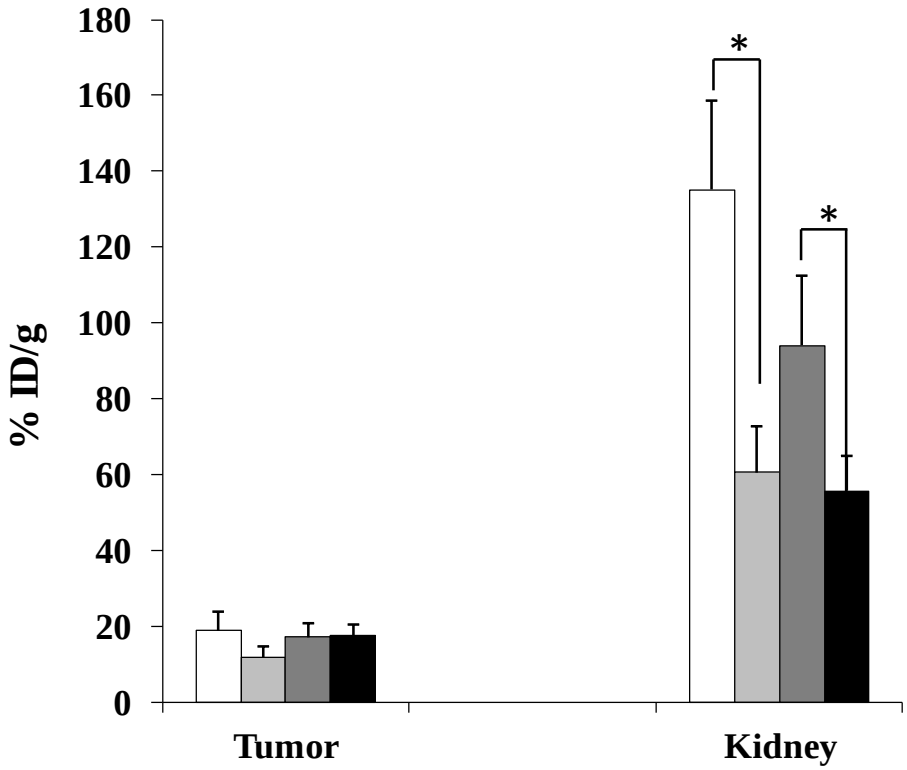

Figure 2.6

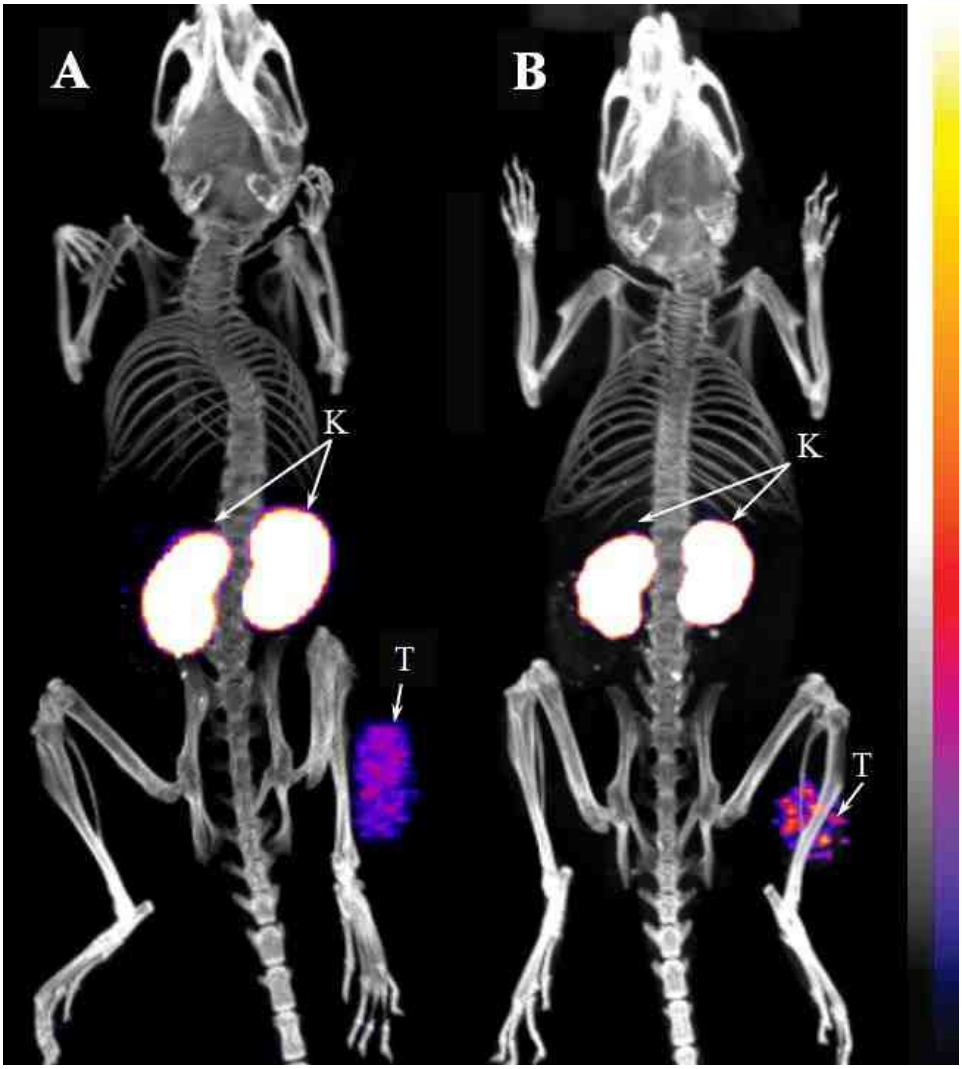

Figure 2.7

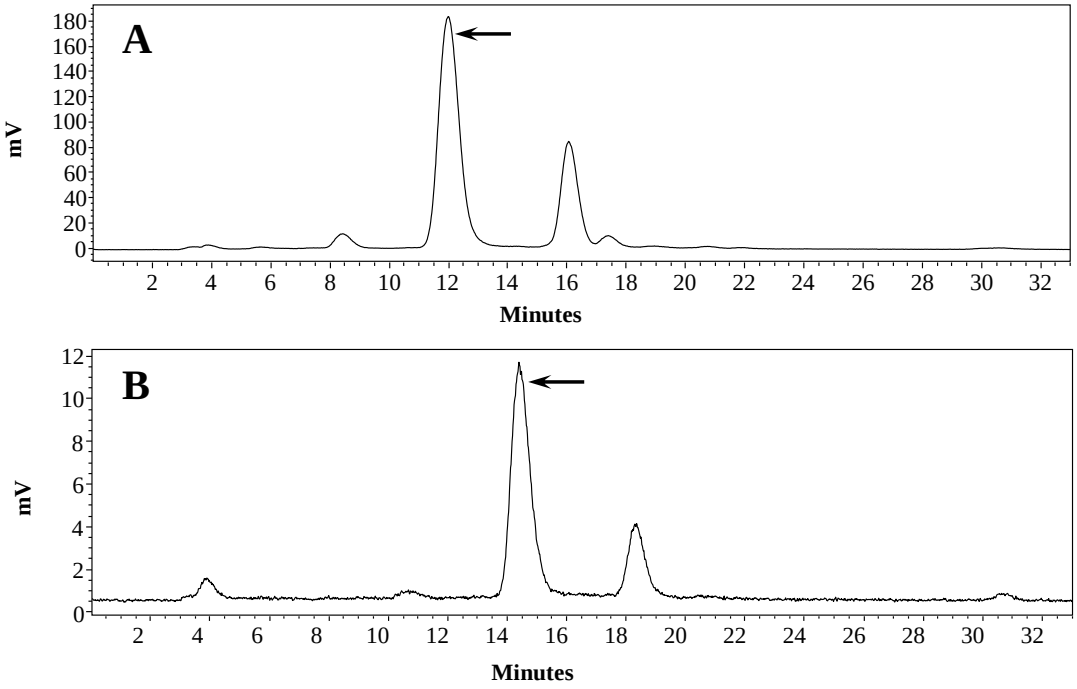
A
mV
180
160
140
120
100
80
60
40
20
0
2 4 6 8 10 12 14 16 18 20 22 24 26 28 30 32
Minutes
B
mV
12
10
8
6
4
2
0
2 4 6 8 10 12 14 16 18 20 22 24 26 28 30 32
Minutes

Chapter 3

Effects of amino acids on melanoma targeting and clearance properties of Tc-99m-labeled Arg-X-Asp-conjugated α-melanocyte stimulating hormone peptides

Introduction

Malignant melanoma is the most lethal form of skin cancer with an increasing incidence [3]. Unfortunately, no curative treatment exists for metastatic melanoma. It is of great interest to develop receptor-targeting imaging probes for melanoma. Both melanocortin-1 (MC1) and $\alpha_v\beta_3$ integrin receptors have been attractive molecular targets for developing melanoma imaging probes [91, 100, 103, 105, 125, 129, 130, 132-134, 136-145, 147]. Generally, the radiolabeled α-melanocyte stimulating hormone (α-MSH) peptides could target the MC1 receptors [91, 100, 103, 105, 129-137], whereas the radiolabeled Arg-Gly-Asp (RGD) peptides could bind to the $\alpha_v\beta_3$ integrin receptors [138-145]. In 2010, we reported a novel α-MSH hybrid peptide which could target both MC1 and $\alpha_v\beta_3$ integrin receptors [127]. Specifically, a cyclic RGD motif {Arg-Gly-Asp-$_D$Tyr-Asp} was attached to [Cys^{3,4,10}, $_D$-Phe^7, Arg^{11}]α-MSH$_{3-13}$ peptide via a lysine linker to yield RGD-Lys-(Arg^{11})CCMSH peptide. The dual receptor-targeting ^{99m}Tc-RGD-Lys-(Arg^{11})CCMSH displayed enhanced melanoma uptake as compared to single receptor-targeting ^{99m}Tc-RAD-Lys-(Arg^{11})CCMSH or ^{99m}Tc-RGD-Lys-(Arg^{11})CCMSHscramble in M21 human melanoma-xenografts [127]. Interestingly, the substitution of Gly in ^{99m}Tc-RGD-Lys-(Arg^{11})CCMSH with Ala,

Thr and Val improved the MC1 receptor binding affinities and enhanced the melanoma uptake in B16/F1 melanoma-bearing C57 mice [127, 128, 148].These interesting findings suggested that the single amino acid at that specific position generated a profound impact on the MC1 receptor binding affinity.

The structural differences among Gly, Ala, Thr and Val were minimal. As compared to Gly, the Ala has one extra -CH_3 group, the Thr has one extra -$CH(OH)CH_3$ group, whereas the Val has one extra -$CH(CH_3)_2$ group. The comparison in biodistribution results of ^{99m}Tc-RXD-Lys-(Arg^{11})CCMSH (X = Gly, Ala, Thr and Val) demonstrated that such subtle structural modification retained high melanoma uptake in B16/F1 melanoma-bearing C57 mice. Thus, we were interested in whether and how other amino acids could affect the melanoma targeting and pharmacokinetic properties of ^{99m}Tc-RXD-Lys-(Arg^{11})CCMSH peptide. For instance, whether and how a long hydrocarbon chain and a bulky benzene ring could affect the receptor binding and melanoma targeting properties of the peptides. In this study, we replaced the Gly with Ser, Nle, Phe and DPhe to generate four new peptides, namely RSD-Lys-(Arg^{11})CCMSH, RNleD-Lys-(Arg^{11})CCMSH, RFD-Lys-(Arg^{11})CCMSH and RfD-Lys-(Arg^{11})CCMSH peptides. The MC1 receptor binding affinities of these four peptides were examined in B16/F1 melanoma cells. Based on the receptor binding affinities, we further radiolabeled RSD-Lys-(Arg^{11})CCMSH, RFD-Lys-(Arg^{11})CCMSH and RfD-Lys-(Arg^{11})CCMSH with ^{99m}Tc. Then we determined the cellular internalization and efflux in B16/F1 melanoma cells and biodistribion properties in B16/F1 melanoma-bearing C57 mice for these three ^{99m}Tc-peptides.

Thereafter, we determined the imaging property of ^{99m}Tc-RSD-Lys-(Arg^{11})CCMSH in B16/F1 melanoma-bearing C57 mice.

Experimental design and methods

Chemicals and Reagents

Amino acids and resin were purchased from Advanced ChemTech Inc. (Louisville, KY) and Novabiochem (San Diego, CA). ^{125}I-Tyr^{2}-[Nle^{4}, DPhe^{7}]-α-MSH {^{125}I-(Tyr^{2})-NDP-MSH} was obtained from PerkinElmer, Inc. (Waltham, MA) for receptor binding assay. $^{99m}TcO_4^-$ was purchased from Cardinal Health (Albuquerque, NM). *L*-lysine was purchased from Sigma-Aldrich (St. Louis, MO). All other chemicals used in this study were purchased from Thermo Fischer Scientific (Waltham, MA) and used without further purification. B16/F1 murine melanoma cells were obtained from American Type Culture Collection (Manassas, VA).

Peptide Synthesis and In Vitro Competitive Binding Assay

The RSD-Lys-(Arg^{11})CCMSH, RNleD-Lys-(Arg^{11})CCMSH, RFD-Lys-(Arg^{11})CCMSH and RfD-Lys-(Arg^{11})CCMSH peptides were synthesized using fluorenylmethyloxycarbonyl (Fmoc) chemistry according to our previously published procedure [146] with slight modification on Sieber amide resin by an Advanced ChemTech multiple-peptide synthesizer (Louisville, KY). Briefly, 70 µmol of Sieber amide resin and 210 µmol of Fmoc-protected amino acids were used for the synthesis. Fmoc-Lys(Boc) was used to generate a Lys linker in each

peptide. Intermediate scaffolds of H_2N-Arg(Pbf)-Ser/Nle/Phe/DPhe-Asp(OtBu)-DTyr(tBu)-Asp(O-2-phenylisopropyl)-Lys(Boc)-Cys(Trt)-Cys(Trt)-Glu(OtBu)-His(Trt)-DPhe-Arg(Pbf)-Trp(Boc)-Cys(Trt)-Arg(Pbf)-Pro-Val were synthesized on Sieber amide resin. The protecting group of 2-phenylisopropyl of each scaffold was removed and each peptide was cleaved from the resin treating with a mixture of 2.5% of trifluoroacetic acid (TFA) and 5% of triisopropylsilane. After the precipitation with ice-cold ether and characterization by MS, each protected peptide was dissolved in H_2O/CH_3CN (50:50) and lyophilized to remove the reagents such as TFA and triisopropylsilane. Each protected peptide was further cyclized by coupling the carboxylic group from the Asp with the alpha amino group from the Arg at the N-terminus. The cyclization reaction was achieved by overnight reaction in dimethylformamide (DMF) using benzotriazole-1-yl-oxy-tris-pyrrolidino-phosphonium-hexafluorophosphate (PyBOP) as a coupling agent in the presence of N,N-diisopropylethylamine (DIPEA). The protecting groups were totally removed by treating with a mixture of TFA, thioanisole, phenol, water, ethanedithiol and triisopropylsilane (87.5:2.5:2.5:2.5:2.5:2.5) for 2 h at room temperature (25 °C). Each peptide was precipitated and washed with ice-cold ether for four times, purified by RP-HPLC and characterized by MS. The chemical purity of each peptide was determined by Waters RP-HPLC (Milford, MA) on a Grace Vydac C-18 reverse phase analytic column (Deerfield, IL) using a 20-min gradient of 16-26% acetonitrile in 20 mM HCl aqueous solution at a flow rate of 1 mL/min. The purities of all four peptides were greater than 95%.

The IC_{50} values of RSD-Lys-(Arg^{11})CCMSH, RNleD-Lys-(Arg^{11})CCMSH, RFD-Lys-(Arg^{11})CCMSH and RfD-Lys-(Arg^{11})CCMSH peptides for the MC1 receptor were determined in B16/F1 melanoma cells. The receptor binding assay was replicated in triplicate for each peptide. The B16/F1 cells were seeded into a 24-well cell culture plate at a density of 2.5×10^5 cells/well and incubated at 37° C overnight. After being washed with binding medium {modified Eagle's medium with 25 mM N-(2-hydroxyethyl)-piperazine-N′-(2-ethanesulfonic acid) (HEPES), pH 7.4, 0.2% bovine serum albumin (BSA), 0.3 mM 1,10-phenathroline}, the cells were incubated at 25 °C for 2 h with approximately 30,000 counts per minute (cpm) of ^{125}I-(Tyr^2)-NDP-MSH in the presence of increasing concentrations (10^{-13} M to 10^{-6} M) of each peptide in 0.3 mL of binding medium. The reaction medium was aspirated after the incubation. The cells were rinsed twice with 0.5 mL of ice-cold pH 7.4, 0.2% BSA/0.01 M phosphate buffered saline (PBS) to remove any unbound radioactivity and lysed in 0.5 mL of 1 M NaOH for 5 min. The activities associated with the cells were measured in a Wallac 2480 automated gamma counter (PerkinElmer, NJ). The IC_{50} value for each peptide was calculated using Prism software (GraphPad Software, La Jolla, CA).

Peptide Radiolabeling

Because RNleD-Lys-(Arg^{11})CCMSH exhibited lowest receptor binding affinity among four peptides, we only further evaluated the other three peptides. RSD-Lys-(Arg^{11})CCMSH, RFD-Lys-(Arg^{11})CCMSH and RfD-Lys-(Arg^{11})CCMSH

peptides were labeled with ^{99m}Tc via a direct reduction reaction with $SnCl_2$. Briefly, 10 µL of 1 mg/mL $SnCl_2$ in 0.1 M HCl, 40 µL of 0.5 M NH_4OAc (pH 5.2), 100 µL of 0.2 M Na_2tartate (pH 9.2), 100 µL of fresh $^{99m}TcO_4^-$ solution (37-74 MBq), and 10 µL of 1 mg/mL of each peptide in aqueous solution were added into a reaction vial and incubated at 25 °C for 20 min to form ^{99m}Tc-labeled peptide. Each ^{99m}Tc-peptide was purified to a single species by Waters RP-HPLC (Milford, MA) on a Grace Vydac C-18 reverse phase analytic column (Deerfield, IL) using a 20-min gradient of 16-26% acetonitrile in 20 mM HCl aqueous solution at a flow rate of 1 mL/min. Each purified peptide was purged with N_2 gas for 20 min to remove the acetonitrile. The pH of final peptide solution was adjusted to 7.4 with 0.1 N NaOH and sterile normal saline for stability, biodistribution and imaging studies. The serum stabilities of ^{99m}Tc-RSD-Lys-(Arg^{11})CCMSH, ^{99m}Tc-RFD-Lys-(Arg^{11})CCMSH and ^{99m}Tc-RfD-Lys-(Arg^{11})CCMSH were determined by incubation in mouse serum at 37 °C for 24 h and monitored for degradation by RP-HPLC. Briefly, 100 µL of HPLC-purified peptide solution (~7.4 MBq) was added into 100 µL of mouse serum (Sigma-Aldrich Corp, St. Louis, MO) and incubated at 37 ^{o}C for 24 h. After the incubation, 200 µL of a mixture of ethanol and acetonitrile (V:V = 1:1) was added to precipitate the serum proteins. The resulting mixture was centrifuged at 16,000 g for 5 min to collect the supernatant. The supernatant was purged with N_2 gas for 30 min to remove the ethanol and acetonitrile. The resulting sample was mixed with 500 µL of water and injected into RP-HPLC for analysis using the gradient described above.

Cellular Internalization and Efflux

Cellular internalization and efflux of ^{99m}Tc-RSD-Lys-(Arg^{11})CCMSH, ^{99m}Tc-RFD-Lys-(Arg^{11})CCMSH and ^{99m}Tc-RfD-Lys-(Arg^{11})CCMSH were evaluated in B16/F1 melanoma cells. The B16/F1 cells were seeded into a 24-well cell culture plate at a density of 2.5×10^5 cells/well and incubated at 37° C overnight. After being washed twice with binding medium [modified Eagle's medium with 25 mM *N*-(2-hydroxyethyl)-piperazine-*N'*-(2-ethanesulfonic acid), pH 7.4, 0.2% bovine serum albumin (BSA), 0.3 mM 1,10-phenathroline], the B16/F1 cells were incubated at 25°C for 20, 40, 60, 90 and 120 min (n=3) in the presence of approximate 300,000 counts per minute (cpm) of HPLC-purified of ^{99m}Tc-RSD-Lys-(Arg^{11})CCMSH, ^{99m}Tc-RFD-Lys-(Arg^{11})CCMSH or ^{99m}Tc-RfD-Lys-(Arg^{11})CCMSH. After incubation, the reaction medium was aspirated and the cells were rinsed with 2 × 0.5 mL of ice-cold pH 7.4, 0.2% BSA / 0.01 M PBS. Cellular internalization was assessed by washing the cells with acidic buffer [40 mM sodium acetate (pH 4.5) containing 0.9% NaCl and 0.2% BSA] to remove the membrane-bound radioactivity. The remaining internalized radioactivity was obtained by lysing the cells with 0.5 mL of 1 N NaOH for 5 min. Membrane-bound and internalized activities were counted in a gamma counter. Cellular efflux was determined by incubating the B16/F1 cells with ^{99m}Tc-RSD-Lys-(Arg^{11})CCMSH, ^{99m}Tc-RFD-Lys-(Arg^{11})CCMSH or ^{99m}Tc-RfD-Lys-(Arg^{11})CCMSH for 2 h at 25°C, removing non-specific-bound activity with 2 × 0.5 mL of ice-cold PBS rinse, and monitoring radioactivity released into cell culture medium. At time points of 20,

40, 60, 90 and 120 min, the radioactivities on the cell surface and inside the cells were separately collected and counted in a gamma counter.

Biodistribution Studies

All the animal studies were conducted in compliance with Institutional Animal Care and Use Committee approval. The biodistribution properties of ^{99m}Tc-RSD-Lys-(Arg^{11})CCMSH, ^{99m}Tc-RFD-Lys-(Arg^{11})CCMSH and ^{99m}Tc-RfD-Lys-(Arg^{11})CCMSH were determined in B16/F1 melanoma-bearing C57 female mice (Harlan, Indianapolis, IN). Each C57 mouse was subcutaneously inoculated on the right flank with 1×10^6 B16/F1 cells. The weight of tumors reached approximately 0.2 g 10 days post cell inoculation. Each melanoma-bearing mouse was injected with 0.037 MBq of ^{99m}Tc-RSD-Lys-(Arg^{11})CCMSH, ^{99m}Tc-RFD-Lys-(Arg^{11})CCMSH or ^{99m}Tc-RfD-Lys-(Arg^{11})CCMSH via the tail vein. Groups of 4 mice were sacrificed at 0.5, 2, 4 and 24 h post-injection, and tumors and organs of interest were harvested, weighed and counted. Blood values were taken as 6.5% of the body weight. The specificity of tumor uptake was determined by co-injecting ^{99m}Tc-RSD-Lys-(Arg^{11})CCMSH, ^{99m}Tc-RFD-Lys-(Arg^{11})CCMSH or ^{99m}Tc-RfD-Lys-(Arg^{11})CCMSH with 10 μg (6.1 nmol) of unlabeled NDP-MSH at 2 h post-injection.

L-lysine co-injection is effective in decreasing the renal uptake of radiolabeled α-MSH peptides. Because ^{99m}Tc-RSD-Lys-(Arg^{11})CCMSH exhibited the highest tumor uptake and fastest urinary clearance among three ^{99m}Tc-

peptdes, we only examined the effect of *L*-lysine co-injection on the renal uptake of ^{99m}Tc-RSD-Lys-(Arg^{11})CCMSH. Briefly, a group of 4 mice were injected with a mixture of 0.037 MBq of ^{99m}Tc-RSD-Lys-(Arg^{11})CCMSH and 15 mg of *L*-lysine. The mice were sacrificed at 2 h post-injection, and tumors and organs of interest were harvested, weighed and counted in a gamma counter.

Melanoma Imaging with ^{99m}Tc-RSD-Lys-(Arg^{11})CCMSH

^{99m}Tc-RSD-Lys-(Arg^{11})CCMSH was the lead peptide due to its higher tumor uptake and faster urinary clearance. Thus, we further determined the melanoma imaging property of ^{99m}Tc-RSD-Lys-(Arg^{11})CCMSH. Approximately 4.1 MBq of ^{99m}Tc-RSD-Lys-(Arg^{11})CCMSH was injected into a B16/F1 melanoma-bearing C57 mouse via the tail vein. The mouse was euthanized for small animal SPECT/CT (Nano-SPECT/CT®, Bioscan, Washington DC) imaging 2 h post-injection. The 9-min CT imaging was immediately followed by the SPECT imaging of whole-body. The SPECT scans of 24 projections were acquired. Reconstructed data from SPECT and CT were visualized and co-registered using InVivoScope (Bioscan, Washington DC).

Urinary Metabolites of ^{99m}Tc-RSD-Lys-(Arg^{11})CCMSH

We also examined the urinary metabolites of ^{99m}Tc-RSD-Lys-(Arg^{11})CCMSH. Approximately 3.7 MBq of ^{99m}Tc-RSD-Lys-(Arg^{11})CCMSH was

injected into a B16/F1 melanoma-bearing C57 mouse via the tail vein to determine the urinary metabolites. The mouse was euthanized to collect urine at 2 h post-injection. The collected urine sample was centrifuged at 16,000 g for 5 min before the HPLC analysis. Thereafter, an aliquot of the urine was injected into the HPLC. A 20-minute gradient of 16-26% acetonitrile / 20 mM HCl with a flow rate of 1 mL/min was used for urine analysis.

Statistical Analysis

Statistical analysis was performed using the Student's t-test for unpaired data to determine the significance of differences in tumor and kidney uptake with/without peptide blockade or with/without *L*-lysine co-injection in biodistribution studies described above. Differences at the 95% confidence level ($p<0.05$) were considered significant.

Results

The schematic structures of RSD-Lys-(Arg^{11})CCMSH, RNleD-Lys-(Arg^{11})CCMSH, RFD-Lys-(Arg^{11})CCMSH and RfD-Lys-(Arg^{11})CCMSH are presented in **Figure 3.1**. The peptides were synthesized and purified by reverse phase-high performance liquid chromatography (RP-HPLC). The overall synthetic yields were 30% for all four peptides. The chemical purities of RSD-Lys-(Arg^{11})CCMSH, RNleD-Lys-(Arg^{11})CCMSH, RFD-Lys-(Arg^{11})CCMSH and RfD-Lys-(Arg^{11})CCMSH were greater than 95% after the HPLC purification. The peptide identities were confirmed by electrospray mass spectrometry (MS). The measured molecular weight was 2180 for RSD-Lys-(Arg^{11})CCMSH, 2206 for RNleD-Lys-(Arg^{11})CCMSH, 2240 for RFD-Lys-(Arg^{11})CCMSH and RfD-Lys-(Arg^{11})CCMSH (**Table 3.1**). The competitive binding curves of the peptides are shown in **Figure 3.2**. The IC_{50} value was 1.30 ± 0.36 nM for RSD-Lys-(Arg^{11})CCMSH, 2.99 ± 0.26 nM for RNleD-Lys-(Arg^{11})CCMSH, 0.82 ± 0.06 nM for RFD-Lys-(Arg^{11})CCMSH, and 1.35 ± 0.08 nM for RfD-Lys-(Arg^{11})CCMSH in B16/F1 melanoma cells, respectively.

Because RNleD-Lys-(Arg^{11})CCMSH exhibited lowest receptor binding affinity among four peptides, as well as lower receptor binding affinity than that of RGD-Lys-(Arg^{11})CCMSH in our previous report [146], we only further evaluated the other three peptides. RSD-Lys-(Arg^{11})CCMSH, RFD-Lys-(Arg^{11})CCMSH and RfD-Lys-(Arg^{11})CCMSH were readily radiolabeled with ^{99m}Tc with greater than 95% radiolabeling yields. All three ^{99m}Tc-peptides were separated from their excess non-labeled peptides by RP-HPLC. The radiochemical purities of three

^{99m}Tc-peptides were greater than 99% (**Table 3.1**). The specific activities of ^{99m}Tc-RSD-Lys-(Arg^{11})CCMSH, ^{99m}Tc-RFD-Lys-(Arg^{11})CCMSH and ^{99m}Tc-RfD-Lys-(Arg^{11})CCMSH were 8.834×10^9, 8.598×10^9 , 8.598×10^9 MBq/g, respectively. The retention times of ^{99m}Tc-RSD-Lys-(Arg^{11})CCMSH, ^{99m}Tc-RFD-Lys-(Arg^{11})CCMSH and ^{99m}Tc-RfD-Lys-(Arg^{11})CCMSH were 12.5, 18.4 and 20.8 min, respectively. ^{99m}Tc-RSD-Lys-(Arg^{11})CCMSH, ^{99m}Tc-RFD-Lys-(Arg^{11})CCMSH and ^{99m}Tc-RfD-Lys-(Arg^{11})CCMSH were stable in mouse serum at 37°C for 24 h (**Figure 3.3**). Cellular internalization and efflux properties of ^{99m}Tc-RSD-Lys-(Arg^{11})CCMSH, ^{99m}Tc-RFD-Lys-(Arg^{11})CCMSH and ^{99m}Tc-RfD-Lys-(Arg^{11})CCMSH were examined in B16/F1 cells. **Figure 3.4** illustrates the internalization and efflux properties of ^{99m}Tc-RSD-Lys-(Arg^{11})CCMSH, ^{99m}Tc-RFD-Lys-(Arg^{11})CCMSH and ^{99m}Tc-RfD-Lys-(Arg^{11})CCMSH. All three ^{99m}Tc-peptides exhibited rapid cellular internalization and prolonged cellular retention. Approximately 69% of ^{99m}Tc-RSD-Lys-(Arg^{11})CCMSH, 87% of ^{99m}Tc-RFD-Lys-(Arg^{11})CCMSH and 87% of ^{99m}Tc-RfD-Lys-(Arg^{11})CCMSH activities were internalized in the cells after 20 min of incubation. Cellular efflux results indicated that 76% of ^{99m}Tc-RSD-Lys-(Arg^{11})CCMSH, 73% of ^{99m}Tc-RFD-Lys-(Arg^{11})CCMSH and 46% of ^{99m}Tc-RfD-Lys-(Arg^{11})CCMSH activities remained inside the cells after 2 h of incubation in the culture medium.

The melanoma targeting and pharmacokinetic properties of ^{99m}Tc-RSD-Lys-(Arg^{11})CCMSH, ^{99m}Tc-RFD-Lys-(Arg^{11})CCMSH and ^{99m}Tc-RfD-Lys-(Arg^{11})CCMSH are shown in **Tables 3.2-3.4**. Both ^{99m}Tc-RFD-Lys-(Arg^{11})CCMSH and ^{99m}Tc-RfD-Lys-(Arg^{11})CCMSH exhibited similar tumor uptake pattern in

B16/F1 melanoma-bearing C57 mice. ^{99m}Tc-RFD-Lys-(Arg^{11})CCMSH exhibited its highest tumor uptake of 15.01 ± 4.40% ID/g at 4 h post-injection, whereas ^{99m}Tc-RfD-Lys-(Arg^{11})CCMSH reached its highest tumor uptake of 13.11 ± 1.21% ID/g at 4 h post-injection. The tumor uptake values of ^{99m}Tc-RFD-Lys-(Arg^{11})CCMSH and ^{99m}Tc-RfD-Lys-(Arg^{11})CCMSH decreased to 7.19 ± 1.02 and 6.29 ± 1.39% ID/g by 24 h post-injection. The tumor blocking studies revealed that co-injection of 10 μg (6.1 nM) of non-radiolabeled NDP-MSH with ^{99m}Tc-RFD-Lys-(Arg^{11})CCMSH or ^{99m}Tc-RfD-Lys-(Arg^{11})CCMSH decreased their tumor uptake values to 2.82 ± 0.48 and 1.57 ± 0.48% ID/g at 2 h post-injection, demonstrating that the tumor uptake was MC1 receptor-mediated. ^{99m}Tc-RSD-Lys-(Arg^{11})CCMSH displayed a different tumor uptake pattern as compared to ^{99m}Tc-RFD-Lys-(Arg^{11})CCMSH and ^{99m}Tc-RfD-Lys-(Arg^{11})CCMSH. ^{99m}Tc-RSD-Lys-(Arg^{11})CCMSH exhibited rapid and high melanoma uptake of 18.01 ± 4.22% ID/g at 30 min post-injection. The tumor uptake of ^{99m}Tc-RSD-Lys-(Arg^{11})CCMSH gradually reduced to 8.04 ± 1.80% ID/g at 24 h post-injection. Furthermore, co-injection of 10 μg (6.1 nM) of non-radiolabeled NDP-MSH with ^{99m}Tc-RSD-Lys-(Arg^{11})CCMSH decreased their tumor uptake value to 2.35 ± 0.01% ID/g at 2 h post-injection, demonstrating that the tumor uptake was MC1 receptor-mediated.

Kidneys were the excretion pathways for ^{99m}Tc-RSD-Lys-(Arg^{11})CCMSH, ^{99m}Tc-RFD-Lys-(Arg^{11})CCMSH and ^{99m}Tc-RfD-Lys-(Arg^{11})CCMSH. The renal uptake values of ^{99m}Tc-RSD-Lys-(Arg^{11})CCMSH, ^{99m}Tc-RFD-Lys-(Arg^{11})CCMSH and ^{99m}Tc-RfD-Lys-(Arg^{11})CCMSH were 80.01 ± 15.67, 88.08 ± 9.31 and 111.54 ± 10.19% ID/g at 2 h post injection, respectively. At 24 h post-injection, The renal

uptake values of for ^{99m}Tc-RSD-Lys-(Arg^{11})CCMSH, ^{99m}Tc-RFD-Lys-(Arg^{11})CCMSH and ^{99m}Tc-RfD-Lys-(Arg^{11})CCMSH decreased to 23.15 ± 2.94, 51.01 ± 3.62 and 73.05 ± 9.87% ID/g, respectively. Liver uptake was different among these three ^{99m}Tc-peptides. ^{99m}Tc-RSD-Lys-(Arg^{11})CCMSH demonstrated lower liver uptake than ^{99m}Tc-RFD-Lys-(Arg^{11})CCMSH and ^{99m}Tc-RfD-Lys-(Arg^{11})CCMSH. The liver uptake of ^{99m}Tc-RSD-Lys-(Arg^{11})CCMSH, ^{99m}Tc-RFD-Lys-(Arg^{11})CCMSH and ^{99m}Tc-RfD-Lys-(Arg^{11})CCMSH were 1.22 ± 0.12, 9.87 ± 1.26 and 5.29 ± 1.30% ID/g at 2 h post injection, respectively.

^{99m}Tc-RSD-Lys-(Arg^{11})CCMSH exhibited faster whole-body clearance than ^{99m}Tc-RFD-Lys-(Arg^{11})CCMSH and ^{99m}Tc-RfD-Lys-(Arg^{11})CCMSH. Approximately 68% of ^{99m}Tc-RSD-Lys-(Arg^{11})CCMSH cleared through the urinary system by 2 h post-injection, whereas approximately 43% of ^{99m}Tc-RFD-Lys-(Arg^{11})CCMSH and 44% of ^{99m}Tc-RfD-Lys-(Arg^{11})CCMSH washed through the urinary system by 2 h post-injection. At 24 h post-injection, 84% of ^{99m}Tc-RSD-Lys-(Arg^{11})CCMSH, 76% of ^{99m}Tc-RFD-Lys-(Arg^{11})CCMSH and 73% of ^{99m}Tc-RfD-Lys-(Arg^{11})CCMSH cleared out the body. ^{99m}Tc-RSD-Lys-(Arg^{11})CCMSH also displayed lower normal organ uptake than ^{99m}Tc-RFD-Lys-(Arg^{11})CCMSH and ^{99m}Tc-RfD-Lys-(Arg^{11})CCMSH. Normal organ uptake of ^{99m}Tc-RSD-Lys-(Arg^{11})CCMSH was minimal (<1.2% ID/g) except for the kidneys after 2 h post-injection.

Since ^{99m}Tc-RSD-Lys-(Arg^{11})CCMSH showed higher tumor uptake and faster urinary clearance than ^{99m}Tc-RFD-Lys-(Arg^{11})CCMSH and ^{99m}Tc-RfD-Lys-(Arg^{11})CCMSH, the effect of *L*-lysine co-injection on the tumor and renal uptake

of ^{99m}Tc-RSD-Lys-(Arg^{11})CCMSH was examined in B16/F1 melanoma-bearing C57 mice. *L*-lysine co-injection significantly (*p<0.05) reduced the renal uptake of ^{99m}Tc-RSD-Lys-(Arg^{11})CCMSH by 37% at 2 h post-injection without affecting the tumor uptake (**Figure 3.5**). Whole-body single photon emission computed tomography (SPECT)/CT image at 2 h post-injection are presented in **Figure 3.6**. Flank B16/F1 melanoma lesions were clearly visualized by SPECT using ^{99m}Tc-RSD-Lys-(Arg^{11})CCMSH peptide as an imaging probe. The SPECT image of tumor accurately matched its anatomical location obtained in the CT image. The SPECT image showed high contrast of tumor to normal organ except for kidneys, which was consistent with the biodistribution results. The urinary metabolites of ^{99m}Tc-RSD-Lys-(Arg^{11})CCMSH at 2 h post-injection are shown in **Figure 3.7**. Approximately 70% of ^{99m}Tc-RSD-Lys-(Arg^{11})CCMSH remained intact in the urine at 2 h post-injection, while 30% of the ^{99m}Tc-RSD-Lys-(Arg^{11})CCMSH was transformed to a more hydrophobic compound.

Discussion

In our previous reports [24-26] we have found the important role of Gly in the tumor targeting property of ^{99m}Tc-RGD-Lys-(Arg^{11})CCMSH in B16/F1 melanoma-bearing C57 mice. Despite the minimal structural differences among Gly, Ala, Thr and Val amino acids, the replacement of Gly in RGD-Lys-(Arg^{11})CCMSH with Ala, Thr and Val enhanced the MC1 receptor binding affinities and B16/F1 melanoma uptake of the peptides [24-26]. In this study, we further investigated whether the substitution of Gly with a longer hydrocarbon chain (Nle) and a bulky benzene ring (Phe or DPhe) could affect the receptor binding and melanoma targeting properties of the peptides. On the other hand, we hypothesized that the replacement of Gly with Ser would facilitate the urinary clearance of the peptide as compared to hydrophobic Nle, Phe and DPhe. Thus, we synthesized and evaluated RSD-Lys-(Arg^{11})CCMSH, RNleD-Lys-(Arg^{11})CCMSH, RFD-Lys-(Arg^{11})CCMSH and RfD-Lys-(Arg^{11})CCMSH peptides in this study.

The introduction of Ser, Nle, Phe and DPhe generated different impact on the MC1 receptor binding affinities of the peptides. The linear long hydrocarbon chain from Nle decreased the MC1 receptor binding affinity of the peptide, whereas the short CH_2OH group from Ser and the bulky benzene ring from Phe and DPhe increased the MC1 receptor binding affinity of the peptides. Among these four new peptides, RNleD-Lys-(Arg^{11})CCMSH displayed the weakest MC1 receptor binding affinity of 2.99 ± 0.26 nM, whereas RSD-Lys-(Arg^{11})CCMSH and RfD-Lys-(Arg^{11})CCMSH exhibited similar strong MC1 receptor binding affinities of

1.30 ± 0.36 and 1.35 ± 0.08 nM. Overall, RfD-Lys-(Arg^{11})CCMSH showed the strongest MC1 receptor binding affinity of 0.82 ± 0.06 nM. Despite that the -His-DPhe-Arg-Trp- motif is the binding moiety to MC1 receptor, the difference in receptor binding affinity indicated that the Ser, Nle, Phe and DPhe interacted with the receptor binding moiety. Such subtle interactions were likely related to the flexibility of lactam bonds among amino acid residues in the peptides. In our previous report [25,26], the MC1 receptor binding affinities were 2.1, 0.3, 0.7 and 1.0 nm for RGD-Lys-(Arg^{11})CCMSH, RAD-Lys-(Arg^{11})CCMSH, RTD-Lys-(Arg^{11})CCMSH and RVD-Lys-(Arg^{11})CCMSH in B16/F1 cells, respectively. Clearly, RNleD-Lys-(Arg^{11})CCMSH displayed the weakest MC1 receptor binding affinity among all RXD-Lys-(Arg^{11})CCMSH peptides. Thus, we further radiolabeled RSD-Lys-(Arg^{11})CCMSH, RFD-Lys-(Arg^{11})CCMSH and RfD-Lys-(Arg^{11})CCMSH with ^{99m}Tc and evaluated their cellular internalization and efflux properties, as well as their in vivo biodistribution and clearance properties. It is worthwhile to note that three cysteine residues in each peptide provide a NS_3 chelating system for ^{99m}Tc. It was reported that non-radioactive rhenium-conjugated (Arg^{11})CCMSH retained comparable nanomolar MC1 receptor binding affinity as (Arg^{11})CCMSH peptide (1.9 vs. 1.7 nM) [149]. Accordingly, the radiolabeling of three RXD-Lys-(Arg^{11})CCMSH peptides with ^{99m}Tc should retain their nanomolar binding affinities.

^{99m}Tc-RSD-Lys-(Arg^{11})CCMSH, ^{99m}Tc-RFD-Lys-(Arg^{11})CCMSH and ^{99m}Tc-RfD-Lys-(Arg^{11})CCMSH exhibited similar rapid internalization and prolonged efflux properties in B16/F1 melanoma cells. Despite the similar pattern in cellular

internalization and efflux properties, ^{99m}Tc-RSD-Lys-(Arg^{11})CCMSH displayed a different tumor uptake pattern as compared to ^{99m}Tc-RFD-Lys-(Arg^{11})CCMSH and ^{99m}Tc-RfD-Lys-(Arg^{11})CCMSH. ^{99m}Tc-RSD-Lys-(Arg^{11})CCMSH exhibited rapid and high melanoma uptake of 18.01 ± 4.22% ID/g at 30 min post-injection. Meanwhile, ^{99m}Tc-RSD-Lys-(Arg^{11})CCMSH displayed lower renal uptake than ^{99m}Tc-RFD-Lys-(Arg^{11})CCMSH and ^{99m}Tc-RfD-Lys-(Arg^{11})CCMSH. The renal uptake of ^{99m}Tc-RSD-Lys-(Arg^{11})CCMSH was 45% of the renal uptake of ^{99m}Tc-RFD-Lys-(Arg^{11})CCMSH, and 32% of the renal uptake of ^{99m}Tc-RfD-Lys-(Arg^{11})CCMSH at 24 h post-injection. Not surprisingly, ^{99m}Tc-RSD-Lys-(Arg^{11})CCMSH also showed lower liver uptake than ^{99m}Tc-RFD-Lys-(Arg^{11})CCMSH and ^{99m}Tc-RfD-Lys-(Arg^{11})CCMSH. The liver uptake of ^{99m}Tc-RSD-Lys-(Arg^{11})CCMSH was 12% of the liver uptake of ^{99m}Tc-RFD-Lys-(Arg^{11})CCMSH, and 23% of the liver uptake of ^{99m}Tc-RfD-Lys-(Arg^{11})CCMSH at 2 h post-injection. Furthermore, ^{99m}Tc-RSD-Lys-(Arg^{11})CCMSH exhibited faster urinary clearance than ^{99m}Tc-RFD-Lys-(Arg^{11})CCMSH and ^{99m}Tc-RfD-Lys-(Arg^{11})CCMSH. Interestingly, the stereochemistry of Phe and DPhe affected the renal and liver uptake. ^{99m}Tc-RFD-Lys-(Arg^{11})CCMSH displayed higher liver uptake than that of ^{99m}Tc-RfD-Lys-(Arg^{11})CCMSH, whereas ^{99m}Tc-RfD-Lys-(Arg^{11})CCMSH displayed higher renal uptake than that of ^{99m}Tc-RFD-Lys-(Arg^{11})CCMSH. Clearly, the tumor targeting and clearance properties of ^{99m}Tc-RSD-Lys-(Arg^{11})CCMSH were more favorable than those of ^{99m}Tc-RFD-Lys-(Arg^{11})CCMSH and ^{99m}Tc-RfD-Lys-(Arg^{11})CCMSH.

The B16/F1 melanoma lesions could be clearly visualized by SPECT/CT using ^{99m}Tc-RSD-Lys-(Arg^{11})CCMSH as an imaging probe. However, the image also indicated very high renal uptake. In fact, extremely high renal uptake (67-135% ID/g at 2 h post-injection) appears to be a common issue for all reported ^{99m}Tc-RXD-Lys-(Arg^{11})CCMSH peptides [128, 146, 148]. Despite that ^{99m}Tc-RSD-Lys-(Arg^{11})CCMSH exhibited the second lowest renal uptake (80.01 ± 15.67% ID/g at 2 h post-injection) among all reported ^{99m}Tc-RXD-Lys-(Arg^{11})CCMSH peptides, it is desirable to reduce the non-specific renal uptake in future studies to facilitate its potential therapeutic application. In this study, *L*-lysine co-injection significantly (*$p<0.05$) reduced the renal uptake of ^{99m}Tc-RSD-Lys-(Arg^{11})CCMSH by 37% at 2 h post-injection without affecting its tumor uptake. Obviously, *L*-lysine co-injection can be utilized to decrease the renal uptake of ^{99m}Tc-RSD-Lys-(Arg^{11})CCMSH in future studies. The effect of *L*-lysine co-injection also highlighted the contribution of the overall positive charge of ^{99m}Tc-RSD-Lys-(Arg^{11})CCMSH to its renal uptake. Clearly, the substitution of the positively-charged Lys linker with a neutral or negatively-charged amino acid (i.e. Gly or Glu) can decrease the overall charge of ^{99m}Tc-RSD-Lys-(Arg^{11})CCMSH. According to the effect of *L*-lysine co-injection in this study, it is very likely that the substitution of Lys with a neutral or negatively-charged amino acid will decrease the renal uptake.

Conclusions

In summary, the substitution of Gly with Ser, Phe and DPhe increased the MC1 receptor binding affinities of the peptides, whereas the substitution of Gly with Nle decreased the MC1 receptor binding affinity of the peptide in B16/F1 melanoma cells. ^{99m}Tc-RSD-Lys-(Arg^{11})CCMSH exhibited higher melanoma uptake and lower kidney and liver uptake than those of ^{99m}Tc-RFD-Lys-(Arg^{11})CCMSH and ^{99m}Tc-RfD-Lys-(Arg^{11})CCMSH. The B16/F1 melanoma lesions could be clearly visualized by SPECT/CT using ^{99m}Tc-RSD-Lys-(Arg^{11})CCMSH as an imaging probe. It is desirable to reduce the non-specific renal uptake of ^{99m}Tc-RSD-Lys-(Arg^{11})CCMSH to facilitate its potential therapeutic application.

Tables

Table 3.1. Peptide properties

Capacity factors, chemical/radiochemical purities and measured molecular weights of RXD-Lys-(Arg^{11})CCMSH peptides and their ^{99m}Tc-conjugates.

Peptide	Capacity factor (k')	Chemical/Radiochemical Purity (%)	Measured Molecular Weight (Da)
RSD-Lys-(Arg^{11})CCMSH	2.19	97.01	2180
RNleD-Lys-(Arg^{11})CCMSH	4.36	95.83	2206
RFD-Lys-(Arg^{11})CCMSH	3.77	98.25	2240
RfD-Lys-(Arg^{11})CCMSH	3.86	95.75	2240
^{99m}Tc-RSD-Lys-(Arg^{11})CCMSH	3.18	99.75	ND
^{99m}Tc-RFD-Lys-(Arg^{11})CCMSH	4.93	99.27	ND
^{99m}Tc-RfD-Lys-(Arg^{11})CCMSH	5.13	99.78	ND

ND = not determined.

Table 3.2. Biodistribution of ^{99m}Tc-RSD-Lys-(Arg^{11})CCMSH

Biodistribution of ^{99m}Tc-RSD-Lys-(Arg^{11})CCMSH in B16/F1 melanoma-bearing C57 mice. The data was presented as percent injected dose/gram or as percent injected dose (mean ± SD, n=4).

Tissue	0.5 h	2 h	4 h	24 h	2 h NDP Blockade
			Percent injected dose/gram (%ID/g)		
Tumor	18.01 ± 4.22	17.42 ± 1.52	10.12 ± 1.72	8.04 ± 1.80	2.35 ± 0.01*
Brain	0.25 ± 0.12	0.02 ± 0.01	0.01 ± 0.01	0.06 ± 0.01	0.05 ± 0.01
Blood	13.59 ± 1.25	0.19 ± 0.11	0.06 ± 0.04	2.01 ± 1.52	0.69 ± 0.42
Heart	2.14 ± 0.49	0.14 ± 0.05	0.09 ± 0.04	0.14 ± 0.05	0.46 ± 0.30
Lung	3.69 ± 1.18	0.33 ± 0.13	0.22 ± 0.06	0.27 ± 0.13	0.65 ± 0.16
Liver	2.25 ± 0.20	1.22 ± 0.12	1.57 ± 0.81	0.70 ± 0.14	1.54 ± 0.11
Skin	5.31 ± 0.63	0.33 ± 0.10	0.27 ± 0.05	2.19 ± 0.58	0.75 ± 0.02
Spleen	1.73 ± 0.17	0.18 ± 0.10	0.38 ± 0.15	0.22 ± 0.07	0.28 ± 0.10
Stomach	2.31 ± 0.31	0.73 ± 0.08	0.61 ± 0.18	0.30 ± 0.17	1.19 ± 0.04
Kidneys	98.25 ± 13.78	80.01 ± 15.67	69.23 ± 17.41	23.15 ± 2.94	90.41 ± 19.21
Muscle	1.42 ± 0.57	0.09 ± 0.04	0.07 ± 0.04	1.01 ± 0.50	0.09 ± 0.06
Pancreas	0.68 ± 0.27	0.04 ± 0.04	0.09 ± 0.06	0.17 ± 0.07	0.15 ± 0.03
Bone	2.11 ± 0.67	0.44 ± 0.18	0.32 ± 0.19	0.59 ± 0.09	0.47 ± 0.13
			Percent injected dose (%ID)		
Intestines	2.02 ± 0.17	0.63 ± 0.08	1.48 ± 0.22	0.66 ± 0.27	1.06 ± 0.79
Urine	36.01 ± 2.73	68.19 ± 9.80	74.72 ± 6.63	84.03 ± 2.67	69.99 ± 4.72
			Uptake ratio of tumor/normal tissue		
Tumor/Blood	1.33	91.68	168.67	4.02	3.41
Tumor/Kidneys	0.18	0.22	0.15	0.35	0.03
Tumor/Lung	4.88	52.79	46.00	29.78	3.62
Tumor/Liver	8.00	14.28	6.45	11.49	1.53
Tumor/Muscle	12.68	193.56	144.57	8.04	26.11

*$p<0.05$ ($p=0.002$) for determining the significance of differences in tumor and kidney uptake between ^{99m}Tc-RSD-Lys-(Arg^{11})CCMSH with or without NDP-MSH peptide blockade at 2 h post-injection.

Table 3.3. Biodistribution of ^{99m}Tc-RFD-Lys-(Arg^{11})CCMSH

Biodistribution of ^{99m}Tc-RFD-Lys-(Arg^{11})CCMSH in B16/F1 melanoma-bearing C57 mice. The data was presented as percent injected dose/gram or as percent injected dose (mean ± SD, n=4).

Tissue	0.5 h	2 h	4 h	24 h	2 h NDP Blockade
			Percent injected dose/gram (%ID/g)		
Tumor	7.42 ± 3.56	11.22 ± 1.53	13.11 ± 1.21	6.29 ± 1.39	1.57 ± 0.48*
Brain	0.21 ± 0.01	0.07 ± 0.01	0.04 ± 0.01	0.01 ± 0.01	0.08 ± 0.01
Blood	6.78 ± 3.79	1.99 ± 0.24	0.91 ± 0.38	0.23 ± 0.01	1.61 ± 0.01
Heart	2.63 ± 1.13	0.94 ± 0.11	0.88 ± 0.35	0.14 ± 0.02	0.76 ± 0.17
Lung	7.51 ± 1.60	3.38 ± 0.48	2.11 ± 0.51	0.38 ± 0.17	2.10 ± 0.29
Liver	6.75 ± 2.44	9.87 ± 1.26	12.11 ± 1.86	4.73 ± 1.53	6.34 ± 2.19
Skin	4.27 ± 1.16	1.54 ± 0.20	0.87 ± 0.17	0.46 ± 0.05	1.48 ± 0.44
Spleen	4.82 ± 1.31	4.40 ± 0.72	4.85 ± 1.33	2.56 ± 0.45	2.40 ± 1.11
Stomach	6.21 ± 0.37	4.40 ± 3.33	3.80 ± 1.14	0.92 ± 0.44	10.65 ± 2.76
Kidneys	56.86 ± 16.58	88.08 ± 9.31	81.89 ± 23.37	51.01 ± 3.62	72.29 ± 6.08
Muscle	1.27 ± 0.42	0.31 ± 0.19	0.21 ± 0.01	0.01 ± 0.01	0.33 ± 0.15
Pancreas	1.17 ± 0.23	0.38 ± 0.17	0.45 ± 0.01	0.20 ± 0.08	0.19 ± 0.08
Bone	1.97 ± 0.32	1.11 ± 0.07	0.44 ± 0.25	0.41 ± 0.25	0.05 ± 0.01
			Percent injected dose (%ID)		
Intestines	3.23 ± 1.73	4.69 ± 1.24	7.02 ± 2.79	1.50 ± 0.50	13.77 ± 11.25
Urine	30.19 ± 11.73	42.61 ± 2.89	61.42 ± 0.29	75.8 ± 5.02	39.05 ± 10.35
			Uptake ratio of tumor/normal tissue		
Tumor/Blood	1.09	5.64	14.41	27.35	0.98
Tumor/Kidneys	0.13	0.13	0.16	0.12	0.02
Tumor/Lung	0.99	3.38	6.21	16.55	0.75
Tumor/Liver	1.10	1.14	1.08	1.33	0.25
Tumor/Muscle	5.84	36.19	62.43	629.00	4.76

*$p<0.05$ ($p=0.001$) for determining the significance of differences in tumor and kidney uptake between ^{99m}Tc-RFD-Lys-(Arg^{11})CCMSH with or without NDP-MSH peptide blockade at 2 h post-injection.

Table 3.4. Biodistribution of ^{99m}Tc-RfD-Lys-(Arg^{11})CCMSH

Biodistribution of ^{99m}Tc-RfD-Lys-(Arg^{11})CCMSH in B16/F1 melanoma-bearing C57 mice. The data was presented as percent injected dose/gram or as percent injected dose (mean ± SD, n=4).

Tissue	0.5 h	2 h	4 h	24 h	2 h NDP Blockade
			Percent injected dose/gram (%ID/g)		
Tumor	9.56 ± 2.36	12.68 ± 2.39	15.01 ± 4.40	7.19 ± 1.02	2.82 ± 0.48*
Brain	0.16 ± 0.01	0.04 ± 0.01	0.03 ± 0.02	0.01 ± 0.01	0.04 ± 0.01
Blood	7.85 ± 2.12	1.01 ± 0.11	0.45 ± 0.12	0.06 ± 0.01	0.74 ± 0.01
Heart	2.67 ± 0.89	0.50 ± 0.17	0.45 ± 0.12	0.21 ± 0.08	0.60 ± 0.09
Lung	6.44 ± 1.81	2.73 ± 1.08	1.19 ± 0.44	0.47 ± 0.22	1.83 ± 0.35
Liver	6.59 ± 0.61	5.29 ± 1.30	4.47 ± 1.63	4.57 ± 0.45	3.77 ± 1.53
Skin	4.87 ± 0.41	1.25 ± 0.29	0.85 ± 0.11	0.34 ± 0.08	1.30 ± 0.43
Spleen	2.98 ± 1.23	1.26 ± 0.45	0.86 ± 0.19	0.76 ± 0.08	0.93 ± 0.36
Stomach	3.37 ± 1.40	2.71 ± 0.75	1.86 ± 0.46	0.51 ± 0.11	4.49 ± 0.85
Kidneys	103.75 ± 11.26	111.54 ± 10.19	104.95 ± 8.06	73.05 ± 9.87	111.34 ± 12.41
Muscle	0.45 ± 0.12	0.04 ± 0.03	0.02 ± 0.01	0.04 ± 0.03	0.03 ± 0.01
Pancreas	0.48 ± 0.16	0.38 ± 0.15	0.18 ± 0.03	0.05 ± 0.01	0.31 ± 0.11
Bone	0.07 ± 0.06	0.43 ± 0.07	0.15 ± 0.03	0.19 ± 0.14	0.38 ± 0.30
			Percent injected dose (%ID)		
Intestines	2.49 ± 0.60	2.58 ± 1.38	3.18 ± 1.08	0.82 ± 0.14	2.65 ± 1.53
Urine	22.56 ± 12.86	44.49 ± 12.39	50.50 ± 8.66	72.74 ± 7.36	54.88 ± 2.72
			Uptake ratio of tumor/normal tissue		
Tumor/Blood	1.22	12.55	33.36	119.83	3.81
Tumor/Kidneys	0.09	0.11	0.14	0.10	0.03
Tumor/Lung	1.48	4.64	12.61	15.30	1.54
Tumor/Liver	1.45	2.40	3.36	1.57	0.75
Tumor/Muscle	21.24	317.00	750.50	179.75	94.00

*$p<0.05$ ($p=0.002$) for determining the significance of differences in tumor and kidney uptake between ^{99m}Tc-RfD-Lys-(Arg^{11})CCMSH with or without NDP-MSH peptide blockade at 2 h post-injection.

Figure Legends

Figure 3.1. Schematic structures of RXD-Lys-(Arg^{11})CCMSH peptides.

Figure 3.2. The competitive binding curves of RSD-Lys-(Arg^{11})CCMSH (●), RNleD-Lys-(Arg^{11})CCMSH (▲), RFD-Lys-(Arg^{11})CCMSH (■), and RfD-Lys-(Arg^{11})CCMSH (♦) in B16/F1 murine melanoma cells. The IC_{50} value was 1.30 ± 0.36 nM for RSD-Lys-(Arg^{11})CCMSH, 2.99 ± 0.26 nM for RNleD-Lys-(Arg^{11})CCMSH, 0.82 ± 0.06 nM for RFD-Lys-(Arg^{11})CCMSH, and 1.35 ± 0.08 nM for RfD-Lys-(Arg^{11})CCMSH, respectively.

Figure 3.3. Radioactive HPLC profiles of ^{99m}Tc-RSD-Lys-(Arg^{11})CCMSH **(A)**, ^{99m}Tc-RFD-Lys-(Arg^{11})CCMSH **(B)** and ^{99m}Tc-RfD-Lys-(Arg^{11})CCMSH **(C)** in mouse serum after incubation at 37 °C for 24 h. The arrows denote the original retention times of ^{99m}Tc-RSD-Lys-(Arg^{11})CCMSH (12.5 min), ^{99m}Tc-RFD-Lys-(Arg^{11})CCMSH (18.4 min) and ^{99m}Tc-RfD-Lys-(Arg^{11})CCMSH (20.8 min) prior to the incubation in mouse serum.

Figure 3.4. Cellular internalization and efflux of ^{99m}Tc-RSD-Lys-(Arg^{11})CCMSH **(A and B)**, ^{99m}Tc-RFD-Lys-(Arg^{11})CCMSH **(C and D)** and ^{99m}Tc-RfD-Lys-(Arg^{11})CCMSH **(E and F)** in B16/F1 melanoma cells. Total bound radioactivity (♦), internalized radioactivity (■) and cell membrane radioactivity (▲) were presented as counts per minute (cpm).

Figure 3.5. Effect of *L*-lysine co-injection on the tumor and kidney uptakes of ^{99m}Tc-RSD-Lys-(Arg^{11})CCMSH at 2 h post-injection in B16/F1 melanoma-bearing C57 mice. The white (□) and black (■) columns represent the tumor and renal uptake of ^{99m}Tc-RSD-Lys-(Arg^{11})CCMSH with or without *L*-lysine co-injection. *L*-lysine co-injection significantly (*$p<0.05$) reduced the renal uptake of ^{99m}Tc-RSD-Lys-(Arg^{11})CCMSH by 37% at 2 h post-injection without affecting the tumor uptake.

Figure 3.6. Representative whole-body SPECT/CT image of B16/F1 melanoma- bearing C57 mice 2 h post injection of 7.4 MBq of ^{99m}Tc-RSD-Lys-(Arg^{11})CCMSH. Flank melanoma lesions (T) are highlighted with an arrow on the image.

Figure 3.7. Radioactive HPLC profiles of urinary metabolites at 2 h post-injection of ^{99m}Tc-RSD-Lys-(Arg^{11})CCMSH. The arrow denotes the original retention time of ^{99m}Tc-RSD-Lys-(Arg^{11})CCMSH (12.5 min) prior to tail vein injection.

Figure 3.1

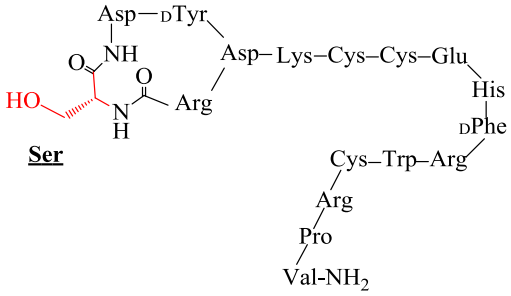

RSD-Lys-(Arg^{11})CCMSH

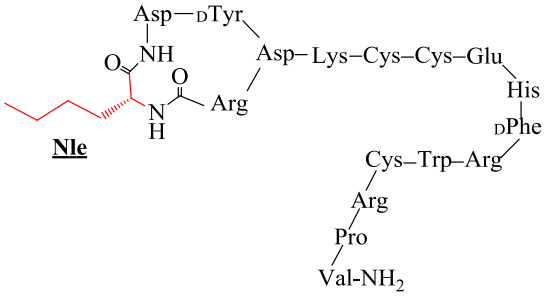

RNleD-Lys-(Arg^{11})CCMSH

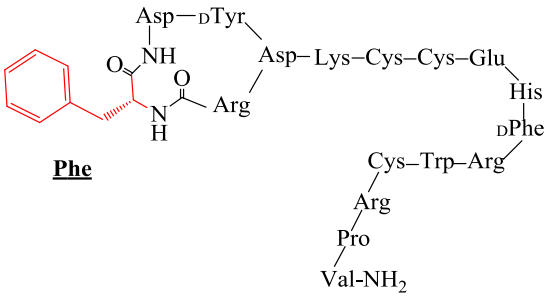

RFD-Lys-(Arg^{11})CCMSH

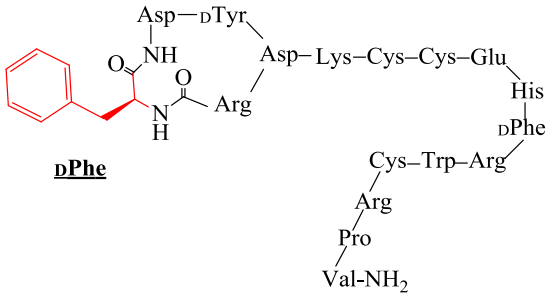

RfD-Lys-(Arg^{11})CCMSH

Figure 3.2

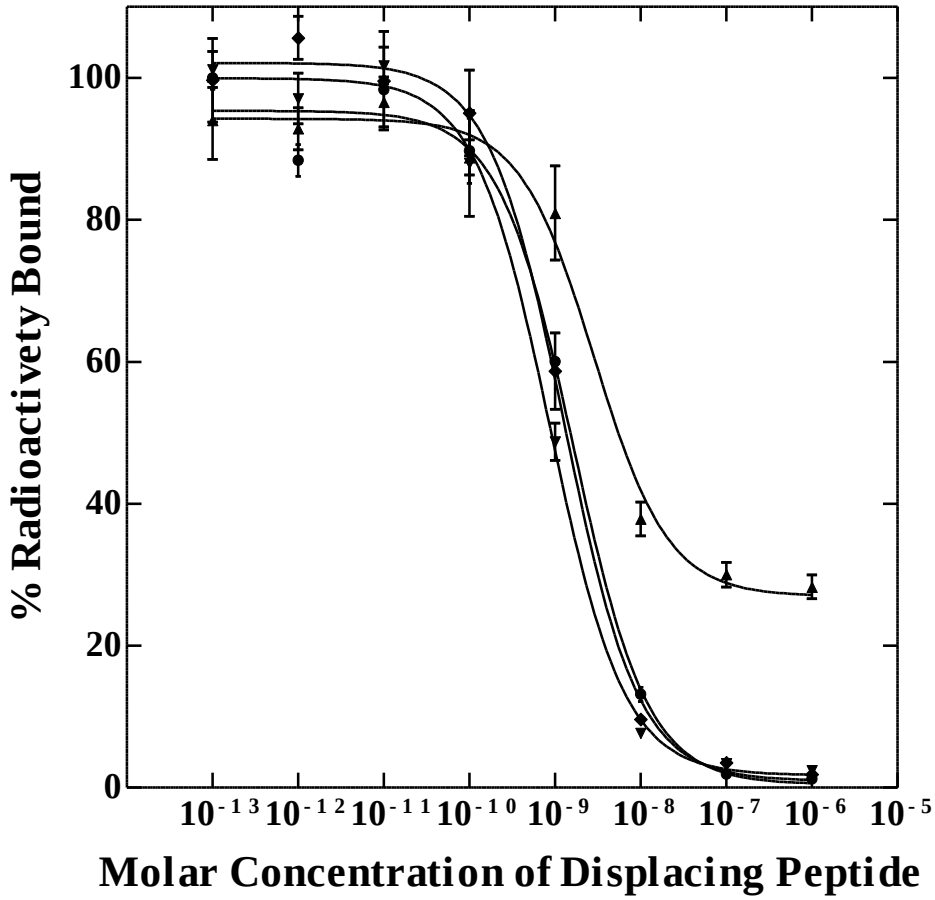
% Radioactivety Bound
100
80
60
40
20
0
10-13 10-12 10-11 10-10 10-9 10-8 10-7 10-6 10-5
Molar Concentration of Displacing Peptide

Figure 3.3

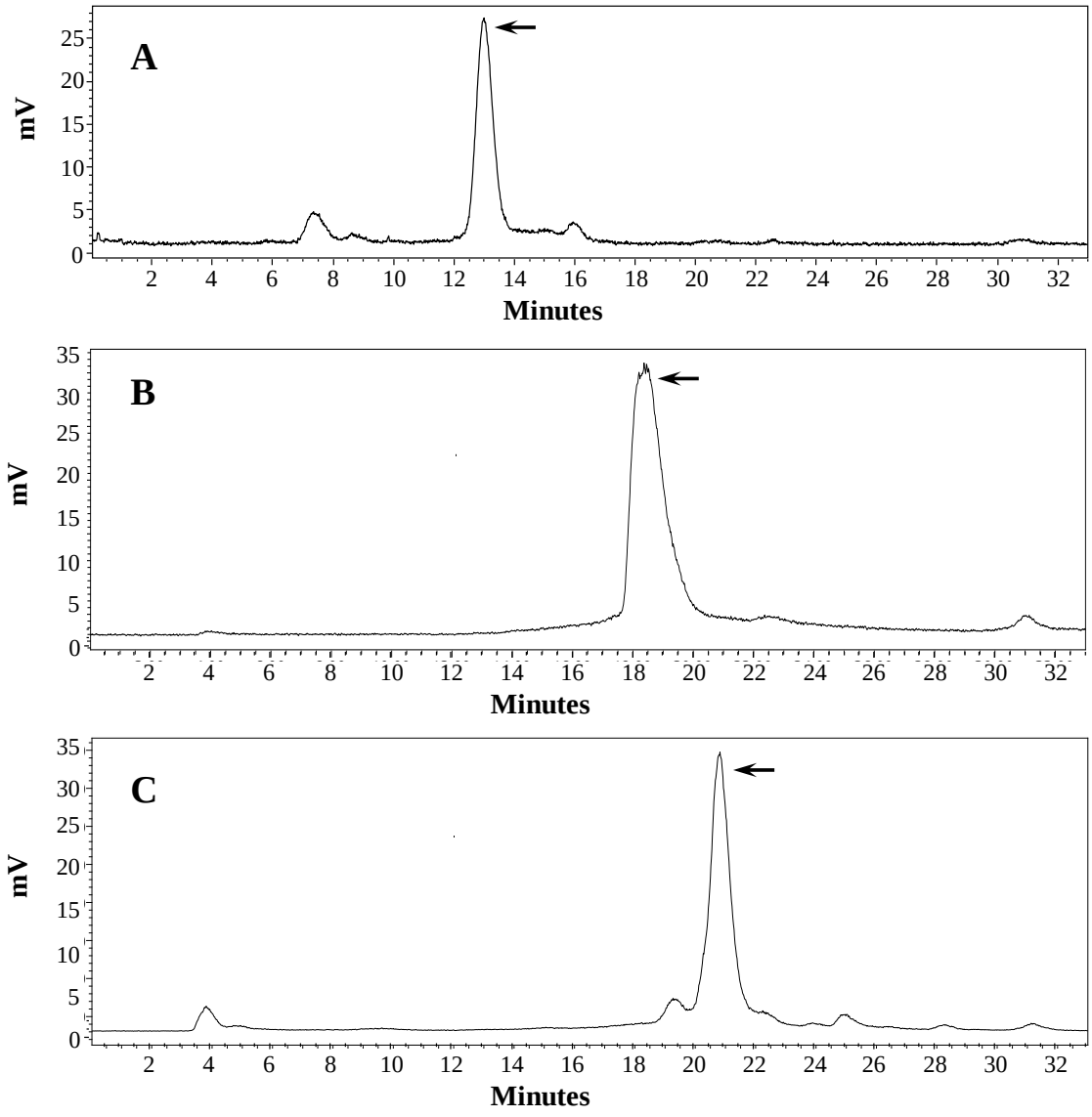

Figure 3.4

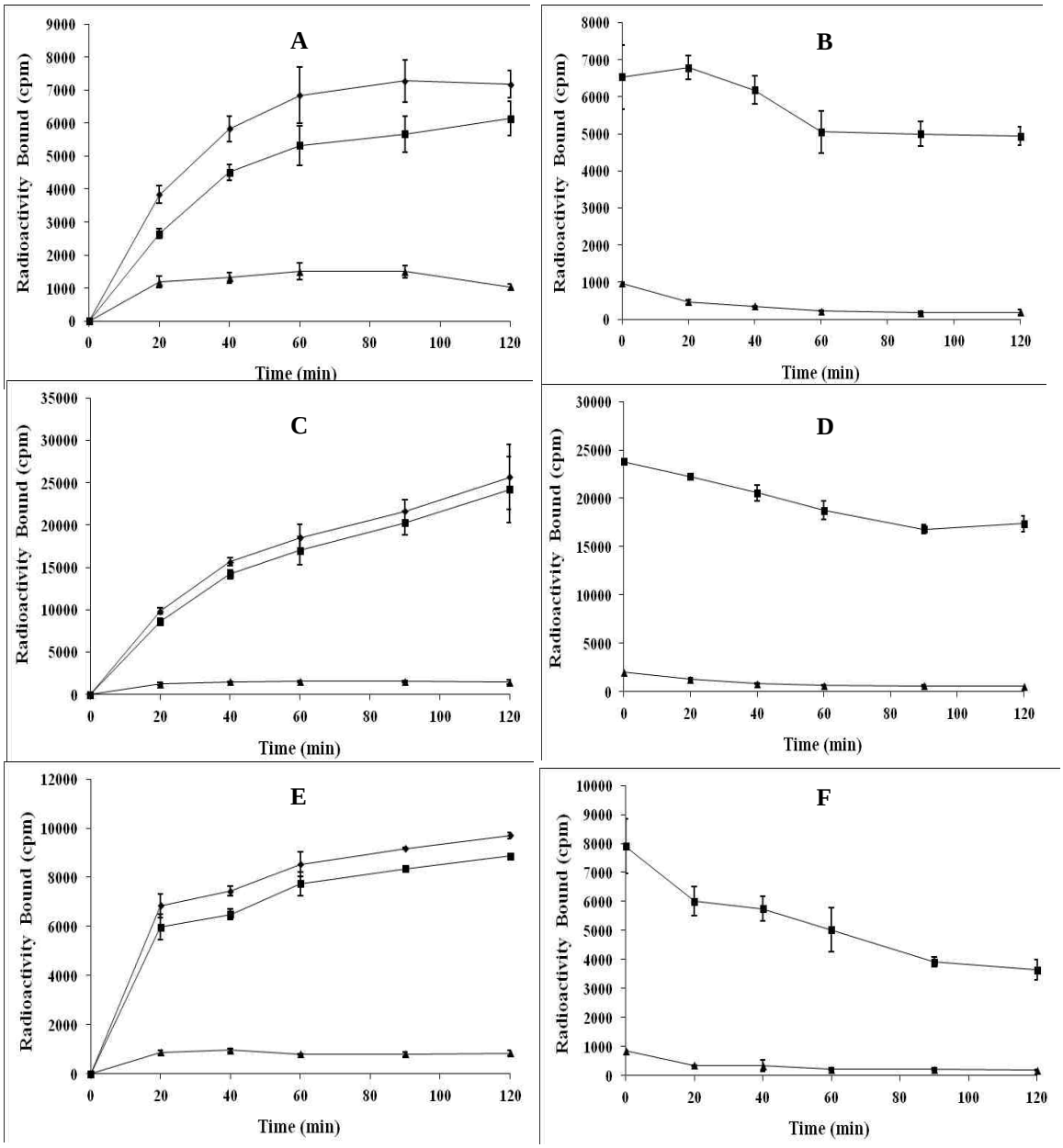

Figure 3.5

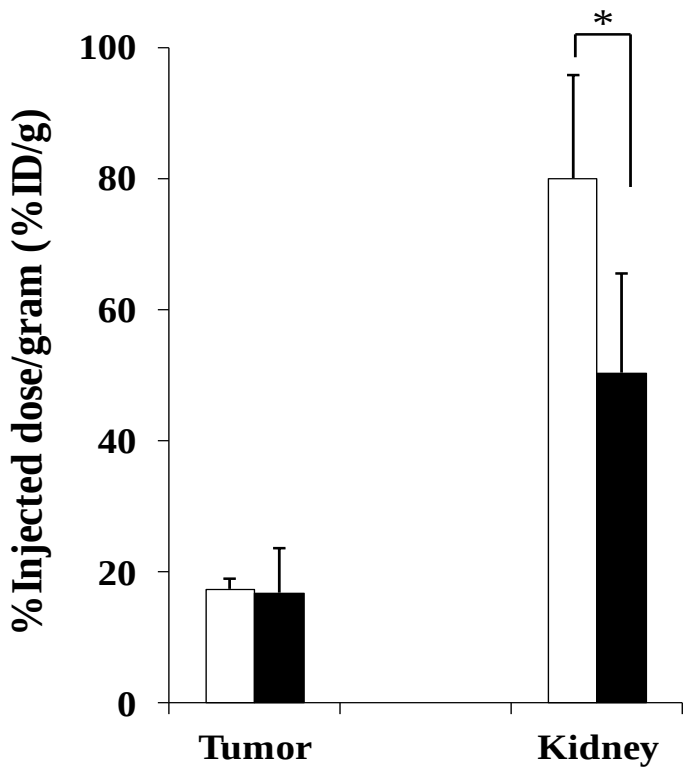

Figure 3.6

Figure 3.7

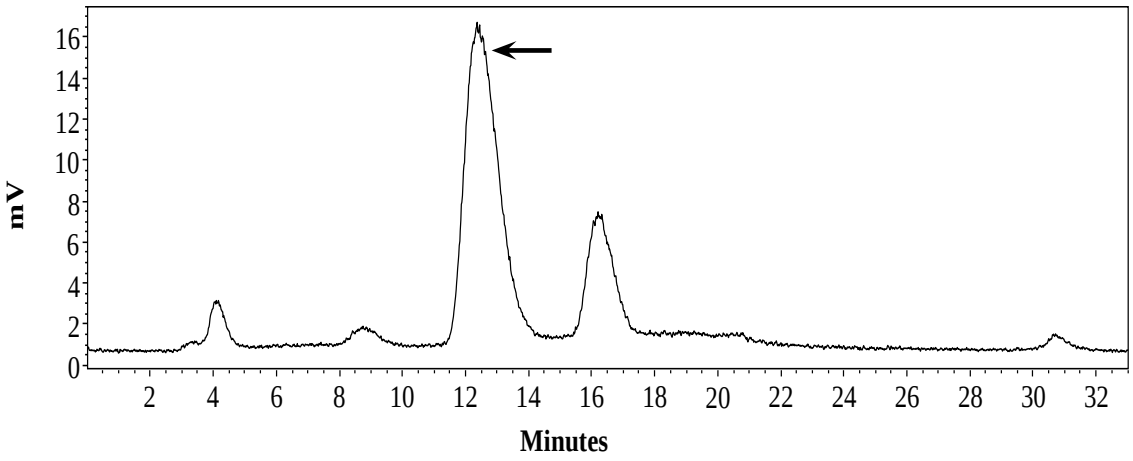
mV
16
14
12
10
8
6
4
2
0
2
4
6
8
10
12
14
16
18
20
22
24
26
28
30
32
Minutes

Chapter 4

Substitution of the Lys linker with the β-Ala linker dramatically decreased the renal uptake of Tc-99m-labeled Arg-X-Asp-conjugated and X-Ala-Asp-conjugated α-MSH peptides

Introduction

Melanocortin-1 (MC1) receptor is an attractive molecular target for melanoma imaging due to its over-expression on both murine and human melanoma cells [90, 91, 95, 100, 101, 105, 127, 129-137]. Recently, we have identified a class of ^{99m}Tc-labeled α-melanocyte stimulating hormone (α-MSH) peptides to target MC1 receptors for melanoma imaging. Specifically, the cyclic RXD motifs {Arg-X-Asp-$_D$Tyr-Asp, X = Gly, Ala, Val, Thr, Ser, Nle, Phe and $_D$Phe} were attached to [Cys^{3,4,10}, $_D$Phe^7, Arg^{11}]α-MSH$_{3-13}$ via a lysine linker to yield RXD-Lys-(Arg^{11})CCMSH peptides. Interestingly, single amino acid substitutions at the X position yielded a profound impact on the melanoma targeting and clearance properties of ^{99m}Tc-RXD-Lys-(Arg^{11})CCMSH peptides. For instance, the substitution of Gly in ^{99m}Tc-RGD-Lys-(Arg^{11})CCMSH with Ala, Thr, Val and Ser improved the MC1 receptor binding affinities and enhanced the melanoma uptake in B16/F1 melanoma-bearing C57 mice [128, 150, 151]. On the other hand, the substitution of Gly in ^{99m}Tc-RGD-Lys-(Arg^{11})CCMSH with Nle decreased the MC1 receptor binding affinity. Although the substitution of Gly in ^{99m}Tc-RGD-Lys-(Arg^{11})CCMSH with Phe and $_D$Phe increased the MC1 receptor binding affinities, both ^{99m}Tc-RFD-Lys-(Arg^{11})CCMSH and ^{99m}Tc-RfD-Lys-

(Arg^{11})CCMSH exhibited much higher liver uptake as compared to ^{99m}Tc-RGD-Lys-(Arg^{11})CCMSH [151].

Despite the promising melanoma targeting results, extremely high renal uptake (67-135% ID/g at 2 h post-injection) is a common issue associated with all ^{99m}Tc-RXD-Lys-(Arg^{11})CCMSH peptides [128, 150, 151]. Thus, it is desirable to reduce the non-specific renal uptake of ^{99m}Tc-RXD-Lys-(Arg^{11})CCMSH peptides to facilitate their potential therapeutic applications. In our previous reports, *L*-lysine co-injection significantly reduced the renal uptake of ^{99m}Tc-RXD-Lys-(Arg^{11})CCMSH peptides by 37%-51% at 2 h post-injection without affecting their tumor uptake [128, 150, 151]. *L*-lysine is a positively-charged amino acid. The effect of *L*-lysine co-injection in reducing the renal uptake indicated that the overall positive charge of the ^{99m}Tc-RXD-Lys-(Arg^{11})CCMSH peptides contributed their non-specific renal uptake. Obviously, the substitution of the positively-charged Lys linker with a neutral amino acid can decrease the overall charges of ^{99m}Tc-RXD-Lys-(Arg^{11})CCMSH peptides. According to the effect of *L*-lysine co-injection in decreasing the renal uptake, we hypothesized that the substitution of the Lys linker with a neutral β-Ala linker would decrease the renal uptake of the ^{99m}Tc-RXD-Lys-(Arg^{11})CCMSH peptides. To examine our hypothesis, we synthesized six peptides with β-Ala linkers, namely RSD-β-Ala-(Arg^{11})CCMSH, RTD-β-Ala-(Arg^{11})CCMSH, RVD-β-Ala-(Arg^{11})CCMSH, RAD-β-Ala-(Arg^{11})CCMSH, NAD-β-Ala-(Arg^{11})CCMSH and EAD-β-Ala-(Arg^{11})CCMSH. The MC1 receptor binding affinities of these six peptides were examined in B16/F1 melanoma cells. The peptides were readily radiolabeled with ^{99m}Tc using $SnCl_2$

as a reducing agent. We further determined the cellular internalization and efflux in B16/F1 melanoma cells and biodistribution properties in B16/F1 melanoma-bearing C57 mice for these six ^{99m}Tc-peptides. Thereafter, we determined the imaging properties of ^{99m}Tc-RAD-β-Ala-(Arg^{11})CCMSH in B16/F1 melanoma-bearing C57 mice.

Experimental Design and Methods

Chemicals and Reagents

Amino acids and resin were purchased from Advanced ChemTech Inc. (Louisville, KY) and Novabiochem (San Diego, CA). ^{125}I-Tyr^{2}-[Nle^{4}, DPhe^{7}]-α-MSH {^{125}I-(Tyr^{2})-NDP-MSH} was obtained from PerkinElmer, Inc. (Waltham, MA) for receptor binding assay. $^{99m}TcO_4^-$ was purchased from Cardinal Health (Albuquerque, NM). All other chemicals used in this study were purchased from Thermo Fischer Scientific (Waltham, MA) and used without further purification. B16/F1 murine melanoma cells were obtained from American Type Culture Collection (Manassas, VA).

Peptide Synthesis and In Vitro Competitive Binding Assay

RSD-β-Ala-(Arg^{11})CCMSH, RTD-β-Ala-(Arg^{11})CCMSH, RVD-β-Ala-(Arg^{11})CCMSH, RAD-β-Ala-(Arg^{11})CCMSH, NAD-β-Ala-(Arg^{11})CCMSH and EAD-β-Ala-(Arg^{11})CCMSH were synthesized using fluorenylmethyloxycarbonyl (Fmoc) chemistry according to our previously published procedures[17-19] with slight modification on Sieber amide resin by an Advanced ChemTech multiple-peptide synthesizer (Louisville, KY). Briefly, 70 µmol of Sieber amide resin and 210 µmol of Fmoc-protected amino acids were used for the synthesis. Fmoc-β-Ala was used to generate a β-Ala linker in the hybrid peptide. Each peptide was purified

by RP-HPLC and characterized by liquid chromatography-mass spectroscopy (LC-MS).

The IC_{50} values of RSD-β-Ala-(Arg^{11})CCMSH, RTD-β-Ala-(Arg^{11})CCMSH, RVD-β-Ala-(Arg^{11})CCMSH, RAD-β-Ala-(Arg^{11})CCMSH, NAD-β-Ala-(Arg^{11})CCMSH and EAD-β-Ala-(Arg^{11})CCMSH for the MC1 receptor were determined in B16/F1 melanoma cells. The receptor binding assay was replicated in triplicate for each peptide. The B16/F1 cells were seeded into a 24-well cell culture plate at a density of 2.5×10^5 cells/well and incubated at 37° C overnight. After being washed with binding medium {modified Eagle's medium with 25 mM N-(2-hydroxyethyl)-piperazine-N′-(2-ethanesulfonic acid) (HEPES), pH 7.4, 0.2% bovine serum albumin (BSA), 0.3 mM 1,10-phenathroline}, the cells were incubated at 25 °C for 2 h with approximately 30,000 counts per minute (cpm) of ^{125}I-(Tyr^2)-NDP-MSH in the presence of increasing concentrations (10^{-13} M to 10^{-6} M) of each peptide in 0.3 mL of binding medium. The reaction medium was aspirated after the incubation. The cells were rinsed twice with 0.5 mL of ice-cold pH 7.4, 0.2% BSA/0.01 M phosphate buffered saline (PBS) to remove any unbound radioactivity and lysed in 0.5 mL of 1 M NaOH for 5 min. The activities associated with the cells were measured in a Wallac 2480 automated gamma counter (PerkinElmer, NJ). The IC_{50} value for each peptide was calculated using Prism software (GraphPad Software, La Jolla, CA).

Peptide Radiolabeling

RSD-β-Ala-(Arg^{11})CCMSH, RTD-β-Ala-(Arg^{11})CCMSH, RVD-β-Ala-(Arg^{11})CCMSH, RAD-β-Ala-(Arg^{11})CCMSH, NAD-β-Ala-(Arg^{11})CCMSH and EAD-β-Ala-(Arg^{11})CCMSH were labeled with ^{99m}Tc via a direct reduction reaction using $SnCl_2$ as a reducing agent. Briefly, 10 µL of 1 mg/mL $SnCl_2$ in 0.1 M HCl, 40 µL of 0.5 M NH_4OAc (pH 5.2), 100 µL of 0.2 M Na_2tartate (pH 9.2), 100 µL of fresh $^{99m}TcO_4^-$ solution (37-74 MBq), and 10 µL of 1 mg/mL of each peptide in aqueous solution were added into a reaction vial and incubated at 25 °C for 20 min to form the ^{99m}Tc-labeled peptide. Each ^{99m}Tc-peptide was purified to a single species by Waters RP-HPLC (Milford, MA) on a Grace Vydac C-18 reverse phase analytic column (Deerfield, IL) using a 20-min gradient of 18-28% acetonitrile in 20 mM HCl aqueous solution at a flow rate of 1 mL/min. Each purified peptide was purged with N_2 gas for 20 min to remove the acetonitrile. The pH of final peptide solution was adjusted to 7.4 with 0.1 N NaOH and sterile normal saline for stability, biodistribution and imaging studies. The serum stabilities of ^{99m}Tc-RSD-β-Ala-(Arg^{11})CCMSH, ^{99m}Tc-RTD-β-Ala-(Arg^{11})CCMSH, ^{99m}Tc-RVD-β-Ala-(Arg^{11})CCMSH, ^{99m}Tc-RAD-β-Ala-(Arg^{11})CCMSH, ^{99m}Tc-NAD-β-Ala-(Arg^{11})CCMSH and ^{99m}Tc-EAD-β-Ala-(Arg^{11})CCMSH were determined by incubation in mouse serum at 37°C for 24 h and monitored for degradation by RP-HPLC. Briefly, 100 µL of each HPLC-purified peptide solution (~7.4 MBq) was added into 100 µL of mouse serum (Sigma-Aldrich Corp, St. Louis, MO) and incubated at 37 ^{o}C for 24 h. After the incubation, 200 µL of a mixture of ethanol

and acetonitrile (V:V = 1:1) was added to precipitate the serum proteins. The resulting mixture was centrifuged at 16,000 g for 5 min to collect the supernatant. The supernatant was purged with N_2 gas for 30 min to remove the ethanol and acetonitrile. The resulting sample was mixed with 500 µL of water and injected into RP-HPLC for analysis using the gradient described above.

Biodistribution Studies

All the animal studies were conducted in compliance with Institutional Animal Care and Use Committee approval. The biodistribution properties of ^{99m}Tc-RSD-β-Ala-(Arg^{11})CCMSH, ^{99m}Tc-RTD-β-Ala-(Arg^{11})CCMSH, ^{99m}Tc-RVD-β-Ala-(Arg^{11})CCMSH, ^{99m}Tc-RAD-β-Ala-(Arg^{11})CCMSH, ^{99m}Tc-NAD-β-Ala-(Arg^{11})CCMSH and ^{99m}Tc-EAD-β-Ala-(Arg^{11})CCMSH were determined in B16/F1 melanoma-bearing C57 female mice (Harlan, Indianapolis, IN). Each C57 mouse was subcutaneously inoculated on the right flank with 1×10^6 B16/F1 cells. The weight of tumors reached approximately 0.2 g 10 days post cell inoculation. Each melanoma-bearing mouse was injected with 0.037 MBq of ^{99m}Tc-RSD-β-Ala-(Arg^{11})CCMSH, ^{99m}Tc-RTD-β-Ala-(Arg^{11})CCMSH, ^{99m}Tc-RVD-β-Ala-(Arg^{11})CCMSH, ^{99m}Tc-RAD-β-Ala-(Arg^{11})CCMSH, ^{99m}Tc-NAD-β-Ala-(Arg^{11})CCMSH or ^{99m}Tc-EAD-β-Ala-(Arg^{11})CCMSH via the tail vein. Groups of 4 mice were sacrificed at 0.5, 2, 4 and 24 h post-injection, and tumors and organs of interest were harvested, weighed and counted. Blood values were taken as 6.5% of the body weight. The specificity of tumor uptake was determined by co-

injecting each ^{99m}Tc-peptide with 10 μg (6.1 nmol) of unlabeled NDP-MSH at 2 h post-injection.

Melanoma Imaging with ^{99m}Tc-RAD-β-Ala-(Arg^{11})CCMSH

^{99m}Tc-RAD-β-Ala-(Arg^{11})CCMSH was the lead peptide due to its highest tumor uptake and the lowest renal uptake. Thus, we further determined the melanoma imaging property of ^{99m}Tc-RAD-β-Ala-(Arg^{11})CCMSH. Approximately 4.1 MBq of ^{99m}Tc-RAD-β-Ala-(Arg^{11})CCMSH was injected into a B16/F1 melanoma-bearing C57 mouse via the tail vein. The mouse was euthanized for small animal SPECT/CT (Nano-SPECT/CT®, Bioscan, Washington DC) imaging 2 h post-injection. The 9-min CT imaging was immediately followed by the SPECT imaging of whole-body. The SPECT scans of 24 projections were acquired. Reconstructed data from SPECT and CT were visualized and co-registered using InVivoScope (Bioscan, Washington DC).

Urinary Metabolites of ^{99m}Tc-RAD-β-Ala-(Arg^{11})CCMSH

We also examined the urinary metabolites of ^{99m}Tc-RAD-β-Ala-(Arg^{11})CCMSH. Approximately 3.7 MBq of ^{99m}Tc-RAD-β-Ala-(Arg^{11})CCMSH was injected into a B16/F1 melanoma-bearing C57 mouse via the tail vein to determine the urinary metabolites. The mouse was euthanized to collect urine at 2 h post-injection. The collected urine sample was centrifuged at 16,000 g for 5

min before the HPLC analysis. Thereafter, an aliquot of the urine was injected into the HPLC. A 20-minute gradient of 16-26% acetonitrile / 20 mM HCl with a flow rate of 1 mL/min was used for urine analysis.

Statistical Analysis

Statistical analysis was performed using the Student's t-test for unpaired data to determine the significance of differences in tumor and kidney uptake with/without peptide blockade in biodistribution studies described above. Differences at the 95% confidence level ($p<0.05$) were considered significant.

Results

The schematic structures of RSD-β-Ala-(Arg^{11})CCMSH, RTD-β-Ala-(Arg^{11})CCMSH, RVD-β-Ala-(Arg^{11})CCMSH, RAD-β-Ala-(Arg^{11})CCMSH, NAD-β-Ala-(Arg^{11})CCMSH and EAD-β-Ala-(Arg^{11})CCMSH are presented in **Figure 4.1**. The peptides were synthesized and purified by reverse phase-high performance liquid chromatography (RP-HPLC) according to our previously published procedures [150, 151]. The overall synthetic yields were 30% for all six peptides. The chemical purities of RSD-β-Ala-(Arg^{11})CCMSH, RTD-β-Ala-(Arg^{11})CCMSH, RVD-β-Ala-(Arg^{11})CCMSH, RAD-β-Ala-(Arg^{11})CCMSH, NAD-β-Ala-(Arg^{11})CCMSH and EAD-β-Ala-(Arg^{11})CCMSH were greater than 95% after the HPLC purification. The peptide identities were confirmed by electrospray mass spectrometry. The measured molecular weight was 2123 Da for RSD-β-Ala-(Arg^{11})CCMSH, 2137 Da for RTD-β-Ala-(Arg^{11})CCMSH, 2135 Da for RVD-β-Ala-(Arg^{11})CCMSH, 2107 Da for RAD-β-Ala-(Arg^{11})CCMSH, 2064 Da for NAD-β-Ala-(Arg^{11})CCMSH and 2080 Da for EAD-β-Ala-(Arg^{11})CCMSH (**Table 4.1**). The competitive binding curves of the peptides are shown in **Figure 4.2**. The IC_{50} value was 2.76 ± 0.51 nM for RSD-β-Ala-(Arg^{11})CCMSH, 1.56 ± 0.63 nM for RTD-β-Ala-(Arg^{11})CCMSH, 1.99 ± 0.16 nM for RVD-β-Ala-(Arg^{11})CCMSH, 0.35 ± 0.01 nM for RAD-β-Ala-(Arg^{11})CCMSH, 3.34 ± 0.28 nM for NAD-β-Ala-(Arg^{11})CCMSH and 3.83 ± 0.71 nM for EAD-β-Ala-(Arg^{11})CCMSH in B16/F1 melanoma cells, respectively.

RSD-β-Ala-(Arg^{11})CCMSH, RTD-β-Ala-(Arg^{11})CCMSH, RVD-β-Ala-(Arg^{11})CCMSH, RAD-β-Ala-(Arg^{11})CCMSH, NAD-β-Ala-(Arg^{11})CCMSH and EAD-

β-Ala-(Arg^{11})CCMSH were readily radiolabeled with ^{99m}Tc with greater than 95% radiolabeling yields (**Table 4.1**). All six ^{99m}Tc-peptides were separated from their excess non-labeled peptides by RP-HPLC. The retention times of ^{99m}Tc-RSD-β-Ala-(Arg^{11})CCMSH, ^{99m}Tc-RTD-β-Ala-(Arg^{11})CCMSH, ^{99m}Tc-RVD-β-Ala-(Arg^{11})CCMSH, ^{99m}Tc-RAD-β-Ala-(Arg^{11})CCMSH, ^{99m}Tc-NAD-β-Ala-(Arg^{11})CCMSH and ^{99m}Tc-EAD-β-Ala-(Arg^{11})CCMSH were 13.1, 13.0, 14.1, 13.7, 17.0 and 14.2 min, respectively. All six ^{99m}Tc-peptides were stable in mouse serum at 37°C for 24 h (**Figure 4.3**).

Cellular internalization and efflux properties of ^{99m}Tc-RSD-β-Ala-(Arg^{11})CCMSH, ^{99m}Tc-RTD-β-Ala-(Arg^{11})CCMSH, ^{99m}Tc-RVD-β-Ala-(Arg^{11})CCMSH, ^{99m}Tc-RAD-β-Ala-(Arg^{11})CCMSH, ^{99m}Tc-NAD-β-Ala-(Arg^{11})CCMSH, and ^{99m}Tc-EAD-β-Ala-(Arg^{11})CCMSH were examined in B16/F1 cells. **Figure 4.4-4.5** illustrates the internalization and efflux properties of ^{99m}Tc-RSD-β-Ala-(Arg^{11})CCMSH, ^{99m}Tc-RTD-β-Ala-(Arg^{11})CCMSH, ^{99m}Tc-RVD-β-Ala-(Arg^{11})CCMSH, ^{99m}Tc-RAD-β-Ala-(Arg^{11})CCMSH, ^{99m}Tc-NAD-β-Ala-(Arg^{11})CCMSH, and ^{99m}Tc-EAD-β-Ala-(Arg^{11})CCMSH. All six ^{99m}Tc-peptides exhibited rapid cellular internalization and prolonged cellular retention. Approximately 64% of ^{99m}Tc-RSD-β-Ala-(Arg^{11})CCMSH, 66% of ^{99m}Tc-RTD-β-Ala-(Arg^{11})CCMSH, 70% of ^{99m}Tc-RVD-β-Ala-(Arg^{11})CCMSH, 77% of ^{99m}Tc-RAD-β-Ala-(Arg^{11})CCMSH, 70% of ^{99m}Tc-NAD-β-Ala-(Arg^{11})CCMSH and 67% of ^{99m}Tc-EAD-β-Ala-(Arg^{11})CCMSH activities were internalized in the cells after 20 min of incubation. Cellular efflux results indicated that 76% of ^{99m}Tc-RSD-β-Ala-(Arg^{11})CCMSH, 56% of ^{99m}Tc-RTD-β-Ala-(Arg^{11})CCMSH, 70% of ^{99m}Tc-RVD-β-

Ala-(Arg^{11})CCMSH, 66% of ^{99m}Tc-RAD-β-Ala-(Arg^{11})CCMSH, 70% of ^{99m}Tc-NAD-β-Ala-(Arg^{11})CCMSH and 54% of ^{99m}Tc-EAD-β-Ala-(Arg^{11})CCMSH activities remained inside the cells after 2 h of incubation in the culture medium.

The melanoma targeting and pharmacokinetic properties of ^{99m}Tc-RSD-β-Ala-(Arg^{11})CCMSH, ^{99m}Tc-RTD-β-Ala-(Arg^{11})CCMSH, ^{99m}Tc-RVD-β-Ala-(Arg^{11})CCMSH, ^{99m}Tc-RAD-β-Ala-(Arg^{11})CCMSH, ^{99m}Tc-NAD-β-Ala-(Arg^{11})CCMSH and ^{99m}Tc-EAD-β-Ala-(Arg^{11})CCMSH are shown in **Tables 4.2-4.7**. All six ^{99m}Tc-peptides exhibited similar tumor uptake pattern in B16/F1 melanoma-bearing C57 mice. The highest tumor uptake appeared either at 2 or 4 h post-injection. Among these six ^{99m}Tc-peptides, ^{99m}Tc-RAD-β-Ala-(Arg^{11})CCMSH showed the highest tumor uptake of 15.66 ± 6.19% ID/g at 2 h post-injection. The tumor uptake of ^{99m}Tc-RAD-β-Ala-(Arg^{11})CCMSH gradually decreased to 14.67 ± 3.81 and 7.79 ± 2.68% ID/g at 4 and 24 h post-injection. Co-injection of 10 μg (6.1 nM) of non-radiolabeled NDP-MSH with ^{99m}Tc-RAD-β-Ala-(Arg^{11})CCMSH decreased the tumor uptake to 2.43 ± 0.53% ID/g at 2 h post-injection, demonstrating that the tumor uptake was MC1 receptor-mediated.

Kidneys were the excretion routes for all six ^{99m}Tc-peptides. Among these six ^{99m}Tc-peptides, ^{99m}Tc-RAD-β-Ala-(Arg^{11})CCMSH showed the lowest renal uptake of 20.18 ± 3.86% ID/g at 2 h post-injection. The renal uptake of ^{99m}Tc-RAD-β-Ala-(Arg^{11})CCMSH gradually decreased to 19.83 ± 6.34 and 3.92 ± 0.99% ID/g at 4 and 24 h post-injection. Co-injection of 10 μg (6.1 nM) of non-radiolabeled NDP-MSH with ^{99m}Tc-RAD-β-Ala-(Arg^{11})CCMSH didn't significantly reduce the renal uptake ($p>0.05$) at 2 h post-injection, indicating that the renal

uptake was non-specific. The substitution of the positively-charged Lys linker with the neutral β-Ala dramatically decreased the renal uptake of ^{99m}Tc-RXD-β-Ala-(Arg^{11})CCMSH peptides. Interestingly, further reduction of the overall positive charge of ^{99m}Tc-NAD-β-Ala-(Arg^{11})CCMSH and ^{99m}Tc-EAD-β-Ala-(Arg^{11})CCMSH peptides did not further decrease the renal uptake as compared to ^{99m}Tc-RAD-β-Ala-(Arg^{11})CCMSH. All six ^{99m}Tc-peptides displayed fast urinary clearance. Approximately 68-78% of ^{99m}Tc-peptides cleared through the urinary system by 2 h post-injection, whereas approximately 77-86% of ^{99m}Tc-peptides washed out through the urinary system by 4 h post-injection. Normal organ uptake of all ^{99m}Tc-peptides was minimal (<3.1 % ID/g) except for kidneys after 2 h post-injection.

Because ^{99m}Tc-RAD-β-Ala-(Arg^{11})CCMSH showed the highest tumor uptake and the lowest renal uptake than the other five ^{99m}Tc-peptides at 2 h post-injection, we further determined the imaging property and urinary metabolites of ^{99m}Tc-RAD-β-Ala-(Arg^{11})CCMSH in B16/F1 melanoma-bearing C57 mice. Whole-body single photon emission computed tomography (SPECT)/CT image at 2 h post-injection is presented in **Figure 4.6**. Flank B16/F1 melanoma lesions were clearly visualized by SPECT using ^{99m}Tc-RAD-β-Ala-(Arg^{11})CCMSH peptide as an imaging probe. The SPECT image of tumor accurately matched its anatomical location obtained in the CT image. The SPECT image showed high contrast of tumor to normal organ except for kidneys, which was consistent with the biodistribution results. The urinary metabolites of ^{99m}Tc-RAD-β-Ala-

(Arg^{11})CCMSH at 2 h post-injection are shown in **Figure 4.7**. ^{99m}Tc-RAD-β-Ala-(Arg^{11})CCMSH remained intact in the urine at 2 h post-injection.

Discussion

In our previous reports [128, 150, 151], we have found the importance of single amino acid at the X position in the tumor targeting properties of ^{99m}Tc-RXD-Lys-(Arg^{11})CCMSH peptides in B16/F1 melanoma-bearing C57 mice. Specifically, the substitution of Gly in ^{99m}Tc-RGD-Lys-(Arg^{11})CCMSH with Ala, Thr, Val and Ser improved the MC1 receptor binding affinities and enhanced the melanoma uptake in B16/F1 melanoma-bearing C57 mice [128, 150, 151]. Despite the promising melanoma targeting results associated with ^{99m}Tc-RXD-Lys-(Arg^{11})CCMSH peptides, it is desirable to reduce the non-specific renal uptake (67-135% ID/g at 2 h post-injection) of ^{99m}Tc-RXD-Lys-(Arg^{11})CCMSH peptides to facilitate their potential therapeutic applications. In this study, we substituted the positively-charged Lys linker with the neutral β-Ala linker to determine whether such linker change could reduce the renal uptake of ^{99m}Tc-RXD-β-Ala-(Arg^{11})CCMSH peptides. Furthermore, we replaced the RAD moiety with NAD and EAD moieties to examine whether the further reduction of the overall positive changes of ^{99m}Tc-NAD-β-Ala-(Arg^{11})CCMSH and ^{99m}Tc-EAD-β-Ala-(Arg^{11})CCMSH could decrease their renal uptake further.

The substitution of Lys linker with β-Ala linker slightly affected the receptor binding affinities of RXD-β-Ala-(Arg^{11})CCMSH peptides. The receptor binding affinities of RXD-β-Ala-(Arg^{11})CCMSH peptides were approximately 2-fold weaker than RXD-Lys-(Arg^{11})CCMSH peptides, respectively. Despite the fact the -His-DPhe-Arg-Trp- motif is the binding moiety to the MC1 receptor, the decrease in receptor binding affinity with the β-Ala linker substitution indicated that the

linker might somehow interact with the receptor binding moiety. Such interaction might be related to the side chain of the Lys linker. The decrease in receptor binding affinities of RXD-β-Ala-(Arg^{11})CCMSH peptides also resulted in the reduction in tumor uptake of ^{99m}Tc-RXD-β-Ala-(Arg^{11})CCMSH peptides by 21-45% in B16/F1 melanoma-bearing C57 mice. Specifically, the tumor uptake of ^{99m}Tc-RAD-β-Ala-(Arg^{11})CCMSH was 79% of the tumor uptake of ^{99m}Tc-RAD-Lys-(Arg^{11})CCMSH at 2 h post-injection [128].

The substitution of Lys linker with β-Ala linker dramatically decreased the renal uptake of ^{99m}Tc-RXD-β-Ala-(Arg^{11})CCMSH peptides by 64-79% in B16/F1 melanoma-bearing C57 mice. For instance, the renal uptake of ^{99m}Tc-RAD-β-Ala-(Arg^{11})CCMSH was only 22% of the renal uptake of ^{99m}Tc-RAD-Lys-(Arg^{11})CCMSH at 2 h post-injection [128]. It is worthwhile to note that there is a positively-charged Arg residue in the RAD moiety of ^{99m}Tc-RAD-Lys-(Arg^{11})CCMSH. Thus, we were interested whether the replacement of Arg with Nle (neutral) and Glu (negatively-charged) could further decrease the renal uptake of ^{99m}Tc-NAD-β-Ala-(Arg^{11})CCMSH and ^{99m}Tc-EAD-β-Ala-(Arg^{11})CCMSH as compared to ^{99m}Tc-RAD-β-Ala-(Arg^{11})CCMSH. Interestingly, the replacement of Arg with Nle and Glu did not further decrease the renal uptake of ^{99m}Tc-NAD-β-Ala-(Arg^{11})CCMSH and ^{99m}Tc-EAD-β-Ala-(Arg^{11})CCMSH as compared to ^{99m}Tc-RAD-β-Ala-(Arg^{11})CCMSH. Clearly, the tumor targeting and clearance properties of ^{99m}Tc-RAD-β-Ala-(Arg^{11})CCMSH were more favorable than the other ^{99m}Tc-peptides investigated in this study. Thus, we further examined its melanoma imaging property and urinary metabolites. The B16/F1 melanoma

lesions could be clearly visualized by SPECT/CT using ^{99m}Tc-RAD-β-Ala-(Arg^{11})CCMSH as an imaging probe.

The dramatic reduction in renal uptake with the substitution of the neutral β-Ala linker demonstrates the importance of the electrostatic interactions of the positive charges on the peptides in renal handling and non-specific uptake *in-vivo*. It is imperative to maintain high contrast of tumor uptake to normal organ tissues for enhanced diagnostic imaging and potential therapeutic applications utilizing radiolabeled peptide conjugates as targeting molecules. ^{99m}Tc-labeled radiopharmaceuticals can be readily translated to therapeutic radiopharmaceuticals through the replacement of ^{99m}Tc with ^{186}Re/ ^{188}Re [152, 153]. Both ^{99m}Tc and ^{186}Re/ ^{188}Re have similar coordination chemistry. The same biomolecule can be labeled with ^{186}Re/ ^{188}Re without structural modification. The combined use of ^{99m}Tc- and ^{186}Re/ ^{188}Re-labeled radiopharmaceuticals for imaging and therapy will enhance the success of targeted radionuclide treatment for individual patients.

Conclusions

The substitution of the Lys linker with the β-Ala linker dramatically decreased the renal uptake of ^{99m}Tc-RXD-β-Ala-(Arg^{11})CCMSH peptides. Among these four ^{99m}Tc-RXD-β-Ala-(Arg^{11})CCMSH peptides, ^{99m}Tc-RAD-β-Ala-(Arg^{11})CCMSH exhibited the highest tumor uptake and the lowest renal uptake at 2 h post-injection. The replacement of Arg with Nle and Glu didn't further decrease the renal uptake of ^{99m}Tc-NAD-β-Ala-(Arg^{11})CCMSH and ^{99m}Tc-EAD-β-Ala-(Arg^{11})CCMSH as compared to ^{99m}Tc-RAD-β-Ala-(Arg^{11})CCMSH. The tumor targeting and clearance properties of ^{99m}Tc-RAD-β-Ala-(Arg^{11})CCMSH highlighted it as a lead peptide for future studies.

Tables

Table 4.1. Peptide properties

Capacity factors, chemical/ radiochemical purities, measured molecular weights, and IC_{50} values of RXD-β-Ala-(Arg^{11})CCMSH and XAD-β-Ala-(Arg^{11})CCMSH peptides and their ^{99m}Tc-conjugates.

Peptide	Capacity factor (k')	Chemical/Radiochemical Purity (%)	Measured Molecular Weight (Da)
RSD-β-Ala-(Arg^{11})CCMSH	1.35	95.32	2123
RTD-β-Ala-(Arg^{11})CCMSH	0.98	95.36	2137
RVD-β-Ala-(Arg^{11})CCMSH	1.94	95.89	2135
RAD-β-Ala-(Arg^{11})CCMSH	3.32	96.51	2107
NAD-β-Ala-(Arg^{11})CCMSH	3.17	95.62	2064
EAD-β-Ala-(Arg^{11})CCMSH	2.28	95.59	2080
^{99m}Tc-RSD-β-Ala-(Arg^{11})CCMSH	3.34	99.91	ND
^{99m}Tc-RTD-β-Ala-(Arg^{11})CCMSH	3.29	98.12	ND
^{99m}Tc-RVD-β-Ala-(Arg^{11})CCMSH	3.40	99.98	ND
^{99m}Tc-RAD-β-Ala-(Arg^{11})CCMSH	4.18	98.40	ND
^{99m}Tc-NAD-β-Ala-(Arg^{11})CCMSH	4.63	98.29	ND
^{99m}Tc-EAD-β-Ala-(Arg^{11})CCMSH	3.47	98.11	ND

ND= Not Determined

Table 4.2. Biodistribution of ^{99m}Tc-RSD-β-Ala-(Arg^{11})CCMSH

Biodistribution of ^{99m}Tc-RSD-β-Ala-(Arg^{11})CCMSH in B16/F1 melanoma-bearing C57 mice. The data was presented as percent injected dose/gram or as percent injected dose (mean ± SD, n=4).

Tissue	0.5 h	2h	4h	24 h	2h NDP-Block
Percentage Injected Dose/Gram (%ID/g)					
Tumor	9.64 ± 1.52	9.62 ± 1.53	12.15 ± 2.36	3.62 ± 1.10	1.12 ± 0.01*
Brain	0.15 ± 0.01	0.02 ± 0.01	0.02 ± 0.02	0.02 ± 0.01	0.02 ± 0.01
Blood	2.66 ± 0.84	0.50 ± 0.14	0.06 ± 0.02	0.61 ± 0.46	0.03 ± 0.01
Heart	1.56 ± 0.13	0.23 ± 0.04	0.10 ± 0.06	0.07 ± 0.03	0.17 ± 0.01
Lung	3.85 ± 0.40	0.64 ± 0.15	0.34 ± 0.11	0.29 ± 0.12	0.48 ± 0.06
Liver	1.41 ± 0.13	0.74 ± 0.08	0.86 ± 0.08	0.31 ± 0.08	0.57 ± 0.05
Skin	3.07 ± 1.85	0.52 ± 0.40	0.32 ± 0.13	0.48 ± 0.24	0.29 ± 0.18
Spleen	1.34 ± 0.15	0.32 ± 0.05	0.35 ± 0.05	0.18 ± 0.06	0.22 ± 0.06
Stomach	1.83 ± 0.20	0.62 ± 0.17	0.77 ± 0.21	0.32 ± 0.16	0.62 ± 0.23
Kidneys	30.5 ± 5.18	28.73 ± 3.40	28.70 ± 5.22	8.12 ± 2.34	13.67 ± 2.54
Muscle	0.25 ± 0.02	0.04 ± 0.03	0.02 ± 0.01	0.05 ± 0.02	0.05 ± 0.07
Pancreas	0.68 ± 0.28	0.11 ± 0.01	0.04 ± 0.02	0.04 ± 0.01	0.08 ± 0.01
Bone	0.93 ± 0.45	0.19 ± 0.06	0.05 ± 0.01	0.42 ± 0.28	0.16 ± 0.09
Percentage Injected Dose (%ID)					
Intestines	1.71 ± 0.21	1.11 ± 0.60	1.59 ± 0.41	0.63 ± 0.19	0.76 ± 0.23
Urine	53.37 ± 4.23	68.46 ± 9.28	83.96 ± 0.88	84.33 ± 3.37	90.95 ± 0.59
Uptake Ratio of Tumor/Normal Tissue					
Tumor/Blood	3.62	19.24	202.50	5.93	37.33
Tumor/Kidneys	0.32	0.33	0.42	0.45	0.08
Tumor/Lung	2.50	15.03	35.74	12.48	2.33
Tumor/Liver	6.84	13.00	14.13	11.68	1.96
Tumor/Muscle	38.56	240.50	607.50	72.40	22.40

$p<0.05$ ($p=0.001$,) for determining the significance of differences in tumor and kidney uptake between ^{99m}Tc-RSD-β-Ala-(Arg^{11})CCMSH with or without NDP-MSH peptide blockade at 2 h post-injection.

Table 4.3. Biodistribution of ^{99m}Tc-RTD-β-Ala-(Arg^{11})CCMSH

Biodistribution of ^{99m}Tc-RTD-β-Ala-(Arg^{11})CCMSH in B16/F1 melanoma-bearing C57 mice. The data was presented as percent injected dose/gram or as percent injected dose (mean ± SD, n=4).

Tissue	0.5 h	2h	4h	24 h	2h NDP-Block
Percentage Injected Dose/Gram (%ID/g)					
Tumor	13.29 ± 2.36	13.85 ± 1.43	9.40 ± 2.86	5.23 ± 1.81	1.19 ± 0.30*
Brain	0.20 ± 0.01	0.02 ± 0.01	0.01 ± 0.01	0.01 ± 0.01	0.01 ± 0.01
Blood	7.53 ± 0.99	1.48 ± 0.02	0.27 ± 0.17	0.06 ± 0.05	3.69 ± 0.01
Heart	2.38 ± 1.75	0.27 ± 0.07	0.14 ± 0.05	0.09 ± 0.02	0.22 ± 0.01
Lung	4.61 ± 3.16	0.53 ± 0.13	0.30 ± 0.01	0.16 ± 0.03	0.39 ± 0.14
Liver	1.36 ± 0.10	0.78 ± 0.02	0.73 ± 0.07	0.43 ± 0.11	0.61 ± 0.08
Skin	6.44 ± 2.64	1.33 ± 0.59	0.22 ± 0.15	0.22 ± 0.04	0.38 ± 0.08
Spleen	1.19 ± 0.58	0.31 ± 0.15	0.27 ± 0.14	0.23 ± 0.06	0.21 ± 0.07
Stomach	2.01 ± 0.72	0.83 ± 0.23	0.66 ± 0.20	0.37 ± 0.26	0.92 ± 0.37
Kidneys	35.79 ± 2.11	28.60 ± 5.14	26.17 ± 4.83	11.50 ± 2.81	18.09 ± 1.89^
Muscle	0.46 ± 0.19	0.06 ± 0.05	0.02 ± 0.01	0.03 ± 0.03	0.04 ± 0.01
Pancreas	1.25 ± 1.00	0.11 ± 0.09	0.02 ± 0.02	0.05 ± 0.03	0.07 ± 0.03
Bone	0.90 ± 0.90	0.29 ± 0.20	0.09 ± 0.07	0.11 ± 0.06	0.11 ± 0.04
Percentage Injected Dose (%ID)					
Intestines	2.28 ± 1.24	0.93 ± 0.21	1.29 ± 0.47	2.03 ± 1.42	0.84 ± 0.22
Urine	53.46 ± 7.42	77.83 ± 2.83	84.94 ± 2.10	90.45 ± 3.66	90.63 ± 2.07**
Uptake Ratio of Tumor/Normal Tissue					
Tumor/Blood	1.76	9.36	34.81	87.17	0.32
Tumor/Kidneys	0.37	0.48	0.36	0.45	0.07
Tumor/Lung	2.88	26.13	31.33	32.69	3.05
Tumor/Liver	9.77	17.76	12.88	12.16	1.95
Tumor/Muscle	28.89	230.83	470.00	174.33	29.75

*p<0.05 (*p=0.003, ^p=.015, **p=0.01) for determining the significance of differences in tumor and kidney uptake between ^{99m}Tc-RTD-β-Ala-(Arg^{11})CCMSH with or without NDP-MSH peptide blockade at 2 h post-injection.

Table 4.4. Biodistribution of ^{99m}Tc-RVD-β-Ala-(Arg^{11})CCMSH

Biodistribution of ^{99m}Tc-RVD-β-Ala-(Arg^{11})CCMSH in B16/F1 melanoma-bearing C57 mice. The data was presented as percent injected dose/gram or as percent injected dose (mean ± SD, n=4).

Tissue	0.5 h	2h	4h	24 h	2h NDP-Block
Percentage Injected Dose/Gram (%ID/g)					
Tumor	12.49 ± 2.10	13.11 ± 4.78	11.18 ± 2.76	4.66 ± 1.92	1.30 ± 0.46*
Brain	0.14 ± 0.01	0.03 ± 0.01	0.01 ± 0.01	0.03 ± 0.02	0.02 ± 0.01
Blood	6.11 ± 0.56	0.78 ± 0.06	0.14 ± 0.08	0.06 ± 0.01	0.43 ± 0.01
Heart	1.99 ± 0.11	0.35 ± 0.07	0.15 ± 0.02	0.08 ± 0.02	0.32 ± 0.06
Lung	2.61 ± 0.26	1.13 ± 0.09	0.41 ± 0.13	0.11 ± 0.02	0.64 ± 0.12
Liver	2.22 ± 0.05	1.36 ± 0.33	1.62 ± 0.34	0.50 ± 0.06	1.34 ± 0.23
Skin	4.86 ± 2.81	0.98 ± 0.44	0.16 ± 0.07	0.34 ± 0.05	0.82 ± 0.18
Spleen	1.36 ± 0.38	0.27 ± 0.14	0.31 ± 0.09	0.08 ± 0.02	0.34 ± 0.08
Stomach	2.82 ± 0.60	1.02 ± 0.48	0.85 ± 0.29	0.39 ± 0.15	1.74 ± 0.27
Kidneys	30.77 ± 2.40	30.37 ± 6.04	27.03 ± 0.71	7.58 ± 1.78	17.96 ± 5.92
Muscle	0.44 ± 0.11	0.17 ± 0.05	0.02 ± 0.02	0.14 ± 0.04	0.12 ± 0.07
Pancreas	0.76 ± 0.36	0.14 ± 0.01	0.10 ± 0.06	0.08 ± 0.06	0.10 ± 0.11
Bone	0.46 ± 0.12	0.60 ± 0.38	0.09 ± 0.09	0.17 ± 0.15	0.10 ± 0.05
Percentage Injected Dose (%ID)					
Intestines	1.89 ± 0.32	0.87 ± 0.22	1.33 ± 0.47	1.00 ± 0.59	0.90 ± 0.17
Urine	49.29 ± 2.66	74.19 ± 7.90	84.10 ± 4.44	84.47 ± 6.30	86.59 ± 4.94
Uptake Ratio of Tumor/Normal Tissue					
Tumor/Blood	2.04	16.81	79.86	77.67	3.02
Tumor/Kidneys	0.41	0.43	0.41	0.61	0.07
Tumor/Lung	4.79	11.60	27.27	42.36	2.03
Tumor/Liver	5.63	9.64	6.90	9.32	0.97
Tumor/Muscle	28.39	77.12	559.00	33.29	10.83

$p<0.05$ ($p=0.001$) for determining the significance of differences in tumor and kidney uptake between ^{99m}Tc-RVD-β-Ala-(Arg^{11})CCMSH with or without NDP-MSH peptide blockade at 2 h post-injection.

Table 4.5. Biodistribution of ^{99m}Tc-RAD-β-Ala-(Arg^{11})CCMSH

Biodistribution of ^{99m}Tc-RAD-β-Ala-(Arg^{11})CCMSH in B16/F1 melanoma-bearing C57 mice. The data was presented as percent injected dose/gram or as percent injected dose (mean ± SD, n=4).

Tissue	0.5 h	2h	4h	24 h	2h NDP-Block
Percentage Injected Dose/Gram (%ID/g)					
Tumor	12.55 ± 3.37	15.66 ± 6.19	14.67 ± 3.81	7.79 ± 2.68	2.43 ± 0.53*
Brain	0.19 ± 0.04	0.05 ± 0.01	0.03 ± 0.01	0.05 ± 0.05	0.02 ± 0.02
Blood	3.82 ± 0.62	1.01 ± 0.42	0.60 ± 0.29	0.46 ± 0.44	0.51 ± 0.10
Heart	2.28 ± 0.29	0.90 ± 0.34	0.69 ± 0.33	0.31 ± 0.21	0.73 ± 0.23
Lung	7.22 ± 1.60	3.15 ± 0.79	2.34 ± 1.19	1.01 ± 0.48	3.12 ± 1.13
Liver	2.39 ± 0.62	1.09 ± 0.13	1.05 ± 0.26	0.56 ± 0.23	1.17 ± 0.33
Skin	5.50 ± 0.60	1.38 ± 0.41	0.70 ± 0.13	0.42 ± 0.24	1.29 ± 0.42
Spleen	1.39 ± 0.51	0.80 ± 0.31	0.55 ± 0.34	0.60 ± 0.38	0.64 ± 0.43
Stomach	7.11 ± 2.20	2.61 ± 1.04	1.88 ± 0.63	0.44 ± 0.20	2.88 ± 0.65
Kidneys	25.64 ± 4.06	20.18 ± 3.86	19.83 ± 6.34	3.92 ± 0.99	19.82 ± 9.39
Muscle	0.90 ± 0.48	0.23 ± 0.14	0.18 ± 0.11	0.34 ± 0.32	0.17 ± 0.08
Pancreas	0.84 ± 0.35	0.29 ± 0.09	0.12 ± 0.08	0.20 ± 0.14	0.14 ± 0.05
Bone	1.60 ± 0.27	0.59 ± 0.16	0.24 ± 0.20	0.50 ± 0.42	0.33 ± 0.20
Percentage Injected Dose (%ID)					
Intestines	2.93 ± 0.44	2.58 ± 1.25	1.90 ± 0.39	0.89 ± 1.10	1.46 ± 0.26
Urine	49.54 ± 2.65	78.28 ± 2.36	83.80 ± 3.67	94.25 ± 1.90	83.61 ± 5.94
Uptake Ratio of Tumor/Normal Tissue					
Tumor/Blood	3.29	15.50	24.45	16.93	4.76
Tumor/Kidneys	0.49	0.78	0.74	1.99	0.12
Tumor/Lung	1.74	4.97	6.27	7.71	0.78
Tumor/Liver	5.25	14.37	13.97	13.91	2.08
Tumor/Muscle	13.94	68.09	81.50	22.91	14.29

*$p<0.05$ ($p=0.002$) for determining the significance of differences in tumor and kidney uptake between ^{99m}Tc-RAD-β-Ala-(Arg^{11})CCMSH with or without NDP-MSH peptide blockade at 2 h post-injection.

Table 4.6. Biodistribution of ^{99m}Tc-NAD-β-Ala-(Arg^{11})CCMSH

Biodistribution of ^{99m}Tc-NAD-β-Ala-(Arg^{11})CCMSH in B16/F1 melanoma-bearing C57 mice. The data was presented as percent injected dose/gram or as percent injected dose (mean ± SD, n=4).

Tissue	0.5 h	2h	4h	24 h	2h NDP-Block
Percentage Injected Dose/Gram (%ID/g)					
Tumor	3.43 ± 1.75	11.38 ± 1.29	10.81 ± 5.48	4.17 ± 1.14	2.06 ± 0.85*
Brain	0.17 ± 0.01	0.01 ± 0.01	0.02 ± 0.01	0.01 ± 0.01	0.05 ± 0.01
Blood	10.13 ± 1.66	1.02 ± 0.48	0.87 ± 0.43	0.14 ± 0.02	1.22 ± 0.01
Heart	1.85 ± 0.56	0.62 ± 0.03	0.56 ± 0.31	0.11 ± 0.03	0.48 ± 0.25
Lung	5.68 ± 1.37	2.31 ± 0.55	1.28 ± 0.27	0.74 ± 0.30	1.92 ± 0.41
Liver	2.03 ± 0.41	1.67 ± 0.39	1.37 ± 0.45	0.50 ± 0.08	1.93 ± 0.77
Skin	3.71 ± 1.95	1.14 ± 0.23	0.62 ± 0.10	0.16 ± 0.04	1.47 ± 0.68
Spleen	1.71 ± 0.74	0.76 ± 0.21	0.55 ± 0.08	0.20 ± 0.13	0.33 ± 0.20
Stomach	2.45 ± 1.72	1.14 ± 0.37	0.75 ± 0.06	0.25 ± 0.09	2.11 ± 0.84
Kidneys	32.37 ± 5.90	37.23 ± 9.69	32.68 ± 6.55	8.39 ± 2.56	22.48 ± 9.23
Muscle	0.33 ± 0.10	0.06 ± 0.06	0.15 ± 0.04	0.05 ± 0.01	0.39 ± 0.29
Pancreas	0.37 ± 0.23	0.22 ± 0.08	0.01 ± 0.01	0.01 ± 0.01	0.25 ± 0.14
Bone	0.75 ± 0.40	0.35 ± 0.29	0.03 ± 0.01	0.09 ± 0.07	0.19 ± 0.08
Percentage Injected Dose (%ID)					
Intestines	1.29 ± 0.67	2.84 ± 1.98	4.77 ± 3.46	0.59 ± 0.18	2.28 ± 0.78
Urine	53.93 ± 19.61	73.27 ± 5.41	77.67 ± 5.88	93.77 ± 1.03	74.78 ± 10.44
Uptake Ratio of Tumor/Normal Tissue					
Tumor/Blood	0.34	11.16	12.43	29.79	1.69
Tumor/Kidneys	0.11	0.31	0.33	0.50	0.09
Tumor/Lung	0.60	4.93	8.45	5.64	1.07
Tumor/Liver	1.69	6.81	7.89	8.34	1.07
Tumor/Muscle	10.39	189.67	72.07	83.40	5.28

*p<0.05 (*p=0.003) for determining the significance of differences in tumor and kidney uptake between ^{99m}Tc-NAD-β-Ala-(Arg^{11})CCMSH with or without NDP-MSH peptide blockade at 2 h post-injection.

Table 4.7. Biodistribution of ^{99m}Tc-EAD-β-Ala-(Arg^{11})CCMSH

Biodistribution of ^{99m}Tc-EAD-β-Ala-(Arg^{11})CCMSH in B16/F1 melanoma-bearing C57 mice. The data was presented as percent injected dose/gram or as percent injected dose (mean ± SD, n=4).

Tissue	0.5 h	2h	4h	24 h	2h NDP-Block
Percentage Injected Dose/Gram (%ID/g)					
Tumor	12.25 ± 1.86	10.13 ± 3.60	13.36 ± 4.12	3.71 ± 1.59	1.20 ± 0.25*
Brain	0.15 ± 0.01	0.02 ± 0.01	0.01 ± 0.01	0.01 ± 0.01	0.01 ± 0.01
Blood	5.94 ± 1.42	0.86 ± 0.04	0.38 ± 0.12	0.08 ± 0.01	0.47 ± 0.01
Heart	1.73 ± 0.35	0.44 ± 0.08	0.35 ± 0.03	0.14 ± 0.08	0.29 ± 0.15
Lung	3.50 ± 1.96	2.57 ± 1.00	1.35 ± 0.51	0.35 ± 0.08	1.73 ± 0.74
Liver	2.06 ± 0.73	1.08 ± 0.41	0.93 ± 0.16	0.26 ± 0.08	0.86 ± 0.03
Skin	5.92 ± 0.76	0.55 ± 0.03	0.64 ± 0.05	0.24 ± 0.02	0.86 ± 0.15
Spleen	1.95 ± 1.15	0.59 ± 0.25	0.49 ± 0.18	0.14 ± 0.11	0.26 ± 0.05
Stomach	2.91 ± 1.36	0.70 ± 0.12	0.89 ± 0.06	0.12 ± 0.02	1.16 ± 0.30
Kidneys	25.65 ± 8.27	25.25 ± 9.26	24.37 ± 7.66	4.12 ± 1.14	25.93 ± 1.62
Muscle	0.85 ± 0.26	0.05 ± 0.03	0.03 ± 0.01	0.10 ± 0.08	0.04 ± 0.04
Pancreas	0.72 ± 0.39	0.14 ± 0.07	0.06 ± 0.04	0.02 ± 0.01	0.07 ± 0.02
Bone	1.43 ± 0.32	0.27 ± 0.12	0.07 ± 0.03	0.14 ± 0.06	0.10 ± 0.05
Percentage Injected Dose (%ID)					
Intestines	2.19 ± 0.72	1.38 ± 0.92	2.29 ± 0.66	0.55 ± 0.16	2.51 ± 0.34
Urine	42.67 ± 21.25	75.09 ± 11.87	86.51 ± 3.43	92.30 ± 1.33	85.18 ± 0.53
Uptake Ratio of Tumor/Normal Tissue					
Tumor/Blood	2.06	11.78	35.16	46.38	2.55
Tumor/Kidneys	0.48	0.40	0.55	0.90	0.05
Tumor/Lung	3.50	3.94	9.90	10.60	0.69
Tumor/Liver	5.95	9.38	14.37	14.27	1.40
Tumor/Muscle	14.41	202.60	445.33	37.10	30.00

$p<0.05$ ($p=0.003$) for determining the significance of differences in tumor and kidney uptake between ^{99m}Tc-EAD-β-Ala-(Arg^{11})CCMSH with or without NDP-MSH peptide blockade at 2 h post-injection.

Figure Legends

Figure 4.1. Schematic structures of RXD-β-Ala-(Arg^{11})CCMSH & XAD-β-Ala-(Arg^{11})CCMSH peptides.

Figure 4.2. The competitive binding curves of RSD-β-Ala-(Arg^{11})CCMSH (●), RTD-β-Ala-(Arg^{11})CCMSH (■), RVD-β-Ala-(Arg^{11})CCMSH (▲), RAD-β-Ala-(Arg^{11})CCMSH (□), NAD-β-Ala-(Arg^{11})CCMSH (▽) and EAD-β-Ala-(Arg^{11})CCMSH (△), and in B16/F1 murine melanoma cells. The IC_{50} value was 2.76 ± 0.51 nM for RSD-β-Ala-(Arg^{11})CCMSH, 1.56 ± 0.63 nM for RTD-β-Ala-(Arg^{11})CCMSH, 1.99 ± 0.16 nM for RVD-β-Ala-(Arg^{11})CCMSH, 0.35 ± 0.01 nM for RAD-β-Ala-(Arg^{11})CCMSH, 3.34 ± 0.28 nM for NAD-β-Ala-(Arg^{11})CCMSH and 3.84 ± 0.71 nM for EAD-β-Ala-(Arg^{11})CCMSH respectively.

Figure 4.3. Radioactive HPLC profiles of ^{99m}Tc-RSD-β-Ala-(Arg^{11})CCMSH (A), ^{99m}Tc-RTD-β-Ala-(Arg^{11})CCMSH (B), ^{99m}Tc-RVD-β-Ala-(Arg^{11})CCMSH (C), ^{99m}Tc-RAD-β-Ala-(Arg^{11})CCMSH (D), ^{99m}Tc-NAD-β-Ala-(Arg^{11})CCMSH (E), and ^{99m}Tc-EAD-β-Ala-(Arg^{11})CCMSH (F) in mouse serum after incubation at 37 °C for 24 h. The arrows denote the original peak retention times of ^{99m}Tc-RSD-β-Ala-(Arg^{11})CCMSH (13.1 min), ^{99m}Tc-RTD-β-Ala-(Arg^{11})CCMSH (13.0 min), ^{99m}Tc-RVD-β-Ala-(Arg^{11})CCMSH (14.1 min), ^{99m}Tc-RAD-β-Ala-(Arg^{11})CCMSH (13.7 min), ^{99m}Tc-NAD-β-Ala-(Arg^{11})CCMSH (17.0 min), and ^{99m}Tc-EAD-β-Ala-(Arg^{11})CCMSH (14.2 min), prior to the incubation in mouse serum.

Figure 4.4. Cellular internalization and efflux of ^{99m}Tc-RSD-β-Ala-(Arg^{11})CCMSH (A and B), ^{99m}Tc-RTD-β-Ala-(Arg^{11})CCMSH (C and D) and ^{99m}Tc-RVD-β-Ala-(Arg^{11})CCMSH (E and F) in B16/F1 melanoma cells. Total bound radioactivity (♦), internalized radioactivity (■) and cell membrane radioactivity (▲) were presented as counts per minute (cpm).

Figure 4.5. Cellular internalization and efflux of ^{99m}Tc-RAD-β-Ala-(Arg^{11})CCMSH (G and H), ^{99m}Tc-NAD-β-Ala-(Arg^{11})CCMSH (I and J) and ^{99m}Tc-EAD-β-Ala-(Arg^{11})CCMSH (K and L) in B16/F1 melanoma cells. Total bound radioactivity (♦), internalized radioactivity (■) and cell membrane radioactivity (▲) were presented as counts per minute (cpm).

Figure 4.6. Representative whole-body SPECT/CT image of B16/F1 melanoma- bearing C57 mice 2 h post injection of 7.4 MBq of ^{99m}Tc-RAD-β-Ala-(Arg^{11})CCMSH. Flank melanoma lesions (T) are highlighted with an arrow on the image.

Figure 4.7. Radioactive HPLC profiles of urinary metabolites at 2 h post-injection of ^{99m}Tc-RAD-β-Ala-(Arg^{11})CCMSH. The arrow denotes the original retention time of ^{99m}Tc-RAD-β-Ala-(Arg^{11})CCMSH (15.98 min) prior to tail vein injection.

Figure 4.1

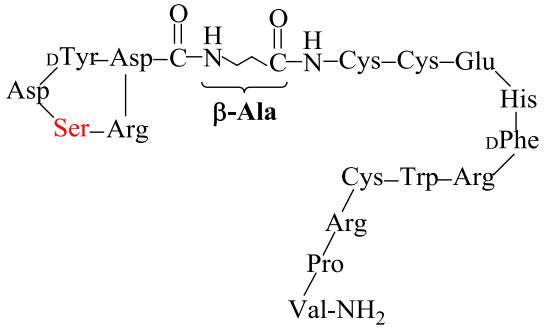

1: RSD-β-Ala-(Arg^{11})CCMSH

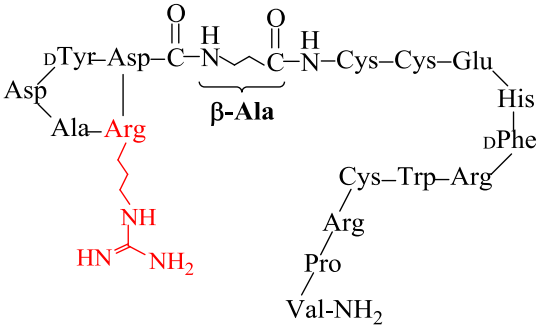

4: RAD-β-Ala-(Arg^{11})CCMSH

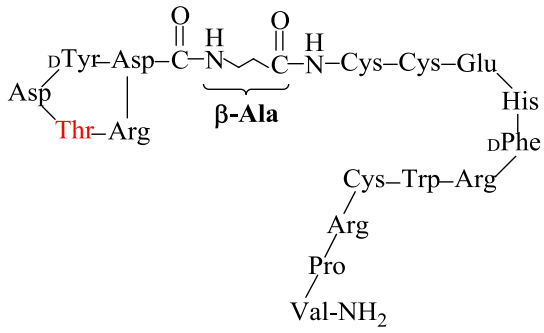

2: RTD-β-Ala-(Arg^{11})CCMSH

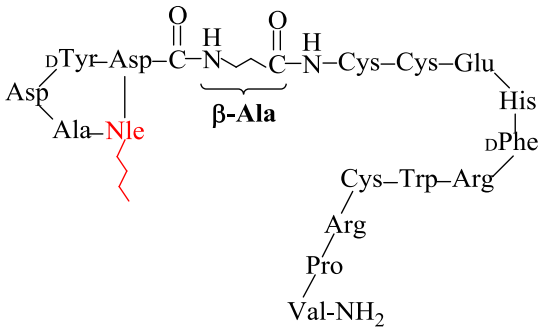

5: NAD-β-Ala-(Arg^{11})CCMSH

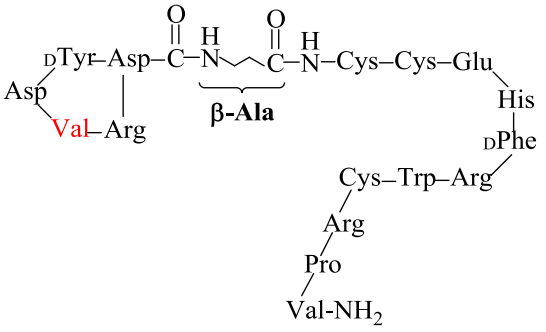

3: RVD-β-Ala-(Arg^{11})CCMSH

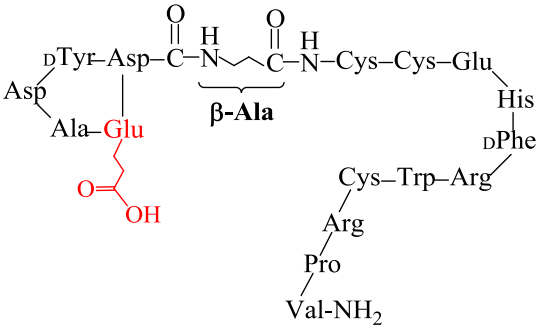

6: EAD-β-Ala-(Arg^{11})CCMSH

Figure 4.2

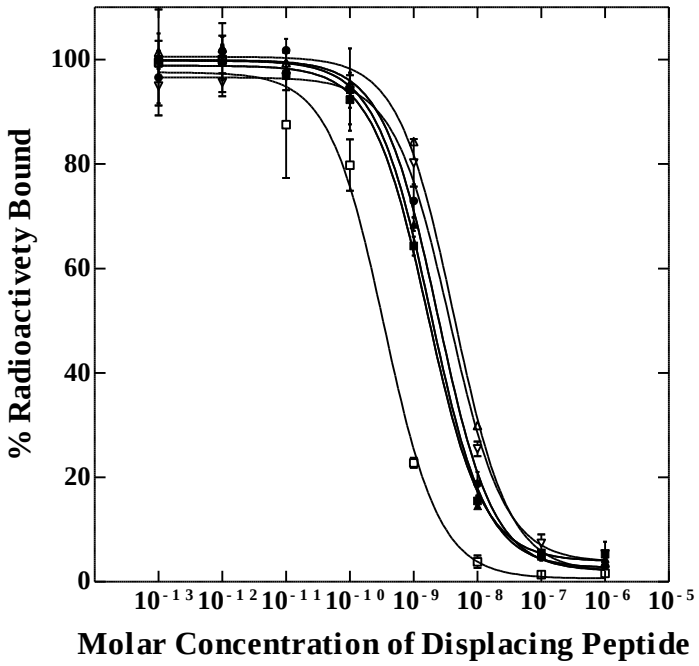
% Radioactivety Bound
100
80
60
40
20
0
10-13 10-12 10-11 10-10 10-9 10-8 10-7 10-6 10-5
Molar Concentration of Displacing Peptide

Figure 4.3

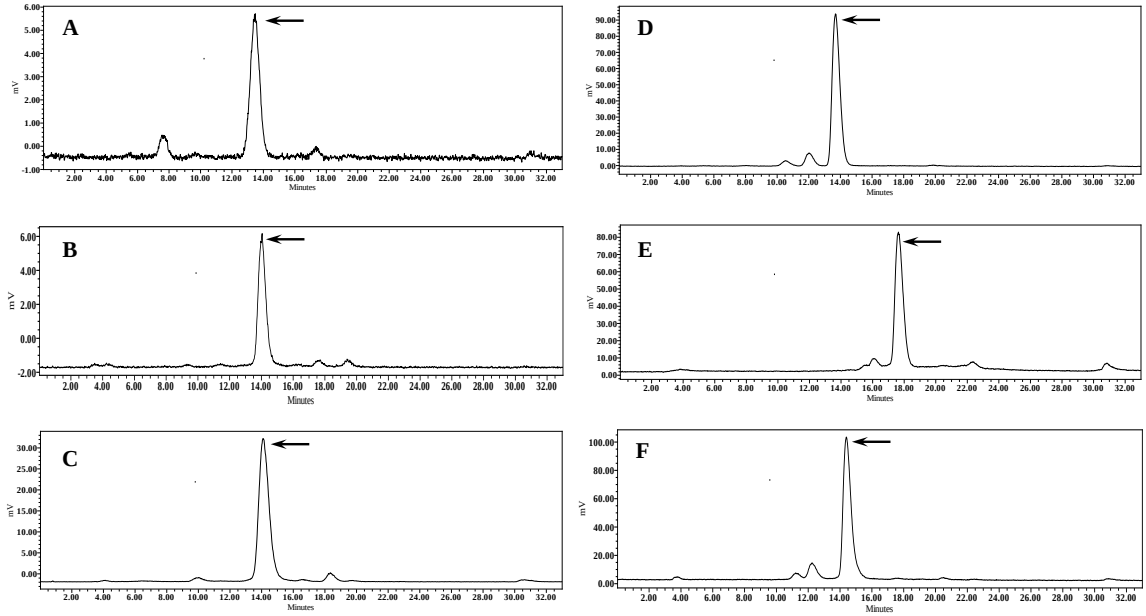

Figure 4.4

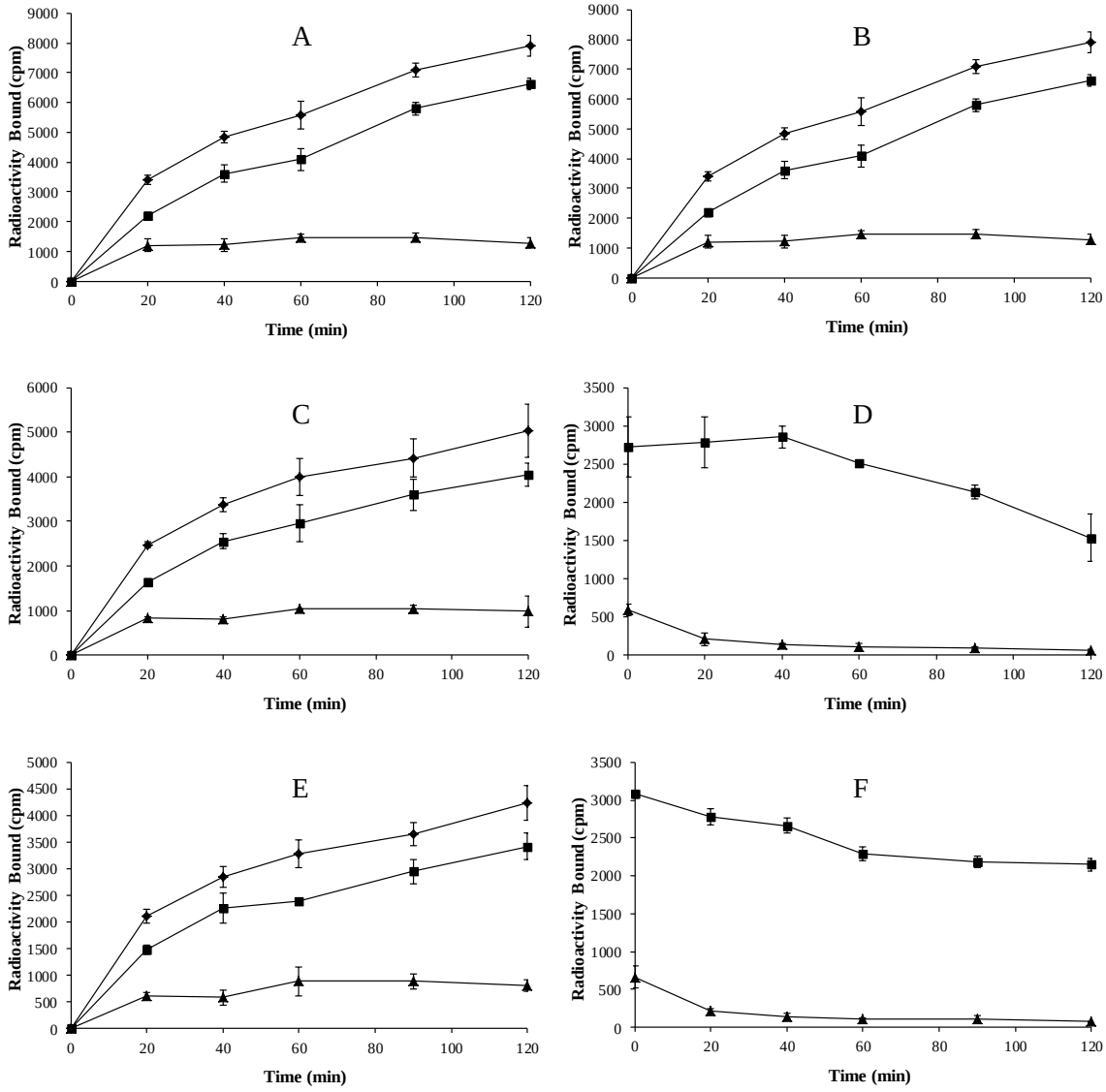

Figure 4.5

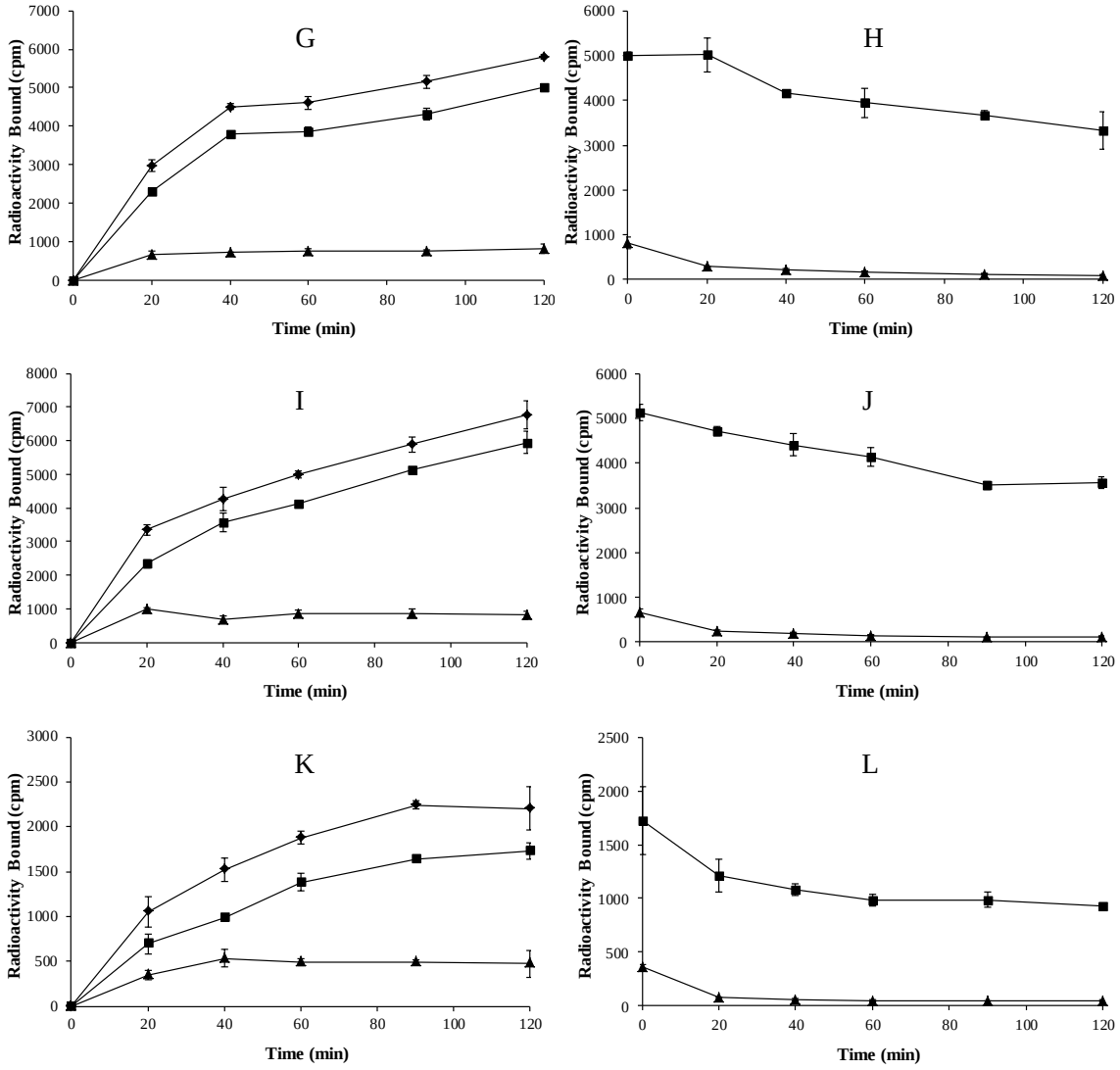

Figure 4.6

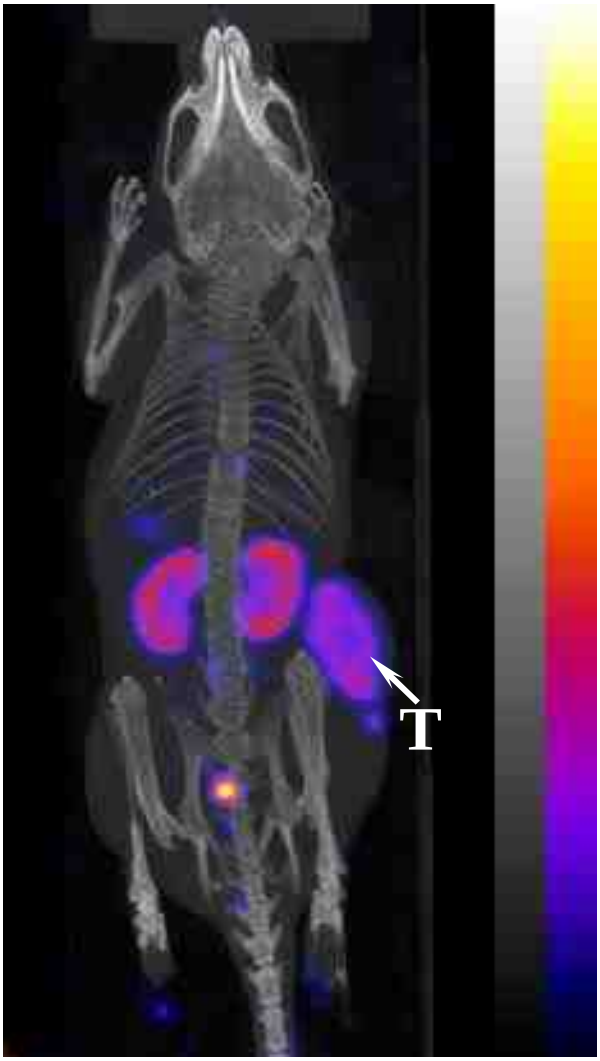

Figure 4.7

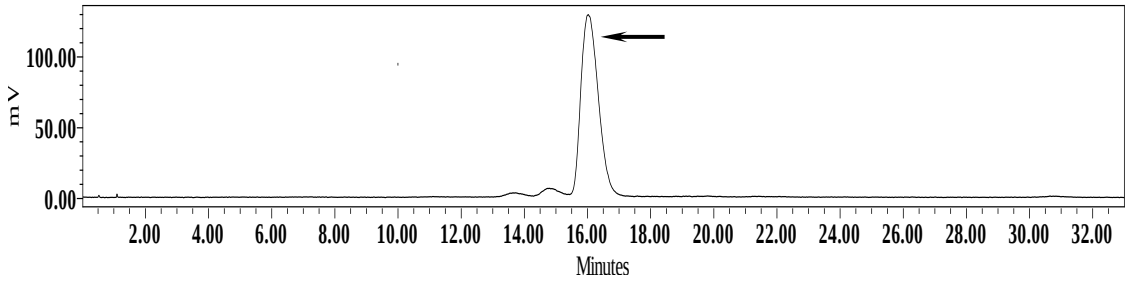
100.00
50.00
0.00
mV
2.00
4.00
6.00
8.00
10.00
12.00
14.00
16.00
18.00
20.00
22.00
24.00
26.00
28.00
30.00
32.00
Minutes

Chapter 5

Project Summary

The development of receptor-targeting diagnostic or therapeutic radiopharmaceuticals, has taken a near herculean effort; understanding the coordination chemistry involved within the metal complexes, determining optimal radiolabeling procedures, and designing the structures of the targeting biomolecules. At the present time, many ^{99m}Tc-labeled radiopharmaceuticals have been widely used as diagnostic imaging agents in various disease states such as cancer, thrombosis, infection, and inflammation. Administration of site-specific targeted radiopharmaceuticals provides the prospect of treating widely disseminated diseases, such as metastatic cancer. Ideally, the targeted radiopharmaceutical is designed to locate with high specificity to cancerous foci at locations undetected and unknown within the human body [152]. The use of small peptides in targeting of radiopharmaceuticals provides a mechanism of targeting specific overexpressed receptors on the cancerous cell surface, enabling high specificity targeting of the cancer cell while minimizing radiation to healthy tissues.

In this project, we developed novel iterations of α-melanocyte stimulating hormone peptides capable of binding the melanoma specific, melanocortin-1 receptor, in order to characterize and determine the most effective small peptides for melanoma targeting. Through previous research, it was determined that a single amino acid substitution of Gly to Ala in the RXD motif of the RGD-Lys-(Arg^{11})CCMSH peptide greatly improved MC1R binding affinity in B16/F1 murine

melanoma cells (2.0 nM vs 0.3 nM, respectively) [127]. In this study, we developed novel α-MSH peptides with further modifications to this same residue in order to examine the influence of the amino acid on *in-vivo* melanoma targeting of the α-MSH peptides. Initially the substitutions of the Gly residue with Thr and Val amino acids were performed to examine the effects of the –$CH(CH_3)OH$ and –$CH(CH_3)_2$ groups on the biodistribution properties of the ^{99m}Tc-labeled RTD-Lys-(Arg^{11})CCMSH and RVD-Lys-(Arg^{11})CCMSH peptides. The RTD-Lys-(Arg^{11})CCMSH and RVD-Lys-(Arg^{11})CCMSH peptides were synthesized via fluorenylmethyloxycarbonyl (Fmoc) chemistry and purified through RP-HPLC, with chemical purities >95%. Cellular binding studies on B16/F1 murine melanoma cells demonstrated increased affinity for the MC1R as compared to the original RGD-Lys-(Arg^{11})CCMSH peptide, but weaker affinity than the RAD-Lys-(Arg^{11})CCMSH peptide with IC_{50} values of 0.70 ± 0.07 nM for RTD-Lys-(Arg^{11})CCMSH and 1.00 ± 0.30 nM for RVD-Lys-(Arg^{11})CCMSH.

RTD-Lys-(Arg^{11})CCMSH and RVD-Lys-(Arg^{11})CCMSH peptides were radiolabeled with ^{99m}Tc and purified via RP-HPLC with radiochemical purities >95%. Both compounds demonstrated to be stable in mouse serum for 24 h at 37°C. *In-vivo* biodistribution studies in B16/F1 bearing female C57BL/6 mice revealed high receptor-mediated melanoma uptake as compared with ^{99m}Tc-RAD-Lys-(Arg^{11})CCMSH but with different uptake patterns. ^{99m}Tc-RTD-Lys-(Arg^{11})CCMSH showed the highest tumor uptake of 18.77 ± 5.13% ID/g at 2 h post-injection, whereas ^{99m}Tc-RVD-Lys-(Arg^{11})CCMSH showed the highest tumor uptake of 19.63 ± 4.68% ID/g at 4 h post-injection. Both the ^{99m}Tc-RTD-Lys-

(Arg^{11})CCMSH and ^{99m}Tc-RVD-Lys-(Arg^{11})CCMSH exhibited extremely high renal uptake at 0.5, 2, and 4 h post-injection with values ranging from 105.54 ± 27.67- 144.56 ± 24.64% ID/g for ^{99m}Tc-RTD-Lys-(Arg^{11})CCMSH and 73.92 ± 3.73- 94.01 ± 18.31% ID/g for ^{99m}Tc-RVD-Lys-(Arg^{11})CCMSH. SPECT/CT imaging studies utilizing ^{99m}Tc-RTD-Lys-(Arg^{11})CCMSH and ^{99m}Tc-RVD-Lys-(Arg^{11})CCMSH as imaging probes demonstrated that B16/F1 lesions could be clearly visualized by SPECT/CT imaging.

Further evaluation of the targeting and pharmacokinetic properties associated with the substitution of the Gly residue in the RXD motif was performed in the second study in which the Gly residue was substituted with Ser, Nle, Phe, and DPhe amino acids. The substitutions were designed to evaluate the effects of the long hydrocarbon chain (Nle), and the bulky benzene rings (Phe and DPhe) on MC1R binding affinity and melanoma targeting properties of the peptides. In addition, the $–CH_2OH$ group (Ser) was substituted in an attempt to facilitate urinary clearance of the peptides compared to the hydrophobic Nle, Phe, and DPhe compounds. The four peptides were synthesized utilizing a similar Fmoc chemistry approach as the previously described RTD-Lys-(Arg^{11})CCMSH and RVD-Lys-(Arg^{11})CCMSH peptides and purified to >95% chemical purity via RP-HPLC. Cellular binding studies on B16/F1 murine melanoma cells demonstrated varying impacts on the MC1R binding affinities of the peptides. The long hydrocarbon chain from the Nle amino acid on RNleD-Lys-(Arg^{11})CCMSH peptide exhibited decreased MC1R binding affinity, whereas the CH_2OH group from the Ser amino acid and the bulky benzene rings from the

Phe and DPhe amino acids increased MC1R binding affinity. IC_{50} values of RSD-Lys-(Arg^{11})CCMSH, RNleD-Lys-(Arg^{11})CCMSH, RFD-Lys-(Arg^{11})CCMSH, and RfD-Lys-(Arg^{11})CCMSH were 1.30 ± 0.36, 2.99 ± 0.26, 0.82 ± 0.06, and 1.35 ± 0.08 nM respectively. The differences in receptor binding affinities of these peptides indicate the Ser, Nle, Phe, and DPhe residues interact with the MC1R binding moiety differently. The subtle differences may be explained by the flexibility of the lactam bonds among the amino acid residues in the peptides.

In order to determine the *in-vivo* melanoma targeting, pharmacokinetic, and imaging properties of the RSD-Lys-(Arg^{11})CCMSH, RFD-Lys-(Arg^{11})CCMSH, and RfD-Lys-(Arg^{11})CCMSH peptides, all peptides were radiolabeled with ^{99m}Tc and purified through RP-HPLC to a radiochemical purity >95%. Due to the poor binding affinity of the RNleD-Lys-(Arg^{11})CCMSH peptide, further evaluation of the *in-vivo* tumor targeting properties was not warranted nor determined. Despite the similar pattern in B16/F1 cellular internalization and efflux, ^{99m}Tc-RSD-Lys-(Arg^{11})CCMSH exhibited a contrast in tumor uptake as compared to the ^{99m}Tc-RFD-Lys-(Arg^{11})CCMSH and ^{99m}Tc-RfD-Lys-(Arg^{11})CCMSH peptides. ^{99m}Tc-RSD-Lys-(Arg^{11})CCMSH exhibited rapid and high receptor-specific melanoma uptake of 18.01 ± 4.22% ID/g at 30 min post-injection, whereas ^{99m}Tc-RFD-Lys-(Arg^{11})CCMSH and ^{99m}Tc-RfD-Lys-(Arg^{11})CCMSH exhibited their peak melanoma uptake values of 13.11 ± 1.21 and 15.01 ± 4.40% ID/g at 4 h post-injection, respectively. In addition, ^{99m}Tc-RSD-Lys-(Arg^{11})CCMSH displayed 45% and 32% lower renal uptake values at 24 h than ^{99m}Tc-RFD-Lys-(Arg^{11})CCMSH and ^{99m}Tc-RfD-Lys-(Arg^{11})CCMSH respectively. Renal uptake values were still

extremely high ranging from 69.23 ± 17.41% ID/g at 4 h post-injection to 80.01 ± 15.67% ID/g at 2 h post-injection. Not surprisingly, however, ^{99m}Tc-RSD-Lys-(Arg^{11})CCMSH showed 12% and 23% lower liver uptake than ^{99m}Tc-RFD-Lys-(Arg^{11})CCMSH and ^{99m}Tc-RfD-Lys-(Arg^{11})CCMSH, due to the absence of the bulky benzene ring. Furthermore, ^{99m}Tc-RSD-Lys-(Arg^{11})CCMSH exhibited faster urinary clearance over all time points as compared to both ^{99m}Tc-RFD-Lys-(Arg^{11})CCMSH and ^{99m}Tc-RfD-Lys-(Arg^{11})CCMSH. SPECT/CT imaging studies utilizing ^{99m}Tc-RSD-Lys-(Arg^{11})CCMSH as an imaging probe demonstrated that B16/F1 lesions could be clearly visualized in B16/F1 bearing female C57BL/6 mice.

The extremely high renal uptake (67-135% ID/g at 2 h post-injection) has become a common implication for all the reported ^{99m}Tc-RXD-Lys-(Arg^{11})CCMSH peptides [128, 146, 150]. In order to facilitate further therapeutic applications of these peptides, non-specific renal uptake must be reduced. In clinical cases today, renal toxicity is the dose limiting factor in peptide-receptor radionuclide therapy (PRRT), as acute nephrotoxicity and acute renal failure seen in patients occurs due to accumulation of radiation dosage in the kidneys [154, 155]. It is hypothesized that renal handling of these radiopharmaceuticals and peptides is facilitated by the charge distribution throughout targeting molecule. In the nephron, evidence has indicated that cationic and neutral molecules are filtered through the glomerulus more efficiently than anionic molecules possibly due to the negatively charged basement membrane of the glomerulus [154, 156]. In addition, the proximal tubule contains negatively charged organic cation transfer

(OCT) cell surface receptors that can interact with positively charged molecules [154].

With the overall positive charge and strong positive charge of the Lys linker in the ^{99m}Tc-RXD-Lys-(Arg^{11})CCMSH peptides, it stands to reason that high renal uptake of these peptides is due to their potential electrostatic interactions with multiple constituents of renal physiology. As a proof-of-concept study, co-injection of purified positively charged L-Lys amino acid with the ^{99m}Tc-RXD-Lys-(Arg^{11})CCMSH peptides was performed. Co-injection of the L-Lys amino acid dramatically decreased non-specific renal uptake of the ^{99m}Tc-RXD-Lys-(Arg^{11})CCMSH peptides 37-50%, without affecting the tumor targeting properties of those peptides. This reduction elucidated the necessity to mitigate the overall positive charge of the ^{99m}Tc-RXD-Lys-(Arg^{11})CCMSH peptides in order to facilitate reduced non-specific renal uptake. Clearly, the substitution of the positively charged Lys linker in the ^{99m}Tc-RXD-Lys-(Arg^{11})CCMSH to a neutral or negatively charged linker (i.e. Gly or Glu) can decrease the overall charge of the ^{99m}Tc-RXD-Lys-(Arg^{11})CCMSH peptides. In previous studies, reducing the overall positive charge of ^{111}In-DOTA-GlyGlu-CycMSH via a negatively charged glutamic acid linker coincided with a 44% reduction in renal uptake as compared to ^{111}In-DOTA-CycMSH [100]. According to the effect seen in the L-Lys co-injection studies and with the introduction of the glutamic acid linker in previous studies, it was likely that such a substitution will provide a significant reduction in non-specific renal uptake of the ^{99m}Tc-RXD-Lys-(Arg^{11})CCMSH peptides.

In the final study of this project we designed a multitude of novel α-MSH peptides with reduced overall net charge. The positively charged Lys linker in the RXD-Lys-(Arg^{11})CCMSH peptides was replaced with a neutral β-Ala linker to yield the novel RAD-β-Ala-(Arg^{11})CCMSH, RSD-β-Ala-(Arg^{11})CCMSH, RTD-β-Ala-(Arg^{11})CCMSH, and RVD-β-Ala-(Arg^{11})CCMSH peptides. In addition, we designed the novel XAD-β-Ala-(Arg^{11})CCMSH peptides containing substitutions of the positively charged Arg residue in the RXD motif with a neutral Nle amino acid and negatively charged Glu residue to create the NAD-β-Ala-(Arg^{11})CCMSH EAD-β-Ala-(Arg^{11})CCMSH peptides, respectively. The substitutions of these amino acids were performed to eliminate as many charge dipoles on the peptide backbone as possible to facilitate reduction in the non-specific renal uptake seen with the RXD-Lys-(Arg^{11})CCMSH peptides.

All peptides were synthesized utilizing a similar Fmoc chemistry approach as described for the RXD-Lys-(Arg^{11})CCMSH peptides and purified via RP-HPLC to a chemical purity >95%. Cellular binding studies performed in B16/F1 cells demonstrated continued low nanomolar binding affinity for the RXD-β-Ala-(Arg^{11})CCMSH and XAD-β-Ala-(Arg^{11})CCMSH peptides. IC_{50} values for the RAD-β-Ala-(Arg^{11})CCMSH, RSD-β-Ala-(Arg^{11})CCMSH, RTD-β-Ala-(Arg^{11})CCMSH, and RVD-β-Ala-(Arg^{11})CCMSH peptides were 0.35 ± 0.01, 2.76 ± 0.51, 1.56 ± 0.63, and 1.99 ± 0.16 nM respectively. These values were comparable to their Lys linker counterparts demonstrating no significant loss in binding affinity for the MC1R. The binding affinity of the XAD-β-Ala-(Arg^{11})CCMSH peptides for the MC1R was slightly lower with IC_{50} values of 3.84

± 0.71 and 3.34 ± 0.28 nM for EAD-β-Ala-(Arg^{11})CCMSH and NAD-β-Ala-(Arg^{11})CCMSH respectively.

In order to determine the *in-vivo* melanoma targeting, pharmacokinetic, and imaging properties of the RXD-β-Ala-(Arg^{11})CCMSH and XAD-β-Ala-(Arg^{11})CCMSH peptides, all peptides were radiolabeled with ^{99m}Tc and purified through RP-HPLC to a radiochemical purity >95%. All RXD-β-Ala-(Arg^{11})CCMSH peptides exhibited rapid and high receptor-specific melanoma uptake similar to their Lys linker counterparts with the exception of RSD-β-Ala-(Arg^{11})CCMSH. RAD-β-Ala-(Arg^{11})CCMSH exhibited peak melanoma uptake of 15.66 ± 6.19% ID/g at 2 h post-injection, not significantly different to RAD-Lys-(Arg^{11})CCMSH with a peak melanoma uptake of 19.91 ± 4.02% ID/g. RTD-β-Ala-(Arg^{11})CCMSH exhibited peak melanoma uptake of 13.85 ± 1.43% ID/g at 2 h post-injection, not significantly different to RTD-Lys-(Arg^{11})CCMSH with a peak melanoma uptake of 18.77 ± 5.13% ID/g. RVD-β-Ala-(Arg^{11})CCMSH exhibited peak melanoma uptake of 13.11 ± 4.78% ID/g at 2 h post-injection, not significantly different to RVD-Lys-(Arg^{11})CCMSH with a peak melanoma uptake of 17.10 ± 3.82% ID/g. As previously stated, RSD-β-Ala-(Arg^{11})CCMSH exhibited peak melanoma uptake of 12.15 ± 2.36% ID/g at 4 h post-injection, which was significantly different to RSD-Lys-(Arg^{11})CCMSH with a peak melanoma uptake of 17.42 ± 1.52% ID/g at 2 h post-injection. EAD-β-Ala-(Arg^{11})CCMSH exhibited peak melanoma uptake of 13.36 ± 4.12% ID/g at 4 h post-injection and NAD-β-Ala-(Arg^{11})CCMSH exhibited peak melanoma uptake of 11.38 ± 1.29% ID/g at 2 h post-injection.

Importantly in this study, we wanted to determine the renal effects of the charge substitutions made to the peptides. Non-specific renal uptake was dramatically reduced in the RXD-β-Ala-(Arg^{11})CCMSH peptides. Non-specific renal uptake of RAD-β-Ala-(Arg^{11})CCMSH, RSD-β-Ala-(Arg^{11})CCMSH, RTD-β-Ala-(Arg^{11})CCMSH, and RVD-β-Ala-(Arg^{11})CCMSH was reduced 79%, 65%, 79%, and 68% at 2 h post-injection as compared to their Lys linker counterparts. All RXD-β-Ala-(Arg^{11})CCMSH exhibited non-specific renal uptake of less than 30% ID/g. The renal uptake of EAD-β-Ala-(Arg^{11})CCMSH and NAD-β-Ala-(Arg^{11})CCMSH was not further reduced as compared to the RXD-β-Ala-(Arg^{11})CCMSH with uptake values of 25.25 ± 9.26% and 37.23 ± 9.69% ID/g 2 h post-injection.

The dramatic reduction in renal uptake with the substitution of the neutral β-Ala linker demonstrates the importance of the electrostatic interactions of the positive charges on the peptides in renal handling and non-specific uptake *in-vivo*. It is imperative to maintain high contrast of tumor uptake to normal organ tissues for enhanced diagnostic imaging and potential therapeutic applications utilizing radiolabeled peptide conjugates as targeting molecules. ^{99m}Tc-labeled radiopharmaceuticals can be readily translated to therapeutic radiopharmaceuticals through the replacement of ^{99m}Tc with ^{186}Re/ ^{188}Re [152, 153]. Both ^{99m}Tc and ^{186}Re/ ^{188}Re have similar coordination chemistry. The same biomolecule can be labeled with ^{186}Re/ ^{188}Re without structural modification. The combined use of ^{99m}Tc- and ^{186}Re/ ^{188}Re-labeled radiopharmaceuticals for imaging and therapy will enhance the success of

targeted radionuclide treatment for individual patients. Imaging patients with ^{99m}Tc-labled radiopharmaceuticals can aid physicians in determining patient-specific dosimetries for safe and efficacious treatment with the ^{186}Re/ ^{188}Re therapeutic radiopharmaceuticals. Furthermore, imaging during the treatment of disease can monitor a patients response to treatment giving critical information to the physician and allow for modification of treatment protocols, should they be warranted, to further aid in therapeutic regimens [157].

Throughout this study, one α-MSH peptide conjugate has been elucidated as a lead compound for further development of both imaging and therapeutic applications. RAD-β-Ala-(Arg^{11})CCMSH has demonstrated high MC1R specific melanoma uptake (15.66 ± 6.19% ID/g at 2 h post-injection) with limited non-specific renal uptake (20.18 ± 3.86% ID/g at 2 h post-injection). This high melanoma uptake and low kidney uptake correlates to a very favorable tumor to kidney uptake ratio of 0.78 at 2 h post injection. The tumor (target) to kidney uptake ratio is important in determining the total accumulation and potential dose limiting exposure of a patient. The higher the ratio, the better the chance of reducing or eliminating the deleterious effects of radiation within the nephron, and allowing for stronger, more aggressive PRRT therapy to proceed [154, 155].

Future Directions

The use of α-MSH peptide analogs for diagnosis and treatment of melanoma in clinical practice today is non-existent. The utilization of these targeting molecules has been confined to the pre-clinical experimental phase.

Further development and characterization on the use of these peptide conjugates in human cell lines and human tissues should be extrapolated in order to facilitate their potential use in patients seeking clinical aide for treatment of this deadly disease. In order to begin the process of moving these novel α-MSH peptides into a more clinical research venture, targeting and pharmacokinetic properties of the lead compounds in human melanoma will need to be established.

1) Defining the 3-D structure of the α-MSH peptides.

To date, it has been extremely difficult to determine the 3-D structure of the α-MSH peptide derivatives. Characterizing the 3-D structure will further allow investigators to understand the interactions of each part of the α-MSH peptide conjugates with the melanocortin-1 receptor. Understanding the interactions will allow for manipulation of the peptides to further enhance MC1R binding affinity and ultimately increase *in-vivo* melanoma uptake. The increased melanoma uptake will facilitate higher quality imaging characteristics and potential therapeutic treatment with PRRT treatment.

2) Utilizing human melanoma cell lines such as TXM13

This entire study was developed around the utilization of the murine B16/F1 melanoma cell line which overexpresses the MC1R at densities around 7,000 receptor sites/cell [158]. Further experimentation into the use of these peptide conjugates in human melanoma cells is imperative due to differences in behavior of both tumors and peptide uptake previously seen. Human TXM13 melanoma cell lines specifically overexpress the MC1R at densities slightly lower than

B16/F1 around 5,500 receptor sites/cell [158]. In addition to lower MC1R density, histopathological analysis of both B16/F1 murine and TXM13 human melanoma tumors revealed striking differences. The B16/F1 murine tumors are highly vascularized gelatinous masses, whereas TXM13 human tumors form solid masses with viable tumor cells surrounding a necrotic core containing few identifiable melanoma cells. Characterizing the targeting and pharmacokinetic properties of our lead α-MSH compounds in human cell lines will enhance our efforts for utilization in human patients.

3) Therapeutic treatment with $^{186}Re/^{188}Re$.

In order to facilitate the potential of our lead α-MSH peptide conjugate as a viable targeting therapeutic molecule, it is necessary to define the efficacy of treatment of both B16/F1 and TXM13 tumors *in-vivo*, utilizing $^{186}Re/^{188}Re$ as the radionuclide for radiation treatment. As stated before, ^{99m}Tc and $^{186}Re/^{188}Re$ share similar coordination chemistry and our α-MSH peptides have been successfully integrated with $^{186}Re/^{188}Re$ in previous studies [158]. A longitudinal study to determine how well treatment with $^{186}Re/^{188}Re$ -labeled α-MSH peptide can decrease overall tumor volume and increase survival time of mice that have been implanted with both B16/F1 and TXM13 melanoma cells is imperative for moving this research into the clinical realm.

REFERENCES

1. Hanahan, D., and Weinberg, R.A. (2000). The Hallmarks of Cancer. Cell *100*, 57-70.
2. Hanahan, D., and Weinberg, Robert A. (2011). Hallmarks of Cancer: The Next Generation. Cell *144*, 646-674.
3. Siegel, R., Naishadham, D., and Jemal, A. (2012). Cancer statistics, 2012. CA: A Cancer Journal for Clinicians *62*, 10-29.
4. Yang, J., Zaja-Milatovic, S., Thu, Y.M., Lee, F., Smykla, R., and Richmond, A. (2009). Molecular determinants of melanoma malignancy: selecting targets for improved efficacy of chemotherapy. Molecular Cancer Therapeutics *8*, 636-647.
5. Sun, W., and Schuchter, L. (2001). Metastatic melanoma. Current Treament Options in Oncology *2*, 193-202.
6. Mehnert, J., and Kluger, H. (2012). Driver Mutations in Melanoma: Lessons Learned From Bench-to-Bedside Studies. Curreent Oncology Reports *14*, 449-457.
7. Palmieri, G., Capone, M., Ascierto, M., Gentilcore, G., Stroncek, D., Casula, M., Sini, M., Palla, M., Mozzillo, N., and Ascierto, P. (2009). Main roads to melanoma. Journal of Translational Medicine *7*, 86.
8. Von Thaler, A.K., Kamenisch, Y., and Berneburg, M. (2010). The role of ultraviolet radiation in melanomagenesis. Experimental Dermatology *19*, 81-88.

9. Weatherhead, S.C., Haniffa, M., and Lawrence, C.M. (2007). Melanomas arising from naevi and de novo melanomas — does origin matter? British Journal of Dermatology *156*, 72-76.

10. Gilchrest, B., Eller, M., Geller, A., and Yaar, M. (1999). The pathogenesis of melanoma induced by ultraviolet radiation. New England Journal of Medicine *340*, 1341-1348.

11. Palmieri, G., Casula, M., Sini, M., Ascierto, P., and Cossu, A. (2007). Issues affecting molecular staging in the management of patients with melanoma. Journal of Cellular and Molecular Medicine *11*, 1052-1068.

12. Giehl, K. (2005). Oncogenic Ras in tumor progression and metastasis. Biolological Chemistry *386*, 193-205.

13. Dhomen, N., and Marais, R. (2009). BRAF Signaling and Targeted Therapies in Melanoma. Hematology/Oncology Clinics of North America *23*, 529-545.

14. Opdecamp, K., Nakayama, A., Nguyen, M., Hodgkinson, C., Pavan, W., and Arnheiter, H. (1997). Melanocyte development in vivo and in neural crest cell cultures: crucial dependence on the MITF basic-helix-loop-helix-zipper transcription factor. Development *124*, 2377-2386.

15. Davies, H., Bignell, G., Cox, C., Stephens, P., Edkins, S., Clegg, S., Teague, J., Woffendin, H., Garnett, M., Bottomley, W., et al. (2002). Mutations of the BRAF gene in human cancer. Nature *417*, 949-954.

16. Wan, P., Garnett, M., Roe, S., Lee, S., Niculescu-Duvaz, D., Good, V., Jones, C., Marshall, C., Springer, C., Barford, D., et al. (2004). Cancer

Genome Project. Mechanism of activation of tha Ras-Erk signaling pathaway by oncogenic mutation on BRAF. Cell *116*, 855-867.

17. Beeram, M., Patnaik, A., and Rowinsky, E. (2005). Raf: a strategic target for therapeutic development against cancer. Journal of Clinical Oncology *23*, 6771-6790.

18. Inamdar, G.S., Madhunapantula, S.V., and Robertson, G.P. (2010). Targeting the MAPK pathway in melanoma: Why some approaches succeed and other fail. Biochemical Pharmacology *80*, 624-637.

19. Loescher, L.J., Janda, M., Soyer, H.P., Shea, K., and Curiel-Lewandrowski, C. (2013). Advances in Skin Cancer Early Detection and Diagnosis. Seminars in Oncology Nursing *29*, 170-181.

20. Rigel, D.S., Friedman, R.J., Kopf, A.W., and Polsky, D. (2005). Abcde—an evolving concept in the early detection of melanoma. Archives of Dermatology *141*, 1032-1034.

21. Haddad, D., Garvey, E.M., Mihalik, L., Pockaj, B.A., Gray, R.J., and Wasif, N. (2013). Preoperative imaging for early-stage cutaneous melanoma: predictors, usage, and utility at a single institution. The American Journal of Surgery *206*, 979-986.

22. Sabel, M.S., and Wong, S.L. (2009). Review of Evidence-Based Support for Pretreatment Imaging in Melanoma. Journal of the National Comprehensive Cancer Network *7*, 281-289.

23. Hafner, J., Schmid, M.H., Kempf, W., Burg, G., Künzi, W., Meuli-Simmen, C., Neff, P., Meyer, V., Mihic, D., Garzoli, E., et al. (2004). Baseline

staging in cutaneous malignant melanoma. British Journal of Dermatology *150*, 677-686.

24. Buzaid, A.C., Tinoco, L., Ross, M.I., Legha, S.S., and Benjamin, R.S. (1995). Role of computed tomography in the staging of patients with local-regional metastases of melanoma. Journal of Clinical Oncology *13*, 2104-2108.

25. La Porta, C.A.M. (2009). Mechanism of Drug Sensitivity and Resistance in Melanoma. Current Cancer Drug Targets *9*, 391-397.

26. Perez-Tomas, R. (2006). Multidrug Resistance: Retrospect and Prospects in Anti-Cancer Drug Treatment. Current Medicinal Chemistry *13*, 1859-1876.

27. Nikolaou, V.A., Stratigos, A.J., Flaherty, K.T., and Tsao, H. (2012). Melanoma: New Insights and New Therapies. Journal of Investigative Dermatology *132*, 854-863.

28. Flaherty, K.T. (2006). Chemotherapy and Targeted Therapy Combinations in Advanced Melanoma. Clinical Cancer Research *12*, 2366s-2370s.

29. Agarwala, S.S. (2009). Current systemic therapy for metastatic melanoma. Expert Review of Anticancer Therapy *9*, 587-595.

30. Helmbach, H., Rossmann, E., Kern, M.A., and Schadendorf, D. (2001). Drug-resistance in human melanoma. International Journal of Cancer *93*, 617-622.

31. Friedman, H.S., Kerby, T., and Calvert, H. (2000). Temozolomide and Treatment of Malignant Glioma. Clinical Cancer Research *6*, 2585-2597.

32. Mouawad, R., Sebert, M., Michels, J., Bloch, J., Spano, J.P., and Khayat, D. (2010). Treatment for metastatic malignant melanoma: Old drugs and new strategies. Critical Reviews in Oncology/Hematology *74*, 27-39.

33. Atallah, E., and Flaherty, L. (2005). Treatment of metastatic malignant melanoma. Current Treatment Options in Oncology *6*, 185-193.

34. Agarwala, S.S., and Kirkwood, J.M. (2000). Temozolomide, a Novel Alkylating Agent with Activity in the Central Nervous System, May Improve the Treatment of Advanced Metastatic Melanoma. The Oncologist *5*, 144-151.

35. Middleton, M.R., Kelly, J., Thatcher, N., Donnelly, D.J., McElhinney, R.S., McMurry, T.B.H., McCormick, J.E., and Margison, G.P. (2000). O^6-(4-bromothenyl)guanine improves the therapeutic index of temozolomide against A375M melanoma xenografts. International Journal of Cancer *85*, 248-252.

36. Hill, H.Z., Hill, G.J., Ii, and Szramowski, J. (1979). Dacarbazine and melphalan: Enhancement by dosage scheduling of the effect in combination treatment on the harding-passey melanoma in c3d2f1 mice. Archives of Surgery *114*, 135-138.

37. Bedikian, A.Y., Weiss, G.R., Legha, S.S., Burris, H.A., Eckardt, J.R., Jenkins, J., Eton, O., Buzaid, A.C., Smetzer, L., and Von Hoff, D.D. (1995). Phase II trial of docetaxel in patients with advanced cutaneous malignant melanoma previously untreated with chemotherapy. Journal of Clinical Oncology *13*, 2895-2899.

38. Einzig, A., Hochster, H., Wiernik, P., Trump, D., Dutcher, J., Garowski, E., Sasloff, J., and Smith, T. (1991). A phase II study of taxol in patients with malignant melanoma. Investigative New Drugs *9*, 59-64.

39. Rosenberg, S.A., Yang, J.C., Schwartzentruber, D.J., Hwu, P., Marincola, F.M., Topalian, S.L., Seipp, C.A., Einhorn, J.H., White, D.E., and Steinberg, S.M. (1999). Prospective Randomized Trial of the Treatment of Patients With Metastatic Melanoma Using Chemotherapy With Cisplatin, Dacarbazine, and Tamoxifen Alone or in Combination With Interleukin-2 and Interferon Alfa-2b. Journal of Clinical Oncology *17*, 968-975.

40. Chapman, P.B., Einhorn, L.H., Meyers, M.L., Saxman, S., Destro, A.N., Panageas, K.S., Begg, C.B., Agarwala, S.S., Schuchter, L.M., Ernstoff, M.S., et al. (1999). Phase III Multicenter Randomized Trial of the Dartmouth Regimen Versus Dacarbazine in Patients With Metastatic Melanoma. Journal of Clinical Oncology *17*, 2745-2751.

41. Atkins, M.B., Lotze, M.T., Dutcher, J.P., Fisher, R.I., Weiss, G., Margolin, K., Abrams, J., Sznol, M., Parkinson, D., Hawkins, M., et al. (1999). High-Dose Recombinant Interleukin 2 Therapy for Patients With Metastatic Melanoma: Analysis of 270 Patients Treated Between 1985 and 1993. Journal of Clinical Oncology *17*, 2105-2116.

42. Legha, S.S., Ring, S., Bedikian, A., Plager, C., Eton, O., Buzaid, A.C., and Papadopoulos, N. (1996). Treatment of metastatic melanoma with combined chemotherapy containing cisplatin, vinblastine and dacarbazine

(CVD) and biotherapy using interleukin-2 and interferon-α. Annals of Oncology *7*, 827-835.

43. Nimmagadda, H.T.a.N. (2009). Targeted therapy in Melanoma. Biologics *3*, 475-484.

44. Eton, O., Legha, S.S., Bedikian, A.Y., Lee, J.J., Buzaid, A.C., Hodges, C., Ring, S.E., Papadopoulos, N.E., Plager, C., East, M.J., et al. (2002). Sequential Biochemotherapy Versus Chemotherapy for Metastatic Melanoma: Results From a Phase III Randomized Trial. Journal of Clinical Oncology *20*, 2045-2052.

45. Hood, J.D., Bednarski, M., Frausto, R., Guccione, S., Reisfeld, R.A., Xiang, R., and Cheresh, D.A. (2002). Tumor Regression by Targeted Gene Delivery to the Neovasculature. Science *296*, 2404-2407.

46. Lyons, J.F., Wilhelm, S., Hibner, B., and Bollag, G. (2001). Discovery of a novel Raf kinase inhibitor. Endocrine-Related Cancer *8*, 219-225.

47. Wilhelm, S.M., Carter, C., Tang, L., Wilkie, D., McNabola, A., Rong, H., Chen, C., Zhang, X., Vincent, P., McHugh, M., et al. (2004). BAY 43-9006 Exhibits Broad Spectrum Oral Antitumor Activity and Targets the RAF/MEK/ERK Pathway and Receptor Tyrosine Kinases Involved in Tumor Progression and Angiogenesis. Cancer Research *64*, 7099-7109.

48. Augustine, C.K., Toshimitsu, H., Jung, S.-H., Zipfel, P.A., Yoo, J.S., Yoshimoto, Y., Selim, M.A., Burchette, J., Beasley, G.M., McMahon, N., et al. (2010). Sorafenib, a Multikinase Inhibitor, Enhances the Response of

Melanoma to Regional Chemotherapy. Molecular Cancer Therapeutics *9*, 2090-2101.

49. Salama, A.S., and Kim, K. (2013). MEK Inhibition in the Treatment of Advanced Melanoma. Curr Oncol Rep *15*, 473-482.

50. Chapman, P.B., Hauschild, A., Robert, C., Haanen, J.B., Ascierto, P., Larkin, J., Dummer, R., Garbe, C., Testori, A., Maio, M., et al. (2011). Improved Survival with Vemurafenib in Melanoma with BRAF V600E Mutation. New England Journal of Medicine *364*, 2507-2516.

51. Fecher, L.A., Amaravadi, R.K., Schuchter, L.M., and Flaherty, K.T. (2009). Drug Targeting of Oncogenic Pathways in Melanoma. Hematology/Oncology Clinics of North America *23*, 599-618.

52. Heimerl, S., Bosserhoff, A.K., Langmann, T., Ecker, J., and Schmitz, G. (2007). Mapping ATP-binding cassette transporter gene expression profiles in melanocytes and melanoma cells. Melanoma Research *17*, 265-273.

53. Walsh, N., Kennedy, S., Larkin, A.M., Tryfonopoulos, D., Eustace, A.J., Mahgoub, T., Conway, C., Oglesby, I., Collins, D., Ballot, J., et al. (2010). Membrane transport proteins in human melanoma: associations with tumour aggressiveness and metastasis. British Journal of Cancer *102*, 1157-1162.

54. Tawbi, H.A., and Buch, S.C. (2010). Chemotherapy resistance Abrogation in Metastatic Melanoma. Clinical Advances in Hematology & Oncology *8*, 259-266.

55. Chen, K.G., Valencia, J.C., Gillet, J.P., Hearing, V.J., and Gottesman, M.M. (2009). Involvement of ABC transporters in melanogenesis and the development of multidrug resistance of melanoma. Pigment Cell & Melanoma Research *22*, 740-749.

56. Ichihashi, N., and Kitajima, Y. (2001). Chemotherapy induces or increases expression of multidrug resistance-associated protein in malignant melanoma cells. British Journal of Dermatology *144*, 745-750.

57. Berger, W., Hauptmann, E., Elbling, L., Vetterlein, M., Kokoschka, E.M., and Micksche, M. (1997). Possible role of the multidrug resistance-associated protein (MRP) in chemoresistance of human melanoma cells. International Journal of Cancer *71*, 108-115.

58. Chen, K.G., Szakács, G., Annereau, J.P., Rouzaud, F., Liang, X.-J., Valencia, J.C., Nagineni, C.N., Hooks, J.J., Hearing, V.J., and Gottesman, M.M. (2005). Principal expression of two mRNA isoforms (ABCB 5α and ABCB 5β) of the ATP-binding cassette transporter gene ABCB5 in melanoma cells and melanocytes. Pigment Cell Research *18*, 102-112.

59. Van der Bliek, A.M., Baas, F., Ten Houte de Lange, T., Kooimna, P.M., Van der Velde-Koerts, T., and Borst, P. (1987). The human mdr3 gene encodes a novel P-glycoprotein homologue and gives rise to alternatively spliced mRNAs in liver. The EMBO Journal *6*, 3325-3331.

60. Fink, D., Aebi, S., and Howell, S.B. (1998). The role of DNA mismatch repair in drug resistance. Clinical Cancer Research *4*, 1-6.

61. Gerson, S.L. (2004). MGMT: its role in cancer aetiology and cancer therapeutics. National Review of Cancer *4*, 296-307.

62. Ma, S., Egyhazi, S., Ueno, T., Lindholm, C., Kreklau, E.L., Stierner, U., Ringborg, U., and Hansson, J. (2003). O^6-methylguanine-DNA-methyltransferase expression and gene polymorphisms in relation to chemotherapeutic response in metastatic melanoma. British Journal of Cancer *89*, 1517-1523.

63. Passagne, I., Evrard, A., Winum, J.Y., Depeille, P., Cuq, P., Montero, J.L., Cupissol, D., and Vian, L. (2003). Cytotoxicity, DNA Damage, and Apoptosis Induced by New Fotemustine Analogs on Human Melanoma Cells in Relation to O^6-Methylguanine DNA-Methyltransferase Expression. Journal of Pharmacology and Experimental Therapeutics *307*, 816-823.

64. Ma, S., Egyházi, S., Martenhed, G., Ringborg, U., and Hansson, J. (2002). Analysis of O^6-methylguanine-DNA methyltransferase in melanoma tumours in patients treated with dacarbazine-based chemotherapy. Melanoma Research *12*, 335-342.

65. Lage, H., Christmann, M., Kern, M.A., Dietel, M., Pick, M., Kaina, B., and Schadendorf, D. (1999). Expression of DNA repair proteins hMSH2, hMSH6, hMLH1, O^6-methylguanine-DNA methyltransferase and N-methylpurine-DNA glycosylase in melanoma cells with acquired drug resistance. International Journal of Cancer *80*, 744-750.

66. Ghanem, G.E., Comunale, G., Libert, A., Vercammen-Grandjean, A., and Lejeune, F.J. (1988). Evidence for alpha-melanocyte-stimulating hormone

(α-MSH) receptors on human malignant melanoma cells. International Journal of Cancer *41*, 248-255.

67. Siegrist, W., Stutz, S., and Eberle, A.N. (1994). Homologous and Heterologous Regulation of α-Melanocyte-stimulating Hormone Receptors in Human and Mouse Melanoma Cell Lines. Cancer Research *54*, 2604-2610.

68. García-Borrón, J.C., Sánchez-Laorden, B.L., and Jiménez-Cervantes, C. (2005). Melanocortin-1 receptor structure and functional regulation. Pigment Cell Research *18*, 393-410.

69. Lu, D., Vage, D.I., and Cone, R.D. (1998). A Ligand-Mimetic Model for Constitutive Activation of the Melanocortin-1 Receptor. Molecular Endocrinology *12*, 592-604.

70. Roberts, D.W., Newton, R.A., Beaumont, K.A., Helen Leonard, J., and Sturm, R.A. (2006). Quantitative analysis of MC1R gene expression in human skin cell cultures. Pigment Cell Research *19*, 76-89.

71. Mountjoy, K.G., Robbins, L.S., Mortrud, M.T., and Cone, R.D. (1992). The Cloning of a Family of Genes that Encode the Melanocortin Receptors. Science *257*, 1248-1251.

72. Abbott, C.R., Rossi, M., Kim, M.S., AlAhmed, S.H., Taylor, G.M., Ghatei, M.A., Smith, D.M., and Bloom, S.R. (2000). Investigation of the melanocyte stimulating hormones on food intake: Lack of evidence to support a role for the melanocortin-3-receptor. Brain Research *869*, 203-210.

73. Chen, W., Kelly, M.A., Opitz-Araya, X., Thomas, R.E., Low, M.J., and Cone, R.D. (1997). Exocrine Gland Dysfunction in MC5-R-Deficient Mice: Evidence for Coordinated Regulation of Exocrine Gland Function by Melanocortin Peptides. Cell *91*, 789-798.

74. Prusis, P., Frandberg, P.A., Muceniece, R., Kalvinsh, I., and Wikberg, J.E.S. (1995). A Three-Dimensional Model for the Interaction of MSH with the Melanocortin-1 Receptor. Biochemical and Biophysical Research Communications *210*, 205-210.

75. Prusis, P., Schiöth, H.B., Muceniece, R., Herzyk, P., Afshar, M., Hubbard, R.E., and Wikberg, J.E.S. (1997). Modeling of the three-dimensional structure of the human melanocortin 1 receptor, using an automated method and docking of a rigid cyclic melanocyte-stimulating hormone core peptide. Journal of Molecular Graphics and Modelling *15*, 307-317.

76. Yang, Y.K., Dickinson, C., Haskell-Luevano, C., and Gantz, I. (1997). Molecular Basis for the Interaction of [Nle^4,d-Phe^7]Melanocyte Stimulating Hormone with the Human Melanocortin-1 Receptor (Melanocyte α-MSH Receptor). Journal of Biological Chemistry *272*, 23000-23010.

77. Rouzaud, F., Kadekaro, A.L., Abdel-Malek, Z.A., and Hearing, V.J. (2005). MC1R and the response of melanocytes to ultraviolet radiation. Mutation Research/Fundamental and Molecular Mechanisms of Mutagenesis *571*, 133-152.

78. Abdel-Malek, Z., Suzuki, I., Tada, A., Im, S., and Akcali, C.A.N. (1999). The Melanocortin-1 Receptor and Human Pigmentation. Annals of the New York Academy of Sciences *885*, 117-133.

79. Abdel-Malek, Z., Scott, M.C., Suzuki, I., Tada, A., Im, S., Lamoreux, L., Ito, S., Barsh, G., and Hearing, V.J. (2000). The Melanocortin-1 Receptor is a Key Regulator of Human Cutaneous Pigmentation. Pigment Cell Research *13*, 156-162.

80. Lee, H.J., Wall, B., and Chen, S. (2008). G-protein-coupled receptors and melanoma. Pigment Cell & Melanoma Research *21*, 415-428.

81. Abdel-Malek, Z.A., Knittel, J., Kadekaro, A.L., Swope, V.B., and Starner, R. (2008). The Melanocortin 1 Receptor and the UV Response of Human Melanocytes—A Shift in Paradigm. Photochemistry and Photobiology *84*, 501-508.

82. Menon, I.A., Persad, S., Ranadive, N.S., and Haberman, H.F. (1983). Effects of Ultraviolet-visible Irradiation in the Presence of Melanin Isolated from Human Black or Red Hair upon Ehrlich Ascites Carcinoma Cells. Cancer Research *43*, 3165-3169.

83. Más, J.S., Gerritsen, I., Hahmann, C., Jiménez-Cervantes, C., and García-Borrón, J.C. (2003). Rate Limiting Factors in Melanocortin 1 Receptor Signalling Throughthe cAMP Pathway. Pigment Cell Research *16*, 540-547.

84. Lin, J.Y., and Fisher, D.E. (2007). Melanocyte biology and skin pigmentation. Nature *445*, 843-850.

85. Kadekaro, A.L., Kanto, H., Kavanagh, R., and Abdel-Malek, Z.A. (2003). Significance of the Melanocortin 1 Receptor in Regulating Human Melanocyte Pigmentation, Proliferation, and Survival. Annals of the New York Academy of Sciences *994*, 359-365.

86. Cardone, M.H., Roy, N., Stennicke, H.R., Salvesen, G.S., Franke, T.F., Stanbridge, E., Frisch, S., and Reed, J.C. (1998). Regulation of Cell Death Protease Caspase-9 by Phosphorylation. Science *282*, 1318-1321.

87. Shinyama, H., Masuzaki, H., Fang, H., and Flier, J.S. (2003). Regulation of Melanocortin-4 Receptor Signaling: Agonist-Mediated Desensitization and Internalization. Endocrinology *144*, 1301-1314.

88. Wong, W., and Minchin, R.F. (1996). Binding and internalization of the melanocyte stimulating hormone receptor ligand [Nle^4, d-Phe^7]α-MSH in B16 melanoma cells. The International Journal of Biochemistry & Cell Biology *28*, 1223-1232.

89. Sánchez-Más, J., Guillo, L.A., Zanna, P., Jiménez-Cervantes, C., and García-Borrón, J.C. (2005). Role of G Protein-Coupled Receptor Kinases in the Homologous Desensitization of the Human and Mouse Melanocortin 1 Receptors. Molecular Endocrinology *19*, 1035-1048.

90. Siegrist, W., Solca, F., Stutz, S., Giuffrè, L., Carrel, S., Girard, J., and Eberle, A.N. (1989). Characterization of Receptors for α-Melanocyte-stimulating Hormone on Human Melanoma Cells. Cancer Research *49*, 6352-6358.

91. Miao, Y., Whitener, D., Feng, W., Owen, N.K., Chen, J., and Quinn, T.P. (2003). Evaluation of the Human Melanoma Targeting Properties of Radiolabeled α-Melanocyte Stimulating Hormone Peptide Analogues. Bioconjugate Chemistry *14*, 1177-1184.

92. Eves, P.C., and Haycock, J.W. (2010). Melanocortin signalling mechanisms. Advances in experimental medicine and biology *681*, 19-28.

93. Hadley, M.E., and Haskell-Luevano, C. (1999). The Proopiomelanocortin System. Annals of the New York Academy of Sciences *885*, 1-21.

94. Castrucci, A.M.d.L., Hadley, M.E., and Hruby, V.J. (1984). Melanotropin bioassays: In vitro and in vivo comparisons. General and Comparative Endocrinology *55*, 104-111.

95. Tatro, J.B., Atkins, M., Mier, J.W., Hardarson, S., Wolfe, H., Smith, T., Entwistle, M.L., and Reichlin, S. (1990). Melanotropin receptors demonstrated in situ in human melanoma. The Journal of Clinical Investigation *85*, 1825-1832.

96. Sawyer, T.K., Sanfilippo, P.J., Hruby, V.J., Engel, M.H., Heward, C.B., Burnett, J.B., and Hadley, M.E. (1980). 4-Norleucine, 7-D-phenylalanine-alpha-melanocyte-stimulating hormone: a highly potent alpha-melanotropin with ultralong biological activity. Proceedings of the National Academy of Sciences *77*, 5754-5758.

97. Quinn, T., Zhang, X., and Miao, Y. (2010). Targeted melanoma imaging and therapy with radiolabeled alpha-melanocyte stimulating hormone peptide analogues. Giornale italiano di dermatologia e venereologia :

organo ufficiale, Societa italiana di dermatologia e sifilografia *145*, 245-258.

98. Chen, J., Cheng, Z., Hoffman, T.J., Jurisson, S.S., and Quinn, T.P. (2000). Melanoma-targeting Properties of ^{99m}Technetium-labeled Cyclic α-Melanocyte-stimulating Hormone Peptide Analogues. Cancer Research *60*, 5649-5658.

99. Miao, Y., and Quinn, T.P. (2007). Alpha-melanocyte stimulating hormone peptide-targeted melanoma imaging. Frontiers in Bioscience *12*, 4514-4524.

100. Miao, Y., Gallazzi, F., Guo, H., and Quinn, T.P. (2008). ^{111}In-Labeled Lactam Bridge-Cyclized α-Melanocyte Stimulating Hormone Peptide Analogues for Melanoma Imaging. Bioconjugate Chemistry *19*, 539-547.

101. Guo, H., Shenoy, N., Gersham, B.M., Yang, J., Sklar, L.A., and Miao, Y. (2009). Metastatic melanoma imaging with an ^{111}In-labeled lactam bridge-cyclized α-melanocyte-stimulating hormone peptide. Nuclear Medicine and Biology *36*, 267-276.

102. Guo, H., Yang, J., Gallazzi, F., Prossnitz, E.R., Sklar, L.A., and Miao, Y. (2009). Effect of DOTA Position on Melanoma Targeting and Pharmacokinetic Properties of ^{111}In-Labeled Lactam Bridge-Cyclized α-Melanocyte Stimulating Hormone Peptide. Bioconjugate Chemistry *20*, 2162-2168.

103. Guo, H., Shenoy, N., Gershman, B.M., Yang, J., Sklar, L.A., and Miao, Y. (2009). Metastatic melanoma imaging with an ^{111}In-labeled lactam bridge-

cyclized [alpha]-melanocyte-stimulating hormone peptide. Nuclear Medicine and Biology *36*, 267-276.

104. Guo, H., Yang, J., Shenoy, N., and Miao, Y. (2009). Gallium-67-Labeled Lactam Bridge-Cyclized α-Melanocyte Stimulating Hormone Peptide for Primary and Metastatic Melanoma Imaging. Bioconjugate Chemistry *20*, 2356-2363.

105. Guo, H., Yang, J., Gallazzi, F., and Miao, Y. (2010). Reduction of the Ring Size of Radiolabeled Lactam Bridge-Cyclized {alpha}-MSH Peptide, Resulting in Enhanced Melanoma Uptake. Journal of Nuclear Medicine *51*, 418-426.

106. Chen, J., Cheng, Z., Owen, N.K., Hoffman, T.J., Miao, Y., Jurisson, S.S., and Quinn, T.P. (2001). Evaluation of an ^{111}In-DOTA-Rhenium Cyclized {alpha}-MSH Analog: A Novel Cyclic-Peptide Analog with Improved Tumor-Targeting Properties. Journal of Nuclear Medicine *42*, 1847-1855.

107. Hoffman, T.J., Gali, H., Smith, C.J., Sieckman, G.L., Hayes, D.L., Owen, N.K., and Volkert, W.A. (2003). Novel Series of ^{111}In-Labeled Bombesin Analogs as Potential Radiopharmaceuticals for Specific Targeting of Gastrin-Releasing Peptide Receptors Expressed on Human Prostate Cancer Cells. Journal of Nuclear Medicine *44*, 823-831.

108. Wang, L., Shi, J., Kim, Y.S., Zhai, S., Jia, B., Zhao, H., Liu, Z., Wang, F., Chen, X., and Liu, S. (2008). Improving Tumor-Targeting Capability and Pharmacokinetics of ^{99m}Tc-Labeled Cyclic RGD Dimers with PEG4 Linkers. Molecular Pharmaceutics *6*, 231-245.

109. Kowalsky, R.J. (2006). Technetium Radiopharmaceutical Chemistry. Volume 12, J.P. Norenberg, ed. (Albuquerque, NM).

110. Steigman, J., and Eckelman, W.C. (1992). The Chemistry of Technetium in Medicine. (Washington, D.C.).

111. Banerjee, S., Pillai, M.R.A., and Ramamoorthy, N. (2001). Evolution of Tc-99m in Diagnostic Radiopharmaceuticals. Seminars in Nuclear Medicine *31*, 260-277.

112. Bartholomä, M.D., Louie, A.S., Valliant, J.F., and Zubieta, J. (2010). Technetium and Gallium Derived Radiopharmaceuticals: Comparing and Contrasting the Chemistry of Two Important Radiometals for the Molecular Imaging Era. Chemical Reviews *110*, 2903-2920.

113. Mease, R.C., and Lambert, C. (2001). Newer Methods of Labeling Diagnostic Agents With Tc-99m. Seminars in Nuclear Medicine *31*, 278-285.

114. Richards, P. (1965). Nuclide Generators. In Radioactive Pharmaceuticals, G.A. Andrews, Kinsley, R.M., Wagner, H.N. Jr., ed. (Oak Ridge, TN: US Atomic Energy Commission), pp. 155-163.

115. Liu, S., and Edwards, D. S. (1999). ^{99m}Tc-Labeled Small Peptides as Diagnostic Radiopharmaceuticals. Chemical Reviews *99*, 2235-2268.

116. Bartholoma, M., Valliant, J., Maresca, K.P., Babich, J., and Zubieta, J. (2009). Single amino acid chelates (SAAC): a strategy for the design of technetium and rhenium radiopharmaceuticals. Chemical Communications, 493-512.

117. Davidson, A., Jones, A.G., and Orvig, C. (1981). A new class of oxotechnetium(5^+) chelate complexes containing a $TcON_2S_2$ core. Inorganic Chemistry *20*, 1629-1632.

118. Liu, S. (2004). The role of coordination chemistry in the development of target-specific radiopharmaceuticals. Chemical Society Reviews *33*, 445-461.

119. Liu, S. (2008). Bifunctional coupling agents for radiolabeling of biomolecules and target-specific delivery of metallic radionuclides. Advanced Drug Delivery Reviews *60*, 1347-1370.

120. Giblin, M.F., Jurisson, S.S., and Quinn, T.P. (1997). Synthesis and Characterization of Rhenium-Complexed α-Melanotropin Analogs. Bioconjugate Chemistry *8*, 347-353.

121. Edwards, S., Liu, S., Barrett, J.A., Harris, A.R., Looby, R.J., Ziegler, M.C., Heminway, S.J., and Carroll, T.R. (1997). New and Versatile Ternary Ligand System for Technetium Radiopharmaceuticals: Water Soluble Phosphines and Tricine as Coligands in Labeling a Hydrazinonicotinamide-Modified Cyclic Glycoprotein IIb/IIIa Receptor Antagonist with ^{99m}Tc. Bioconjugate Chemistry *8*, 146-154.

122. Ramos-Suzarte, M., Pintado, A.P., Mesa, N.R., Oliva, J.P., Iznaga-Escobar, N., Aroche, L.T., Pimentel, G., González, J., Cordero, M., Rodríguez, O.T., Crombet, R.T, and Perez, R. (2007). Diagnostic efficacy and safety of ^{99m}Tc-Labeled monoclonal antibody ior c5 in patients with

colorectal and anal carcinomas: Final report clinical trial phase I/II. Cancer Biology and Therapy *6*, 22-29.

123. de Kieviet, W. (1981). Technetium Radiopharmaceuticals: Chemical Characterization and Tissue Distribution of Tc-Glucoheptonate Using Tc-99m and Carrier Tc-99. Journal of Nuclear Medicine *22*, 703-709.

124. Yang, J., Guo, H., Padilla, R.S., Berwick, M., and Miao, Y. (2010). Replacement of the Lys linker with an Arg linker resulting in improved melanoma uptake and reduced renal uptake of Tc-99m-labeled Arg-Gly-Asp-conjugated alpha-melanocyte stimulating hormone hybrid peptide. Bioorganic & Medicinal Chemistry *18*, 6695-6700.

125. Miao, Y., Benwell, K., and Quinn, T.P. (2007). ^{99m}Tc- and ^{111}In-Labeled {alpha}-Melanocyte-Stimulating Hormone Peptides as Imaging Probes for Primary and Pulmonary Metastatic Melanoma Detection. Journal of Nuclear Medicine *48*, 73-80.

126. Chen, J., Cheng, Z., Miao, Y., Jurisson, S.S., and Quinn, T.P. (2002). α–melanocyte-stimulating hormone peptide analogs labeled with technetium-99m and indium-111 for malignant melanoma targeting. Cancer *94*, 1196-1201.

127. Yang, J., Guo, H., and Miao, Y. (2010). Technetium-99m-labeled Arg-Gly-Asp-conjugated alpha-melanocyte stimulating hormone hybrid peptides for human melanoma imaging. Nuclear Medicine and Biology *37*, 873-883.

128. Yang, J., and Miao, Y. (2012). Substitution of Gly with Ala enhanced the melanoma uptake of technetium-99m-labeled Arg-Ala-Asp-conjugated

alpha-melanocyte stimulating hormone peptide. Bioorganic & Medicinal Chemistry Letters *22*, 1541-1545.

129. Giblin, M.F., Wang, N., Hoffman, T.J., Jurisson, S.S., and Quinn, T.P. (1998). Design and Characterization of α -melanotropin Peptide Analogs Cyclized through Rhenium and Technetium Metal Coordination. Proceedings of the National Academy of Sciences of the United States of America *95*, 12814-12818.

130. Froidevaux, S., Calame-Christe, M., Tanner, H., Sumanovski, L., and Eberle, A.N. (2002). A Novel DOTA-α-Melanocyte–Stimulating Hormone Analog for Metastatic Melanoma Diagnosis. Journal of Nuclear Medicine *43*, 1699-1706.

131. Froidevaux, S., Calame-Christe, M., Schuhmacher, J., Tanner, H., Saffrich, R., Henze, M., and Eberle, A.N. (2004). A Gallium-Labeled DOTA-{alpha}-Melanocyte- Stimulating Hormone Analog for PET Imaging of Melanoma Metastases. Journal of Nuclear Medicine *45*, 116-123.

132. McQuade, P., Miao, Y., Yoo, J., Quinn, T.P., Welch, M.J., and Lewis, J.S. (2005). Imaging of Melanoma Using ^{64}Cu− and ^{86}Y−DOTA−ReCCMSH(Arg^{11}), a Cyclized Peptide Analogue of α-MSH. Journal of Medicinal Chemistry *48*, 2985-2992.

133. Wei, L., Butcher, C., Miao, Y., Gallazzi, F., Quinn, T.P., Welch, M.J., and Lewis, J.S. (2007). Synthesis and Biologic Evaluation of ^{64}Cu-Labeled Rhenium-Cyclized {alpha}-MSH Peptide Analog Using a Cross-Bridged Cyclam Chelator. Journal of Nuclear Medicine *48*, 64-72.

134. Cheng, Z., Xiong, Z., Subbarayan, M., Chen, X., and Gambhir, S.S. (2007). ^{64}Cu-Labeled Alpha-Melanocyte-Stimulating Hormone Analog for MicroPET Imaging of Melanocortin 1 Receptor Expression. Bioconjugate Chemistry *18*, 765-772.

135. Miao, Y., Benwell, K., and Quinn, T.P. (2007). ^{99m}Tc- and ^{111}In-Labeled {alpha}-Melanocyte-Stimulating Hormone Peptides as Imaging Probes for Primary and Pulmonary Metastatic Melanoma Detection. Journal of Nuclear Medicine *48*, 73-80.

136. Miao, Y., Figueroa, S.D., Fisher, D.R., Moore, H.A., Testa, R.F., Hoffman, T.J., and Quinn, T.P. (2008). ^{203}Pb-Labeled {alpha}-Melanocyte-Stimulating Hormone Peptide as an Imaging Probe for Melanoma Detection. Journal of Nuclear Medicine *49*, 823-829.

137. Guo, H., Yang, J., Gallazzi, F., and Miao, Y. (2011). Effects of the Amino Acid Linkers on the Melanoma-Targeting and Pharmacokinetic Properties of ^{111}In-Labeled Lactam Bridge-Cyclized {alpha}-MSH Peptides. Journal of Nuclear Medicine *52*, 608-616.

138. Haubner, R., Wester, H.J., Reuning, U., Senekowitsch-Schmidtke, R., Diefenbach, B., Kessler, H., Stöcklin, G., and Schwaiger, M. (1999). Radiolabeled $\alpha_v\beta_3$ Integrin Antagonists: A New Class of Tracers for Tumor Targeting. Journal of Nuclear Medicine *40*, 1061-1071.

139. Poethko, T., Schottelius, M., Thumshirn, G., Hersel, U., Herz, M., Henriksen, G., Kessler, H., Schwaiger, M., and Wester, H.J. (2004). Two-Step Methodology for High-Yield Routine Radiohalogenation of Peptides:

^{18}F-Labeled RGD and Octreotide Analogs. Journal of Nuclear Medicine *45*, 892-902.

140. Li, C., Wang, W., Wu, Q., Ke, S., Houston, J., Sevick-Muraca, E., Dong, L., Chow, D., Charnsangavej, C., and Gelovani, J.G. (2006). Dual optical and nuclear imaging in human melanoma xenografts using a single targeted imaging probe. Nuclear Medicine and Biology *33*, 349-358.

141. Decristoforo, C., Faintuch-Linkowski, B., Rey, A., von Guggenberg, E., Rupprich, M., Hernandez-Gonzales, I., Rodrigo, T., and Haubner, R. (2006). [^{99m}Tc]HYNIC-RGD for imaging integrin $\alpha_v\beta_3$ expression. Nuclear Medicine and Biology *33*, 945-952.

142. Alves, S., Correia, J.D.G., Gano, L., Rold, T.L., Prasanphanich, A., Haubner, R., Rupprich, M., Alberto, R., Decristoforo, C., Santos, I., et al. (2007). In Vitro and In Vivo Evaluation of a Novel ^{99m}Tc(CO)3-Pyrazolyl Conjugate of cyclo-(Arg-Gly-Asp-d-Tyr-Lys). Bioconjugate Chemistry *18*, 530-537.

143. Decristoforo, C., Hernandez Gonzalez, I., Carlsen, J., Rupprich, M., Huisman, M., Virgolini, I., Wester, H.J., and Haubner, R. (2008). ^{68}Ga- and ^{111}In-labelled DOTA-RGD peptides for imaging of $\alpha_v\beta_3$ integrin expression. European Journal of Nuclear Medicine and Molecular Imaging *35*, 1507-1515.

144. Hultsch, C., Schottelius, M., Auernheimer, J., Alke, A., and Wester, H.J. (2009). ^{18}F-Fluoroglucosylation of peptides, exemplified on cyclo(RGDfK).

European Journal of Nuclear Medicine and Molecular Imaging *36*, 1469-1474.

145. Wei, L., Ye, Y., Wadas, T.J., Lewis, J.S., Welch, M.J., Achilefu, S., and Anderson, C.J. (2009). ^{64}Cu-Labeled CB-TE2A and diamsar-conjugated RGD peptide analogs for targeting angiogenesis: comparison of their biological activity. Nuclear Medicine and Biology *36*, 277-285.

146. Yang, J., Guo, H., Gallazzi, F., Berwick, M., Padilla, R.S., and Miao, Y. (2009). Evaluation of a Novel Arg-Gly-Asp-Conjugated α-Melanocyte Stimulating Hormone Hybrid Peptide for Potential Melanoma Therapy. Bioconjugate Chemistry *20*, 1634-1642.

147. Froidevaux, S., Calame-Christe, M., Schuhmacher, J., Tanner, H., Saffrich, R., Henze, M., and Eberle, A.N. (2004). A Gallium-Labeled DOTA-α-Melanocyte-Stimulating Hormone Analog for PET Imaging of Melanoma Metastases. Journal of Nuclear Medicine *45*, 116-123.

148. Flook, A.M., Yang, J., and Miao, Y. (2013). Evaluation of New Tc-99m-Labeled Arg-X-Asp-Conjugated α-Melanocyte Stimulating Hormone Peptides for Melanoma Imaging. Molecular Pharmaceutics *10*, 3147-3142.

149. Miao, Y., Owen, N.K., Whitener, D., Gallazzi, F., Hoffman, T.J., and Quinn, T.P. (2002). In vivo evaluation of ^{188}Re-labeled alpha-melanocyte stimulating hormone peptide analogs for melanoma therapy. International Journal of Cancer *101*, 480-487.

150. Flook, A.M., Yang, J., and Miao, Y. (2013). Evaluation of New Tc-99m-Labeled Arg-X-Asp-Conjugated α-Melanocyte Stimulating Hormone Peptides for Melanoma Imaging. Molecular Pharmaceutics *10*, 3417-3424.

151. Flook, A.M., Yang, J., and Miao, Y. (2013). Effects of Amino Acids on Melanoma Targeting and Clearance Properties of Tc-99m-Labeled Arg-X-Asp-Conjugated α-Melanocyte Stimulating Hormone Peptides. Journal of Medicinal Chemistry *56*, 8793-8802.

152. Volkert, W.A., and Hoffman, T.J. (1999). Therapeutic Radiopharmaceuticals. Chemical Reviews *99*, 2269-2292.

153. Lim, N.C., Ewart, C.B., Bowen, M.L., Ferreira, C.L., Barta, C.A., Adam, M.J., and Orvig, C. (2008). Pyridine−tert-Nitrogen−Phenol Ligands: N,N,O-Type Tripodal Chelates for the [M(CO)3]+ Core (M = Re, Tc). Inorganic Chemistry *47*, 1337-1345.

154. Vegt, E., de Jong, M., Wetzels, J.F.M., Masereeuw, R., Melis, M., Oyen, W.J.G., Gotthardt, M., and Boerman, O.C. (2010). Renal Toxicity of Radiolabeled Peptides and Antibody Fragments: Mechanisms, Impact on Radionuclide Therapy, and Strategies for Prevention. Journal of Nuclear Medicine *51*, 1049-1058.

155. Wessels, B.W., Konijnenberg, M.W., Dale, R.G., Breitz, H.B., Cremonesi, M., Meredith, R.F., Green, A.J., Bouchet, L.G., Brill, A.B., Bolch, W.E., et al. (2008). MIRD Pamphlet No. 20: The Effect of Model Assumptions on Kidney Dosimetry and Response—Implications for Radionuclide Therapy. Journal of Nuclear Medicine *49*, 1884-1899.

156. BM, B. (2008). Brenner and Rector's The Kidney, Volume 1, (Philadelphia: Saunders Elsevier).

157. Yang, J., Guo, H., Padilla, R.S., Berwick, M., and Miao, Y. (2010). Replacement of the Lys linker with an Arg linker resulting in improved melanoma uptake and reduced renal uptake of Tc-99m-labeled Arg-Gly-Asp-conjugated alpha-melanocyte stimulating hormone hybrid peptide. Bioorganic & Medicinal Chemistry *18*, 6695-6700.

158. Miao, Y., Owen, N.K., Fisher, D.R., Hoffman, T.J., and Quinn, T.P. (2005). Therapeutic Efficacy of a ^{188}Re-Labeled {alpha}-Melanocyte-Stimulating Hormone Peptide Analog in Murine and Human Melanoma-Bearing Mouse Models. Journal of Nuclear Medicine *46*, 121-129.